

**The Antimicrobial Efficacy and Cytotoxic Effects of
2D-MoS₂ surfaces**

Mohsin Amin

**A Thesis submitted in fulfilment of the requirements of the
Manchester Metropolitan University for the degree of
Master of Science (by Research)**

School of Healthcare Sciences

Manchester Metropolitan University

September 2017

Acknowledgements

I would like to thank Dr. Kathryn Whitehead for her help and support throughout the entirety of this project.

Declaration

With the exception of any statements to the contrary, all the data presented in this report are the results of my own efforts and have not previously been submitted in candidature for any other degree or diploma. In addition, no parts of this report have been copied from other sources. I understand that any evidence of plagiarism and/or the use of unacknowledged third party data will be dealt with as a very serious matter.

Signed: Mohsin Amin

Date: 25/09/2017

Abstract

The requirement for antimicrobial surfaces to inhibit or control bacterial growth in the healthcare and environmental industries is increasing and the use of conventional antimicrobial surfaces are showing signs of microbial resistance. This study would investigate a potential antimicrobial and non-cytotoxic surface that would inhibit microbial retention and biofilm formation against two medically relevant pathogens, whilst having minimal effects on human cells. The roughness parameters of two dimensional molybdenum disulphide (2D-MoS₂) surfaces produced using particles sizes of 90 nm, 2 μm and 6 μm at 5 %, 10 %, 15 % and 20 % concentrations were characterised using white light profilometry (micro-topography and surface features). Scanning electron microscopy was used to identify surface structure and determine if any differences were present in MoS₂ distribution per particle size and concentration. Inductively coupled plasma emission spectroscopy (ICP-AES) was used to measure concentrations of molybdenum and sulphur ions that leached from the 2D-MoS₂ surfaces. Microbiological assays were carried out in order to determine the retention and antimicrobial efficacy against planktonic and biofilm *Staphylococcus aureus* and *Pseudomonas aeruginosa* on the 2D-MoS₂ surfaces. Optical profiling of the 2D-MoS₂ surfaces showed that increases in particle sizes, increased the surface roughness. It was observed that an increase in 2D-MoS₂ particle size of the surfaces resulted in an increase in heterogeneity of bacterial distribution. Results demonstrated an increasing trend of MoS₂ leaching; this however was negligible due to results achieving the lower limits of ICP-AES detection. Zone of inhibition assays demonstrated no antimicrobial activity of the surfaces on the bacteria due to minimal leeching of the molybdenum in the surfaces. Crystal violet biofilm assays were successful in determining the antimicrobial effects of the surfaces against both *S. aureus* and *P. aeruginosa*. Growth curves demonstrated that, 2 μm was the most effective particle size of 2D-MoS₂ at inhibiting both *S. aureus* and *P. aeruginosa* growth. Moreover, *S. aureus* showed the greatest susceptibility towards the 2D-MoS₂ surfaces at all particle sizes. Retention assays demonstrated the surfaces influenced the retention of both bacteria and showed that *P. aeruginosa*, had a greater affinity towards binding to the 2D-MoS₂ surface, resulting in increased retention. Scanning electron microscopy of the bacteria after contact with the 2D-MoS₂ surfaces, alongside the analysis of the ICP-AES and zone

of inhibition assays suggested that the surfaces mechanism of action was through contact kill, with *S. aureus* demonstrating different morphologies when in contact with the 2D-MoS₂ and without. *P. aeruginosa* showed a hollowed bacterial cell structure after 0 h, with the bacteria being flattened or pressed. This effect had become more noticeable after 24 h with *P. aeruginosa* showing shrinkage at higher MoS₂ concentrations. Cytotoxicity analysis against human kidney cells evaluated that after 24 h of incubation, 6 μm 2D-MoS₂ demonstrated the least cytotoxicity, in contrast to 48 h where 90 nm 2D-MoS₂ showed the least cytotoxicity. A potential application for these novel 2D-MoS₂ surfaces would be as antimicrobial surfaces within the healthcare and environmental industries. Due to the antimicrobial efficacies of the surfaces alongside the low cytotoxic effects towards renal cells, catheter surface coatings may be a potential application for the 2D-MoS₂ surfaces, due to existing complications with catheter acquired infections. This suggested that different particle sized surfaces of 2D-MoS₂ should be used depending on the duration of contact with the host. This work suggests that 2 μm 2D-MoS₂ was the most effective antimicrobial surface whereas, both 90 nm and 6 μm demonstrated the best biocompatibility, suggesting that a compromise of antimicrobial activity and human cell cytotoxicity would be required to achieve the most effective 2D-MoS₂ surface.

Contents

Introduction	1
1.0 Overview	1
1.01 Antimicrobial resistance	1
1.02 Metals as antimicrobials	2
1.03 Retention of surfaces	3
1.04 <i>Staphylococcus aureus</i>	3
1.05 <i>Pseudomonas aeruginosa</i>	4
1.06 Biofilms	5
1.07 Biototoxicity	5
Aim and objectives	6
1.1 Aim	6
1.12 Objectives	6
Methods	7
2.0 2D-MoS ₂ screen printed surface fabrication	7
2.01 2D-MoS ₂ surface preparation	7
2.02 Scanning electron microscopy	7
2.03 Surface Characterisation	8
2.04 Inductively coupled plasma emission spectroscopy	8
2.1 Cultures and preparation	8
2.11 Stock cultures	8
2.12 Preparation of bacterial suspension	9
2.2 Antimicrobial testing	9
2.21 Retention assay with epifluorescence microscopy	9
2.22 Zones of inhibition	10
2.23 Crystal violet biofilm assay	10
2.24 Bacterial growth curves	11
2.3 Renal human cell cytotoxicity	12
2.31 Immortalised renal human proximal tubular cell preparation	12
2.32 Immortalised renal human proximal tubular cell viability assay	12
2.4 Statistical analysis	12
Results – Surfaces	13
3.0 Scanning electron microscopy of 2D-MoS ₂	13

3.11 Roughness values	16
3.2 Roughness profiles	19
3.2 Leaching of ions using inductively coupled plasma atomic emission spectroscopy	25
Surface retention	27
3.3 Retention of <i>Staphylococcus aureus</i>	27
3.31 Retention of <i>Pseudomonas aeruginosa</i>	32
Antimicrobial effects of 2D-MoS₂	38
3.4 Zones of inhibition	38
3.41 Crystal violet biofilm assay	38
3.42 Growth Curve of <i>Staphylococcus aureus</i>	39
3.43 Growth curve of <i>Pseudomonas aeruginosa</i>	43
Scanning electron microscopy of bacteria after growth curves	46
3.5 <i>Staphylococcus aureus</i>	46
3.51 <i>Pseudomonas aeruginosa</i>	50
Scanning electron microscopy of retained bacteria on 2D-MoS₂ surfaces	54
3.6 <i>Staphylococcus aureus</i>	54
3.61 <i>Pseudomonas aeruginosa</i>	58
Renal human cell cytotoxicity	62
3.7 Immortalised renal human proximal tubular cell viability in response to media incubated with 2D-MoS ₂ surfaces at 24, 25 and 26 hours	62
3.71 Immortalised human renal cell viability in response to media incubated with 2D-MoS ₂ surface at hours 48, 49 and 50	63
Discussion	66
4.0 Surface roughness	66
4.01 ICP–AES	66
4.02 2D-MoS ₂ retention of bacteria	67
4.03 Zones of inhibition	68
4.04 Growth Curve	68
4.05 Bacterial biofilms	69
4.06 2D-MoS ₂ effects on bacteria	69
4.07 Cytotoxicity of MoS ₂	71
5.0 Future work	74
6.0 Conclusion	75

Index of Figures

Figure 1. Scanning electron microscopy images of 90 nm 2D-MoS ₂ surfaces at MoS ₂ concentrations of a) 5 %, b) 10 %, c) 15 % and d) 20 %	14
Figure 2. Scanning electron microscopy images of 2 μm 2D-MoS ₂ surfaces at MoS ₂ concentrations of a) 5 %, b) 10 %, c) 15 % and d) 20 %	15
Figure 3. Scanning electron microscopy images of 6 μm 2D-MoS ₂ surfaces at MoS ₂ concentrations of a) 5 %, b) 10 %, c) 15 % and d) 20 %	16
Figure 4. a) Average surface roughness (S_a) values b) Surface mean square roughness values (S_q) and c) Average maximum height of 2D-MoS ₂ surfaces (S_{pv}) with 2D-MoS ₂ at increasing molybdenum concentrations of 5 %, 10 %, 15 % and 20 %.	18
Figure 5. Line profiles taken using white light profilometry, of 90 nm 2D-MoS ₂ surfaces at concentrations of a) 5 %, b) 10 %, c) 15 % and d) 20 %	21
Figure 6. Line profiles taken using white light profilometry, of 2 μm 2D-MoS ₂ surfaces at concentrations of a) 5 %, b) 10 %, c) 15 % and d) 20 %	22
Figure 7. Line profiles taken using white light profilometry, of 6 μm 2D-MoS ₂ surfaces at concentrations of a) 5 %, b) 10 %, c) 15 % and d) 20 %	23
Figure 8. Mass spectrometry used for the detection of trace volumes of molybdenum from an aqueous solution of sterile distilled water and 2D-MoS ₂ . Note y axis scale max = 0.01ppm	26
Figure 9. Average sulphur concentration measurements taken from leached MoS ₂ into sterilised distilled water, detected using mass spectrometry. Note y axis scale max = 0.4ppm	26
Figure 10. Epifluorescence images demonstrating the retention of <i>S. aureus</i> on 90 nm 2D-MoS ₂ surfaces at concentration of a) 5 %, b) 10 %, c) 15 % and d) 20 % MoS ₂	29

Figure 11. Epifluorescence images demonstrating the retention of *S. aureus* on 2 μm 2D-MoS₂ surfaces at concentration of a) 5 %, b) 10 %, c) 15 % and d) 20 % MoS₂

30

Figure 12. Epifluorescence images demonstrating the retention of *S. aureus* on 6 μm 2D-MoS₂ surfaces at concentration of a) 5 %, b) 10 %, c) 15 % and d) 20 % MoS₂

31

Figure 13. Percentage coverage of *S. aureus* on 90 nm, 2 μm and 6 μm 2D-MoS₂ surfaces at increasing concentrations of MoS₂

32

Figure 14. Epifluorescence images demonstrating the retention of *P. aeruginosa* on 90 nm 2D-MoS₂ surfaces at concentrations of a) 5 %, b) 10 %, c) 15 % and d) 20 % MoS₂

34

Figure 15. Epifluorescence images demonstrating the retention of *P. aeruginosa* on 2 μm 2D-MoS₂ surfaces at concentrations of a) 5 %, b) 10 %, c) 15 % and d) 20 % MoS₂

35

Figure 16. Epifluorescence images describing the retention of *P. aeruginosa* on 6 μm 2D-MoS₂ surfaces at concentrations of a) 5 %, b) 10 %, c) 15 % and d) 20 % MoS₂

36

Figure 17. Percentage coverage of *P. aeruginosa* on 90 nm, 2 μm and 6 μm 2D-MoS₂ surfaces at increasing concentrations of MoS₂

37

Figure 18. Average optical density reading of *S. aureus* and *P. aeruginosa* against 2D-MoS₂ at increasing concentrations of MoS₂ (5 %, 10 %, 15 % and 20 %)

39

Figure 19. Average colony forming units of *S. aureus* over 24 h growth curves, tested against a) 90 nm, b) 2 μm and c) 6 μm 2D-MoS₂ particle sized surfaces, at concentrations of 5 %, 10 %, 15 % and 20 % MoS₂

42

Figure 20. Average colony forming units of *P. aeruginosa* over 24 h growth curves, tested against a) 90 nm, b) 2 μm and c) 6 μm 2D-MoS₂ particle sized surfaces, at concentrations of 5 %, 10 %, 15 % and 20 % MoS₂ 45

Figure 21. Scanning electron microscopy images of *S. aureus* (a, c, e and g) (0 h) alongside *S. aureus* after 2D-MoS₂ 90 nm growth curves (b, d, f and h) (24 h) at MoS₂ concentrations of a) b) 5 %, c) d) 10 %, e) f) 15 % and g) h) 20 % 47

Figure 22. Scanning electron microscopy images of *S. aureus* (a, c, e and g) (0 h) alongside *S. aureus* after 2D-MoS₂ 2 μm growth curves (b, d, f and h) (24 h) at MoS₂ concentrations of a) b) 5 %, c) d) 10 %, e) f) 15 % and g) h) 20 % 48

Figure 23. Scanning electron microscopy images of *S. aureus* (a, c, e and g) (0 h) alongside *S. aureus* after 2D-MoS₂ 6 μm growth curves (b, d, f and h) (24 h) at MoS₂ concentrations of a) b) 5 %, c) d) 10 %, e) f) 15 % and g) h) 20 % 49

Figure 24. Scanning electron microscopy images of *P. aeruginosa* (a, c, e and g) (0 h) alongside *P. aeruginosa* after 2D-MoS₂ 90 nm growth curves (b, d, f and h) (24 h) at MoS₂ concentrations of a) b) 5 %, c) d) 10 %, e) f) 15 % and g) h) 20 % 51

Figure 25. Scanning electron microscopy images of *P. aeruginosa* (a, c, e and g) (0 h) alongside *P. aeruginosa* after 2D-MoS₂ 2 μm growth curves (b, d, f and h) (24 h) at MoS₂ concentrations of a) b) 5 %, c) d) 10 %, e) f) 15 % and g) h) 20 % 51

Figure 26. Scanning electron microscopy images of *P. aeruginosa* (a, c, e and g) (0 h) alongside *P. aeruginosa* after 2D-MoS₂ 6 μm growth curves (b, d, f and h) (24 h) at MoS₂ concentrations of a) b) 5 %, c) d) 10 %, e) f) 15 % and g) h) 20 % 52

Figure 27. Scanning electron microscopy images of *S. aureus* (a, c, e, g) (0 h) on 2D-MoS₂ surfaces, alongside *S. aureus* after 24 h of 90 nm 2D-MoS₂ contact (b, d, f, h) (24 h), at MoS₂ concentrations of a) b) 5 %, c) d) 10 %, e) f) 15 % and g) h) 20 % 54

Figure 28. Scanning electron microscopy images of *S. aureus* (a, c, e, g) (0 h) on 2D-MoS₂ surfaces, alongside *S. aureus* after 24 h of 2 μm 2D-MoS₂ contact (b, d, f, h) (24 h), at MoS₂ concentrations of a) b) 5 %, c) d) 10 %, e) f) 15 % and g) h) 20 % 55

Figure 29. Scanning electron microscopy images of *S. aureus* (a, c, e, g) (0 h) on 2D-MoS₂ surfaces, alongside *S. aureus* after 24 h of 6 μm 2D-MoS₂ contact (b, d, f, h) (2 4 h), at MoS₂ concentrations of a) b) 5 %, c) d) 10 %, e) f) 15 % and g) h) 20 % 56

Figure 30. Scanning electron microscopy images of *P. aeruginosa* (a, c, e, g) (0 h) on 2D-MoS₂ surfaces, alongside *P. aeruginosa* after 24 h of 90 nm 2D-MoS₂ contact (b, d, f, h) (2 4 h), at MoS₂ concentrations of a) b) 5 %, c) d) 10 %, e) f) 15 % and g) h) 20 % 58

Figure 31. Scanning electron microscopy images of *P. aeruginosa* (a, c, e, g) (0 h) on 2D-MoS₂ surfaces, alongside *P. aeruginosa* after 24 h of 2 μm 2D-MoS₂ contact (b, d, f, h) (2 4 h), at MoS₂ concentrations of a) b) 5 %, c) d) 10 %, e) f) 15 % and g) h) 20 % 59

Figure 32. Scanning electron microscopy images of *P. aeruginosa* (a, c, e, g) (0 h) on 2D-MoS₂ surfaces, alongside *P. aeruginosa* after 24 h of 6 μm 2D-MoS₂ contact (b, d, f, h) (2 4 h), at MoS₂ concentrations of a) b) 5 %, c) d) 10 %, e) f) 15 % and g) h) 20 % 60

Figure 33. HK-2 cell viability when incubated with SFM and 20 % MoS₂ concentrations of 2D-MoS₂ surfaces, at particle sizes of 90 nm, 2 μm and 6 μm. Cells were tested after 24, 25 and 26 h 62

Figure 34. HK-2 cell viability when incubated with SFM and 20 % MoS₂ concentrations of 2D-MoS₂ surfaces, at particle sizes of 90 nm, 2 μm and 6 μm. Cells were tested after 48, 49 and 50 h 64

Index of Tables

Table 1. Average peak and valley heights across 2D-MoS₂ surfaces with increasing particle size and concentration 23

Introduction

1.0 Overview

Antimicrobial resistance is a growing health threat. This vast increase in antimicrobial resistance was thought to have arisen through multiple factors, stemming from inappropriate use of antibiotics, the extensive use of antimicrobial agents in animal feeds for growth promotion. Furthermore, the increase in regional and international travel allowing antimicrobial resistant bacteria to be transported across geographical barriers that were previously inaccessible to them, as well as the lack of new drug development from the pharmaceutical industry due to reduced incentives and an increase in regulatory requirements (Ventola, 2015).

1.01 Antimicrobial resistance

Unfortunately, the increase in antimicrobial resistance has become a threatening accomplishment, critically jeopardizing ill patients whom have acquired such infection. This has led to the World Health Organisation (WHO) to place antimicrobial resistance in one of three priority threats to 21st century health (WHO, 2016).

Multiple mechanisms of antimicrobial resistance have spread through a variety of bacterial genomes. The acquisition of genetic material through horizontal gene transfer is one of the most important factors in the development and spread of antimicrobial resistance. This distinct mechanism of movement of bacterial genes allows favourable genetic mutations to be passed through genera (Gaze *et al.*, 2013). Through mutation and selection, along with genetic material exchange mechanisms enabling bacteria to adapt quickly and efficiently to the introduction of antimicrobial agents within their surrounding environment (Tenover, 2006).

Previous studies have suggested that metal ions induce significant stress on bacteria, effectively inhibiting growth (Seniya *et al.*, 2012). Although, most bacteria are able to develop resistance to such metals as a response to metal toxicity. The resistance to antimicrobial metals come mostly from plasmid – encoded bacteria, but are highly specific to a single anion or cation (Chudobova *et al.*, 2015). The resistance genes encoding for this information are changed based on external in internal factors, such as long-term effects of heavy metals in the soil or water (Ohlsen *et al.*, 2003).

There has been an emergence of drug and multidrug resistant *Staphylococcus aureus* and *Pseudomonas aeruginosa* (Lowy, 2003). A recent study in 2014 conducted tests on 306 clinical *S. aureus* isolates using various antibiotic susceptibility profiles. From the data obtained, penicillin resistance amounted to 94.7 % in all the clinical samples taken, whilst methicillin resistance was found in 43.1 % of the samples and inducible clindamycin resistance was shown in 12.4 % of the cases, concluding that the rates of resistance for methicillin are alarmingly high and continue to increase (Ansari *et al.*, 2014). Moreover, the rates of *P. aeruginosa* infections are increasing worldwide, particularly in healthcare environments. It was recently reported that *P. aeruginosa* infections were the second most common cause of pneumonia at 18.1 % and the third most common cause of urinary tract infections at 16.3 % (Hirsch and Tam, 2010).

1.02 Metals as Antimicrobials

The use of metals as antimicrobials has been around for hundreds of years; their modes of actions however, have remained somewhat unclear. Recent studies have found that some prescribed mechanisms include bacterial cell damage via oxidative stress, protein dysfunction or membrane damage (Lemire *et al.*, 2013). Throughout the Twenty First century, due to the discovery of antibiotics and other organic antimicrobial compounds, the general use of metal derived antimicrobials saw a decline in use. This was true except for silver, which has seen continued use in a number of medical and industrial applications (Hobman and Crossman, 2015).

Inside a microbial cell, metals may target different antimicrobial sites depending on their concentration and chemical properties (Bruins *et al.*, 2000). Molybdenum disulphide (MoS_2) and other two-dimensional (2D) materials have gained a large interest in multiple fields within the recent years, due to their chemical, physical and electronic properties (Cao *et al.*, 2017). Previous studies have suggested that key similarities in multiple 2D-compounds such as graphene, MoS_2 , graphene oxide and reduced graphene oxide in terms of antimicrobial mechanisms. The compounds all similarly demonstrated oxidative stress related bacterial cell destruction. A study in 2014 identified that 2D- MoS_2 as a 2D surface, produced an increased number of reactive oxygen species (ROS), which resulted in increased bacterial cell death of up to 40 %. It has also been demonstrated that 2D- MoS_2 surfaces have the ability to

effectively produce ROS whereas the graphene-based compounds could not (Yang *et al.*, 2014).

1.03 Retention of surfaces

Biofouling is an issue that is of great concern to many industries, causing critical problems in food professions and the healthcare sector, leading to increased costs worldwide. This tendency of bacteria to become retained onto a surface is highly undesirable due to the potential of bio transfer post adherence (Whitehead and Verran, 2009). The interaction of bacteria with surfaces has many implications in a wide array of areas including, biofouling, biofilm formation and the spread of infection through plants and animals. The role of solid material surface chemistry in biosensors and bioelectronics is critical as the resistance to nonspecific binding reduces any background interferences (Somorjai and Li, 2010). In addition, the role of bacterial adherence is of the uttermost importance when designing surfaces for implants or other biomedical diagnostic tools (Hall-Stoodley *et al.*, 2004). Bacterial attachment and its corresponding influential factors have been the focus of extensive study through the recent years. This being so because antimicrobial surfaces are requiring more uses, thus antifouling being a more prominent research area (Bos *et al.*, 1999). The current key strategies for disrupting bacterial attachment are targeted towards preventing biofoulants from attaching or degrading them. Surfaces combined with antimicrobials or other biocidal agents have the advantage of the antimicrobial compounds being in contact with the bacteria resulting in locally high antimicrobial doses without systemic toxicity limits being exceeded. Throughout literature, many antimicrobial coatings have been discussed including silver, zinc and nitric oxide. However, many have been associated with increased cytotoxicity, anaphylaxis or low antimicrobial efficacies (Costa *et al.*, 2011).

1.04 *Staphylococcus aureus*

S. aureus is a Gram positive, coagulase and catalyase positive bacteria. It is a common microorganism of the human flora, and it is among the bacteria that are most resilient to the external environment (Rağbetli *et al.*, 2017). *S. aureus* is an important opportunistic pathogen, colonising roughly 20 % of the world's population (Foster *et al.*, 2013). *S. aureus* infections occur frequently because they are resident skin flora and thus easily contaminate open wounds. Initial exposure of *S. aureus* to host

tissues beyond the preliminary barriers is thought to trigger upregulation of its virulence genes (Novick, 2003). *S. aureus* has been well known to survive inside and outside of host cells. Within the host, *S. aureus* must overcome opsonisation by antibodies and complement, which directly leads to killing of *S. aureus* or uptake by phagocytes through complement or Fc receptors (Liu, 2009). *S. aureus* now being a pathogen of great concern due to its intrinsic virulence, its ability to cause a wide array of life threatening infections and its inherent ability to adapt to an array of environments. Due to its effective pathogenicity, the mortality rates of *S. aureus* remain within 20-30 % even with all the currently effective antimicrobial agents. *S. aureus* remains the leading problematic pathogen in both community and healthcare acquired infections (Yilmaz *et al.*, 2016). Retention of *S. aureus* plays a significant role in biomaterial associated infections, leading to failure of implants and other biomedical devices (Alam and Balani, 2017). Staphylococcal adhesion to both abiotic and biotic surfaces is the initial stage in the establishment of infection through surface contact. *S. aureus* uses a variety of proteinaceous adhesins alongside extracellular matrix and plasma proteins to form effective biofilms on surfaces (Heilmann, 2011).

1.05 *Pseudomonas aeruginosa*

The prevention and treatment for bacterial infections and colonisation with each passing year is becoming more challenging; this being especially true for the opportunistic pathogen *P. aeruginosa* (Lister *et al.*, 2009). *P. aeruginosa* is a Gram negative, rod shaped, aerobic bacterium, belonging to the *Pseudomonadaceae* family (Yayan, *et al.*, 2015). *P. aeruginosa* rarely causes infection in immunocompetent hosts however complications arise in those whom are immunocompromised, whether that be from malignancies, HIV or patients that are mechanically ventilated (Sadikot *et al.*, 2005). Due to *P. aeruginosa* metabolic plasticity and versatility, it is capable of colonising a vast range of ecological niches including plants, soil, animals and aquatic environments (Cabot *et al.*, 2016). Having inherent resistances, being adaptively or intrinsically acquired, enable treatment or prevention of *P. aeruginosa* colonisation and infection a challenge to combat (Driscoll, 2007). Furthermore, *P. aeruginosa* ability to form biofilms when attached to a surface promotes long-term colonisation, leading to complications with medical devices and instruments. Such mechanisms exist which aid *P. aeruginosa* in attachment to a surface, for example;

the adaptation of type IV pili have been acquired by *P. aeruginosa* to aid in motility, ultimately helping mediate surface adherence and biofilm formation (Lavery *et al.*, 2014). Because of its pathogenicity, *P. aeruginosa* is widely considered as a model for antimicrobial resistance (Cabot *et al.*, 2016).

1.06 Biofilms

A biofilm is a conglomeration of microbial cells, extracellular DNA, polysaccharides and proteins that are irreversibly associated with a surface (Donlan, 2002). Biofilms are able to attach to a wide array of surfaces and tend to develop in moist environments that are accompanied with rich nutrient flow and cellular metabolites aiding in surface adhesion (Sarjit *et al.*, 2015). Biofilms are living communities that are found attached to either living or abiotic surfaces. Initially bacteria will attach to a substrate that is or has previously been in contact with fluids containing a number of macromolecules such as DNA, proteins and various humic acids (Renner and Weibel, 2011).

Bacterial organisms that dwell in biofilms differ from their planktonic counterparts. The mechanism of antimicrobial resistance such as modifying enzymes and efflux pumps do not seem to be directly responsible for antimicrobial resistance within a biofilm. Bacteria that were known to not exhibit genetic resistance have found significant reductions in susceptibility when forming biofilms. The evidence for biofilm resistance arises when investigating resistance under free-floating and biofilm conditions (Stewart and Costerton, 2001). Under such conditions, bacteria tested in biofilms demonstrated increased antimicrobial resistance however, upon removal of the biofilm and the bacteria enter a free-floating state, susceptibility to previously susceptible antimicrobials, increased significantly (Donlan and Costerton, 2002).

1.07 Biotoxicity

Ideally, an antimicrobial agent should demonstrate the maximum toxicity towards a pathogen whilst causing minimal damage to host cells. The ways in which this is most effectively achieved is through selective toxicity, in which the antimicrobial agent targets a specific metabolic pathway or a part of the pathogens morphology that would normally be absent from mammalian cells (Sefton, 2002). Biotoxicity of antimicrobial surfaces can be tested in a number of ways that include the use of

tetrazolium based dyes to induce formazan based reduction. The WST-8 (tetrazolium salt) colorimetric assay is one of the most common methods of determining cell cytotoxicity, which the WST-8 reagent yields a water soluble formazan derivate that is quantifiable colorimetrically (Tsukatani et al., 2012)

Aim and objectives

1.11 Aim

The aim of this research was to determine the retention, antimicrobial effects and cytotoxicity of 2D-MoS₂ surfaces produced with particle sizes of 90 nm, 2 μm and 6 μm at concentrations of 5 %, 10 %, 15 % and 20 % against two pathogens, *S. aureus* and *P. aeruginosa*

1.12 Objectives

- Determine the surface topographies of the 2D-MoS₂ surfaces
- Quantify the leaching of molybdenum and sulphur ions from the surfaces
- Carry out retention assays using *S. aureus* and *P. aeruginosa* on the 2D-MoS₂ surfaces at all particle sizes and concentrations
- Use microbiological techniques (zone of inhibition, crystal violet biofilm assays, growth curves and retention assays) to determine the antimicrobial efficacy of the 2D-MoS₂ surfaces
- Visualise microbial damage using scanning electron microscopy
- Evaluate the cytotoxicity of 2D-MoS₂ against immortalised renal human proximal tubular cells over multiple time points

Methods

2.0 2D-MoS₂ screen printed surface fabrication

Particle sizes of 90 nm, 2 μm and 6 μm 2D-MoS₂ (Sigma, UK) were used to produce the surfaces using a screen printing method. These were contained in a commercial graphitic ink (Gwent Electronic Materials, UK) since it could be used for many print cycles without screen-blocking and still providing advantageous electrochemical properties whilst also allowing for the increased production of the 2D-MoS₂ electrodes. Concentrations of 5 %, 10 %, 15 % and 20 % MoS₂ were used. The thickness of the screen-printed surface depended on the consistency of the ink, the screen itself and other various printing parameters. In the production of the surfaces used in this study, the thickness of the printed surfaces was between the ranges of 12 μm to 15 μm. To reduce the amount of 2D-MoS₂ material utilized in the fabrication of the 2D-MoS₂ surfaces, the aforementioned mixture was screen-printed on top of an initial screen-printed surface, which had been printed using only carbon – graphite ink. Following the screen-printing of the 2D-MoS₂ modified ink, a curing step was required. An optimised time of 30 min at 60 °C was implemented since previous work had demonstrated that such parameters resulted in optical electrochemical properties of the screen printed electrodes.

2.01 2D-MoS₂ surface preparation

The 2D-MoS₂ electrodes were cut using scissors at the base of the electrode channel to form a 1 cm by 1 cm square. The surface was sterilized using 70 % ethanol (Sigma, UK) for 10 min. Then the 2D-MoS₂ surface were rinsed for two seconds with 25 mL of sterile distilled water to remove ethanol residue and placed in a class II airflow cabinet to dry for 1 h.

2.02 Scanning electron microscopy (SEM)

2D-MoS₂ surfaces were prepared as described in section (*2D-MoS₂ surface preparation*). One of each concentration and particle size of the 2D-MoS₂ surfaces were fixed using 30 mL of 4.0 % glutaraldehyde solution (Agar Scientific, UK) over night. The samples were dehydrated using an ethanol gradient and stored in a desiccator to dry. The fixed and dried 2D-MoS₂ surfaces were mounted on pin type aluminium SEM mounts (Agar Scientific, UK) with double-sided conducting carbon

tape (Agar Scientific, UK). The samples were coated a 10 nm thick gold using a magnetron sputtering system and characterised in three random locations on the surface using SEM (Zeiss Supra 40VP) at magnifications of 100,000 x, 50,000 x, 25,000 x and 10,000 x (n = 3)

2.03 Surface Characterisation

Using optical profilometry (Zemetrics), the surface topography of the 2D-MoS₂ surfaces was measured directly and indirectly from surface replicas (n = 3), locating a different area of the surface for each replicate. Analysis of the surface roughness qualitatively via images, and quantitatively via *S* values (Zemaps). The average peak and valley values from the line profiles were also taken (n = 10).

2.04 Inductively coupled plasma atomic emission spectroscopy

The 2D-MoS₂ surfaces were prepared as in section (*2D-MoS₂ surface preparation*) and placed in separate 15 mL falcon tubes (Fisher Scientific, Loughborough), to which 8 mL of sterile distilled water was added. The falcon tubes were incubated at 37 °C for 24 h under agitation (150 *rpm*). The 2D-MoS₂ surface solution was syringe filtered using leur lock syringes (ThermoFisher, UK) and 0.2 µm sterile syringe filters (Starstead, UK) into new 15 mL flacon tubes and analysed using Inductively coupled plasma atomic emission spectroscopy (ICP–AES) (Thermo scientific, UK) model: iCAP6300 DUO. Analysis parameters used were; pump settings: flush pump rate – 50 *rpm*, analysis pump rate – 50 repetitions per min (*rpm*) and pump tubing – Tygon Orange / White. The source setting were as follows; RF power – 1250W, auxiliary gas flow – 0.5 L / min and nebuliser gas flow – 0.55 L / min with a sample flush time of 46 s (n = 3).

2.1 Cultures and preparation

2.11 Stock cultures

Stock cultures of *S. aureus* (NCTC 12981) and *P. aeruginosa* (PA01) were used for all microbiological assays. Stock solutions were stored in the freezer at 80 °C. Cultures were thawed and inoculated onto tryptone soya agar (TSA) (Oxoid, UK) and incubated for 24 h at 37 °C. Stock cultures were re-frozen after use. For

maintenance of bacterial physiology, inoculated plates were stored in the fridge at 4 °C and replaced every month.

2.12 Preparation of bacterial suspensions

A single colony of *S. aureus* and *P. aeruginosa* was added to 10 mL of tryptone soya broth (TSB) and vortexed for 10 s. The bacterial inoculums were incubated at 37 °C for 24 h in an orbital incubator at 150 *rpm*. Bacterial cultures were spun down in a centrifuge (Sigma 3-16L, UK) at 3000 *rpm* for 10 min, and the bacterial pellet was washed in 10 mL of 0.85 % saline solution (Oxoid, UK) and vortexed for 10 s. The washing procedure was carried out twice. The bacteria were re-suspended to an optical density (OD) of 1.0 ± 0.1 at 540 nm using a spectrophotometer (Jenway 6305, UK). Colony forming units (CFU / mL) were performed using serial dilutions. These counts were 8.40×10^8 CFU / mL for *S. aureus* and 2.88×10^8 CFU / mL for *P. aeruginosa*.

2.2 Antimicrobial testing

2.21 Retention assay with epifluorescence microscopy

Cultures were grown and washed (*Cultures and preparation*). Three 2D-MoS₂ surfaces at each particle size and concentration (n = 6) were sterilized by submerging in 70 % ethanol for 10 min before being rinsed thoroughly with sterile distilled water. Two sections of double sided tape were fixed to the bottom of a sterile Petri dish, onto which each sterilized 2D-MoS₂ surface was placed using sterile forceps. Thirty milliliters of bacterial inoculation were added to each Petri dish to ensure full submersion of each surface. The Petri dish was incubated for 1 h at 37 °C without agitation, after which, the bacterial inoculum was removed and discarded using a sterile 10 mL pipette. Non-adhered cells were gently removed from the surfaces with sterile distilled water (2.5 mL), rinsing at a 45° angle for 5 s. The surfaces were dried in a Class two airflow cabinet for 1 h before being stained with 0.03 % acridine orange (Sigma, UK) (excitation / emission of 460/6560 RNA and 500/526 DNA) suspended in a glacial acetic acid solution (Sigma-Aldrich, UK). The stain was left on for 2 min before removing the surface from the tape and rinsing at a 45 ° angle for 5 s with 2.5 mL of sterile distilled water, to remove excess stain. The surface was air dried in the dark for 1 h. Stained surfaces were visualized using epifluorescence microscopy on a Nikon Eclipse E600 (Nikon, Japan) mounted with an F-View II

black and white digital camera. The surfaces with retained bacteria were visualized using 100 x oil immersion optical lens with a Nikon B-2A fluorescence filter at three different locations (n = 3).

The 2D-MoS₂ surfaces with retained bacteria were also tested to determine percentage coverage of bacteria across the surfaces. Epifluorescence images were uploaded to ImageJ software and percentage coverage was calculated by manually adjusting the threshold to acquire a greyscale image of only visible bacterial cells. This was followed by percentage area measurements to evaluate total percentage coverage for both bacteria. This was repeated twice times per 2D-MoS₂ surface concentration and particle size.

2.22 Zones of inhibition

Bacterial and 2D-MoS₂ samples were prepared as in section (*Cultures and preparation*) One hundred microliters of prepared bacterial inoculum was pipetted onto Petri dishes containing TSA and spread across the agar. The plates were dried for 10 min before placing three separate sterilized 2D-MoS₂ surfaces, of the same concentration onto each plate. This was repeated for all particle sizes as well as each concentration of 2D-MoS₂. The plates were incubated at 37 °C for 24 h. Following incubation, the diameter of the zones of inhibition were measured across the diameter of whole clear zone and recorded using a 120 - millimetre ruler for each surface concertation (n = 3).

2.23 Crystal violet biofilm assay

A bacterial inoculum was prepared as described in section (*Cultures and preparation*) for both bacterial species, however the second broth re-suspension was done using TSB instead of saline. Using 70% ethanol each of the 2D-MoS₂ surfaces were sterilised for 10 min, then rinsed with sterile water and dried in a class II cabinet. A 12 well plate (Fisher Scientific, Loughborough) was used for each bacterium and 1 mL of inoculated broth was added to each well. Column four served as a negative control while rows 1-3 in columns 1-3 each had a surface of 2D-MoS₂ added. This was repeated until all the individual 2D-MoS₂ concentrations had been placed in wells for both bacteria. Following inoculation, the plates were wrapped in Parafilm (Fisher Scientific, Loughborough) and incubated at 37 °C for 24 h. After incubation, the broth containing bacteria was removed from the wells, leaving behind the 2D-

MoS₂ surface with attached biofilm. The surfaces were gently rinsed with sterile water at a 45 ° angle for five seconds, to avoid removing the attached biofilm. One millilitre of crystal violet (Prolab, UK) dye was added to each well and left to stand for 30 min before removing the crystal violet from the well and rinsing again with sterile water. Washing of the wells was repeating a further two times to ensure removal of all excess stain and loosely adhered cells. One millilitre of 33 % glacial acetic acid (Fisher Scientific, Loughborough) was added to each well and left to stand for a further 30 min. The optical densities of each well were measured by removing the glacial acetic acid from each well, placing into a cuvette and observing it at a wavelength of 540 nm, against a blank of 33 % glacial acetic acid (n = 3).

2.24 Bacterial growth curves

Bacterial cultures were grown and prepared as in section (*Cultures and Preparation*). One milliliter of OD 1.0 ± 0.1 bacterial inoculum of *S. aureus* or *P. aeruginosa* was added to each 100 mL of TSB. One milliliter of TSB was removed from each flask and its optical density measured and recorded for time point zero. A further 1 mL was used to determine the CFU / mL using serial dilutions. Time points were taken at 0, 1, 2, 3, 4, 5, 6, 7 and 24 h (n = 2) for each separate bacterium. During the production of the growth curves, samples were taken at each applicable time point for scanning electron microscope (SEM) imaging of bacterial damage after being in contact with the 2D-MoS₂ surfaces. Prior to imaging, the bacterial samples (10 µL) were fixed to 1 cm x 1 cm silicon wafers using 30 mL of 4.0 % glutaraldehyde solution (Agar Scientific, UK), after overnight submersion. The samples were dehydrated using an ethanol gradient and stored in a desiccator to dry. The silicon substrates, bearing the fixed and dried bacteria, were mounted on pin type aluminium SEM mounts (Agar Scientific, UK) with double-sided conducting carbon tape (Agar Scientific, UK). The samples were coated a 10 nm thick gold using a magnetron sputtering system and characterised using SEM (Zeiss Supra 40VP) at magnifications of 100,000 x, 50,000 x, 25,000 x and 10,000 x.

2.3 Renal human cell cytotoxicity

2.31 Immortalised renal human proximal tubular cell preparation

Immortalised renal human proximal tubular (HK-2) cells (ATCC (CRL-2190)) were defrosted from liquid nitrogen and were seeded into a sterile T25 flask, in growth media medium (1:1 of Dulbecco's modified eagle medium (DMEM): Ham's F-12 medium supplemented with 10% fetal bovine serum and penicillin/streptomycin; Life Technologies, UK). The flask was placed in an incubator at 37 °C in 5 % CO₂ and the cells were grown to 80 % confluence. The medium as refreshed every 48 h. Upon reaching the desired confluency the cells were rinsed with sterile phosphate buffered saline and trypsin solution (Life Technologies, 25200-056). Trypsin was used to detached the cell number in suspension was counted using a haemocytometer.

HK-2 cells were prepared as previously described in section (*renal human cell cytotoxicity*). Two 96 well plates (Thermo scientific, UK) were seeded with 5,000 HK-2 cells per well and both plates were incubated for 48 h at 37 °C in 5 % CO₂. Following incubation, the growth media was removed from each well via aspiration and was replaced with 200 µL of serum – free media (SFM) (DMEM: Ham's F-12 medium supplemented with penicillin/streptomycin) to growth-arrest the cells. The 96 well plates were incubated for 24 h at 37 °C in 5 % CO₂.

2.32 Immortalised renal human proximal tubular cell viability assay

Sterile 2D-MoS₂ surfaces and blank surfaces were inserted into two 96 well plates. Two hundred µL of SFM was added to each well and plated were incubated for 24 h and 48 h respectively at 37 °C in 5 % CO₂. After 24 h, 170 µL of SFM or media incubated with 2D-MoS₂ or blank surfaces were added to HK-2 cells in the 96 well plates, which were prepared in section (*Immortalised renal human proximal tubular cell preparation*). The plates were incubated for a further 23 h at 37 °C in 5 % CO₂. This was repeated for the 48 h plate after 48 h of incubation.

Following incubation for the 24 h or the 48 h plate, 9 µL of viability reagent (WST-8(2-(2-methoxy-4-nitrophenyl)-3-(4-nitrophenyl)-5-(2,4-disulfophenyl)-2H-tetrazolium, monosodium salt) (Sigma-Aldrich, UK) was added to each well containing HK-2 cells and absorbance was measured using a plate reader (Multiscan

Go – Thermo scientific, UK) at wavelengths of 450 nm and 650 nm at 24 h, 25 h and 26 h or 48 h, 49 h and 50 h (n = 3)

2.4 Statistical analysis

Statistical analysis was carried out using student *t*-tests. The results were reported as \pm standard error. The differences observed between samples were considered significant at $p < 0.05$.

Results - Surfaces

3.0 Scanning electron microscopy of 2D-MoS₂

Scanning electron microscopy (SEM) was carried out on sterile 2D-MoS₂ surfaces at MoS₂ particle sizes of 90 nm (figure 1), 2 μ m (figure 2) and 6 μ m (figure 3). Each SEM micrograph was taken at 100,000 x, 50,000 x, 25,000 x and 10,000 x and three replicates were taken per surface at different locations. Of these magnifications, 10,000 x was chosen for representation in these results, due to increased MoS₂ particle clarity. On the 2D-MoS₂ images each MoS₂ surface was observed to show a powder like coating, which was identified to be the binder used for fixing the MoS₂ particles together, preventing the surface from collapsing. The 2D-MoS₂ surfaces were in increasing concentrations of MoS₂ from 5 %, 10 %, 15 % and 20 %. Each 2D-MoS₂ surface (90 nm at 5 % - 20 %) demonstrated heterogeneous distribution of MoS₂ particles, and showed no trends with regards to increasing MoS₂ concentrations and the spread of MoS₂ particles across the surfaces. At increased particle sizes of 2 μ m and 6 μ m, the same heterogeneous trends were demonstrated by the 2D-MoS₂ surfaces. In summary, the increases in particle sizes did not affect the spread of the MoS₂ particles across the surfaces.

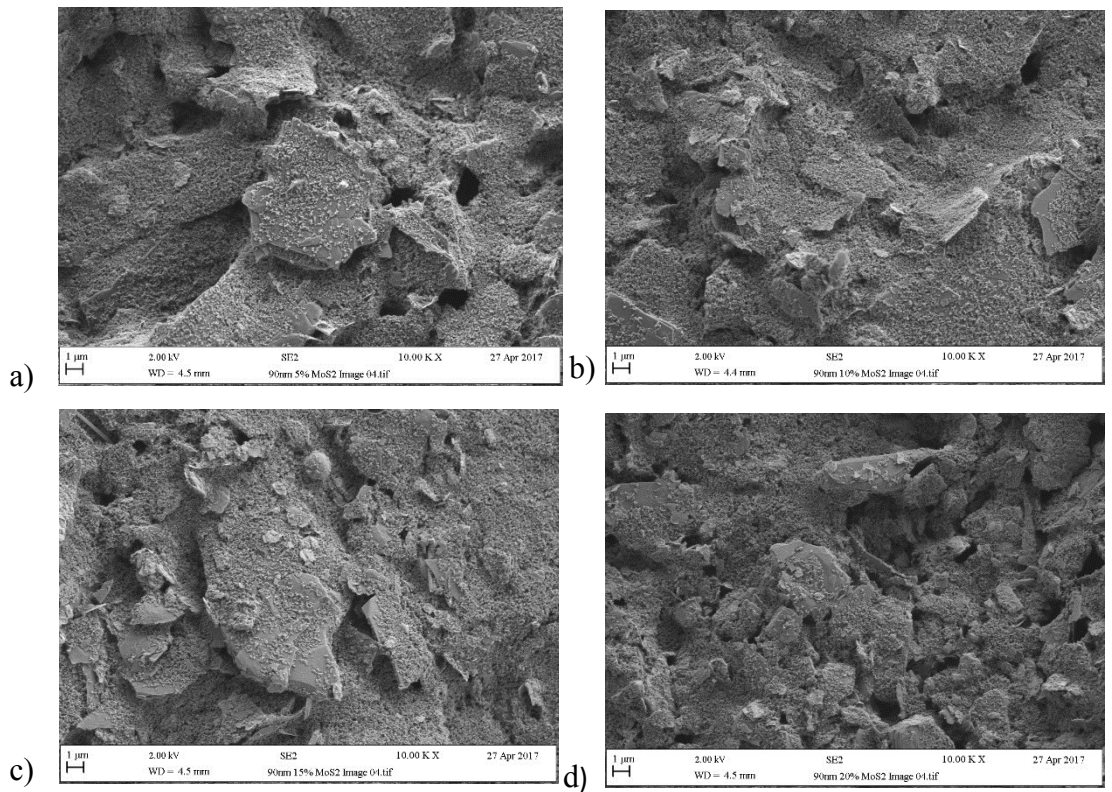


Figure 1. Scanning electron microscopy images of 90 nm 2D-MoS₂ surfaces at MoS₂ concentrations of a) 5 %, b) 10 %, c) 15 % and d) 20 % (n = 3)

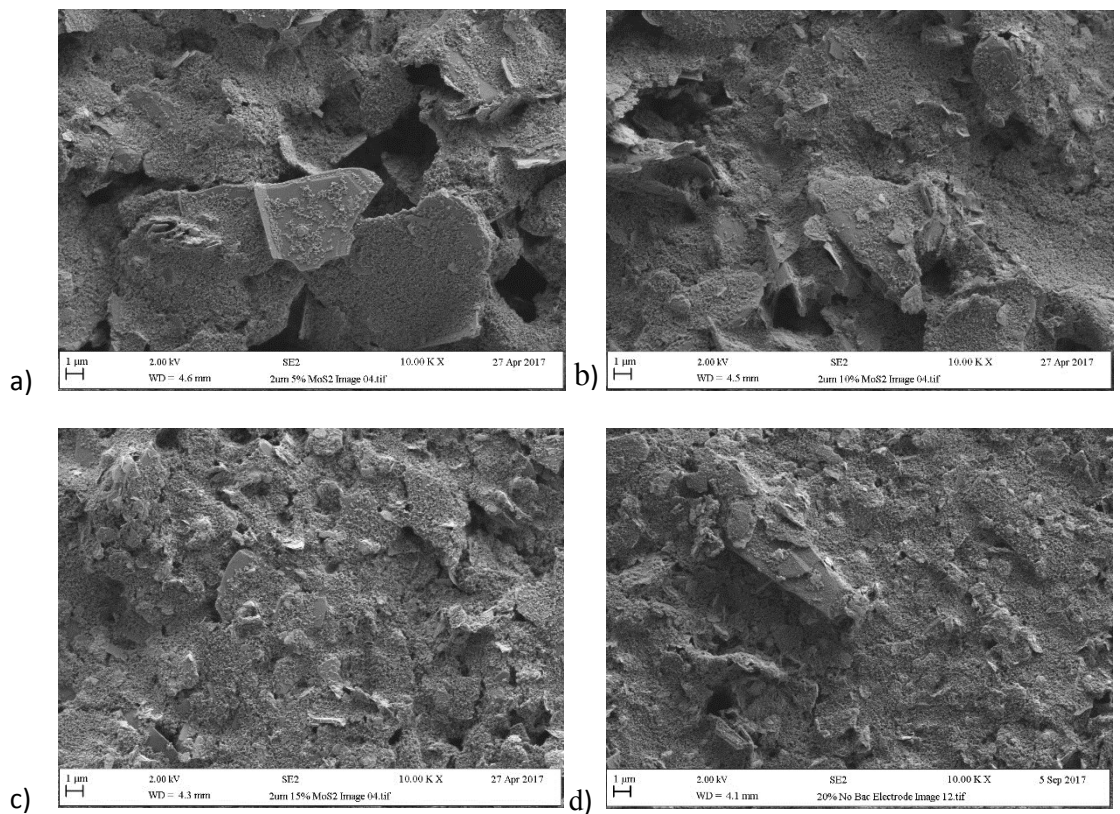


Figure 2. Scanning electron microscopy images of 2 μm 2D-MoS₂ surfaces at MoS₂ concentrations of a) 5 %, b) 10 %, c) 15 % and d) 20 % (n = 3)

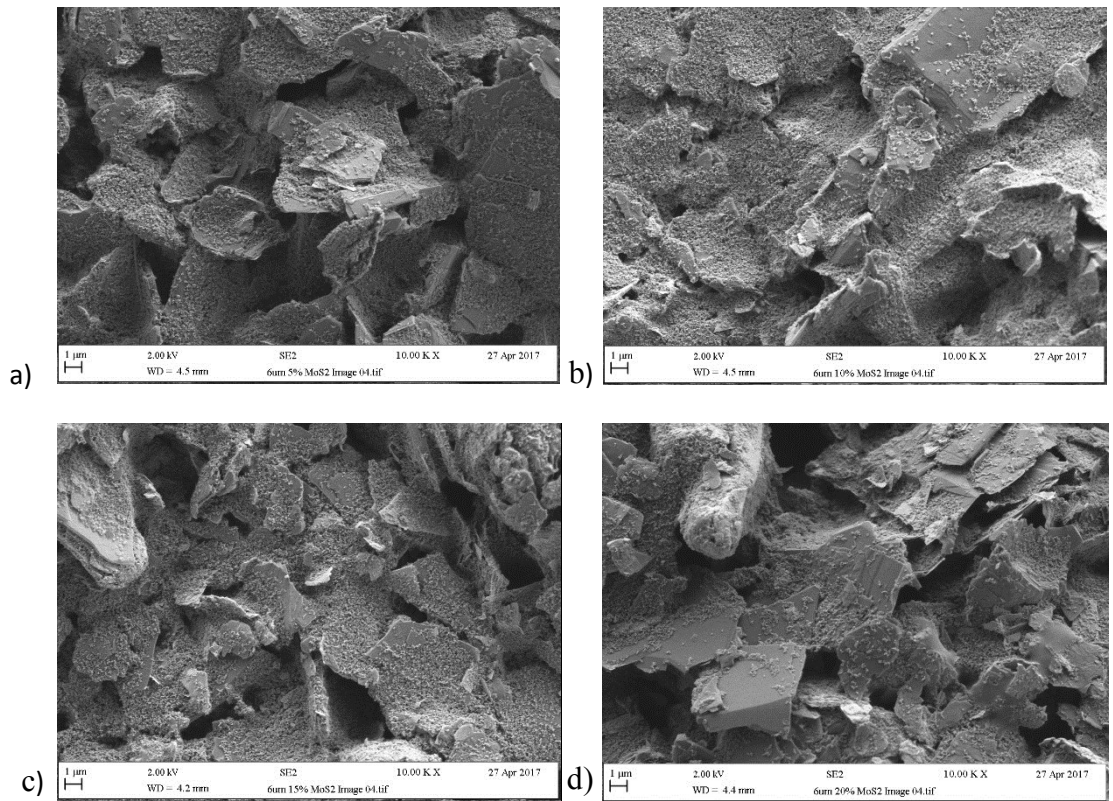


Figure 3. Scanning electron microscopy images of 6 μm 2D-MoS₂ surfaces at MoS₂ concentrations of a) 5 %, b) 10 %, c) 15 % and d) 20 % (n = 3)

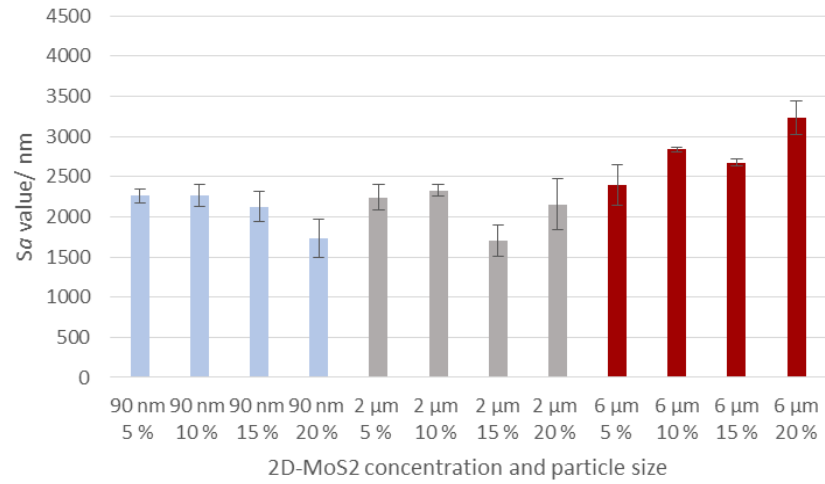
3.1 Roughness values

Surface roughness (S_a) was used to determine the roughness of the surfaces, and whether this would affect the surfaces ability to retain or inhibit the bacteria. S_a values were used to identify changes in surface roughness through different 2D-MoS₂ particle sizes and concentrations. S_q values were used to determine the mean square heights of the sample areas, and S_{pv} values were used to identify the average maximum height values for the 2D-MoS₂ surfaces and for each S value tested, three replicated were taken. The results demonstrated that on the 90 nm and 2 μm 2D-MoS₂ surfaces, the S_a and S_q values showed the same trends whereby the 5 %, 10 % and 15 % 90 nm and 5 %, 10 % and 20 % 2 μm surfaces demonstrated no significant differences in values. However, the 20 % 90 nm and 15% 2 μm 2D-MoS₂ surface values were lower (1729.5 nm and 1703.9 nm respectively). For the 2 μm 2D-MoS₂ surface, the same trends (reduction in all roughness values at 15 % MoS₂) were demonstrated for all the surfaces tested in terms of S_a , S_q and S_{pv} , and there was no significant difference ($p < 0.05$) between these values. The 2 μm 15 % 2D-MoS₂

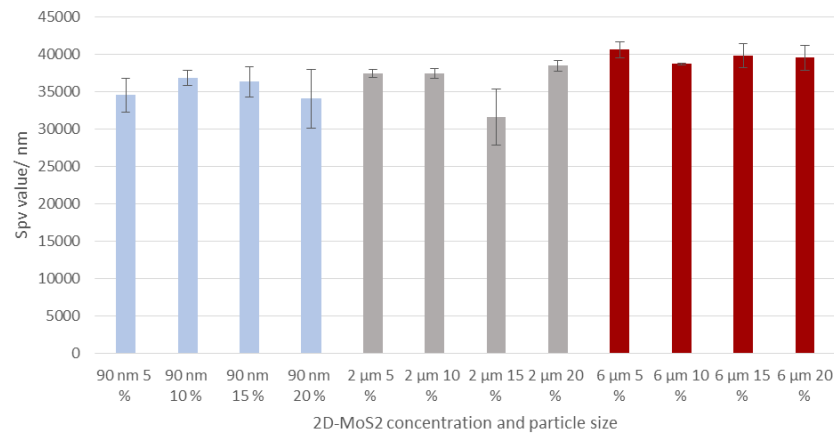
surface was lower in all the roughness variables tested (1703.933 nm for S_a , 2119.2 nm for S_q and S_{pv} of 31668.67 nm). However, no significant differences between the S_a , S_q and S_{pv} values for 2 μm at 15 % MoS_2 , and the 2 μm surfaces at 5 %, 10 % or 20 % was determined as a p value of greater than 0.05 was obtained. In addition, statistical analysis was carried out to analyse significant differences between particle sizes. It was demonstrated that there was no significant difference between the all the roughness values for 2D- MoS_2 surfaces at particle sizes 90 nm and 2 μm ($p < 0.05$).

For the 6 μm 2D- MoS_2 , an increase in S_a was demonstrated from 2397.4 - 3233.533 nm as concentrations of 2D- MoS_2 increased (5 % - 20 %). At 15 % 2D- MoS_2 for the 6 μm surface size, a decrease of 161.3 nm from the 6 μm 10 % 2D- MoS_2 surface was observed. This trend was the same for both the S_a and S_q values for the 6 μm surface. S_q values for 6 μm 2D- MoS_2 showed no trends in relation to the S_a or S_{pv} values. Trends were identified in both S_a and S_q values for 90 nm and 6 μm 2D- MoS_2 surfaces. Statistical tests were performed between S_a , S_q and S_{pv} values, and a significant difference between 90 nm and 6 μm 2D- MoS_2 surfaces was observed (p values of 0.02, 0.01 and 0.001 respectively).

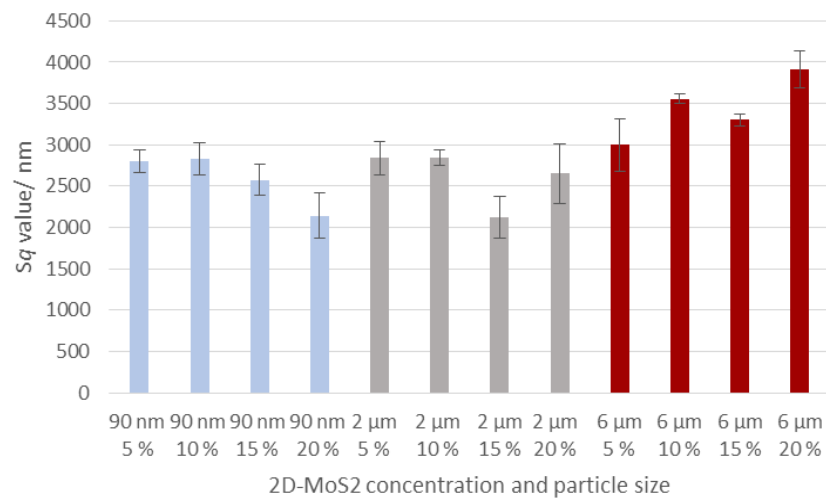
There were no significant differences between the S_{pv} values of 2 μm and 6 μm 2D- MoS_2 ($p = 0.08$). This was different from both the S_a and S_q values between the 90 nm and 2 μm surfaces as a significant difference was observed in both. Overall trends between the 90 nm and 6 μm surfaces were similar, with both having different S_{pv} values. The 2 μm 2D- MoS_2 surface had similar trends throughout each roughness value. Overall, both 90 nm and 2 μm had similar trends across all roughness values tested and 6 μm demonstrated similar trends with regards to S_a and S_q values, but different trends when measuring S_{pv} values.



a)



b)



c)

Figure 4. a) Average surface roughness (S_a) values b) Surface mean square roughness values (S_q) and c) Average maximum height of 2D-MoS₂ surfaces (S_{pv}) with 2D-MoS₂ at increasing molybdenum concentrations of 5 %, 10 %, 15 % and 20 % ($n = 3$).

3.2 Roughness profiles

The roughness profiles of 90 nm 2D-MoS₂ at increasing concentrations from 5 % – 20 % were taken (Figure 5). The 5 % (a) and 10 % (b) 2D-MoS₂ line profiles demonstrated rounded peaks that were larger for 5 % 2D-MoS₂ than 10 % 2D-MoS₂ (51.78- 10.55 nm and 40.94- 9.08 nm respectively), and curved valleys. The 5 % and 10 % 2D-MoS₂ surfaces were rounded in shape, with an almost hill like structure, but which contained many smaller rounded peaks across their surface (0.004 - 0.01 nm and 0.003- 0.04 nm respectively). There was no significant difference demonstrated by the largest peak heights however, a significant difference was identified between the smallest peaks between 90 nm 5 % and 10 % 2D-MoS₂. The widths of the peaks and valleys followed a different trend, 5 % 2D-MoS₂ demonstrated smaller sized widths (83.39 – 10.22 nm) than 10 % 2D-MoS₂ (129.58 – 12.26). Statistical analysis tests were performed on the width sizes and a significant difference between 5 % and 10 % 2D-MoS₂ was observed ($p < 0.0007$). As MoS₂ concentrations of 90 nm 2D-MoS₂ increased, the peak heights of the surfaces increased, with exceptions to the 10 % surface. At higher concentrations, more nanofeatures on the surfaces became prominent (Figure 2d). The shape of the surface was more compact with a single hump presenting many nanofactors. The 20 % 2D-MoS₂ surface's peaks were larger than previous concentrations (67.77 – 9.23 nm) in height, but widths were smaller than both 10 and 15 % 2D-MoS₂ surfaces at an average width of 88.71 nm.

Both 5 % (a) and 20 % (d) 2 μ m 2D-MoS₂ surfaces (Figure 6) demonstrated the same trend with regards to the surface shape. They presented a distinct hump with small peaks across the hump's surface from 71.04 – 8.2 and 47.86 – 8.50 nm respectively in size. These peaks were not as sharp as the nanofactors identified in Figure 2d. Average peak heights across on all the 2 μ m 2D-MoS₂ surfaces demonstrated a trend as surface MoS₂ concentration increased (27.46 -16.70 nm, from 5% to 20 %). It was observed that there was no significant difference between the average surface widths and MoS₂ concentration ($p < 0.15$). Compared to the 90 nm 2D-MoS₂ surfaces, the 2 μ m surfaces demonstrated a trend in that all the surfaces showed less distinct factors across the surface, resulting in flatter line profiles.

The 6 μm 2D-MoS₂ surfaces, demonstrated an increasing trend of average peak height as concentrations of MoS₂ per surface increased, with the exception of 10 % 6 μm 2D-MoS₂, which was significantly different to 5 %, 15 % and 20 % 6 μm 2D-MoS₂. Peak height increased from 774.23 – 1133.77 from 5 % to 20 % 6 μm respectively. This trend was demonstrated in both largest and smallest widths, where an increase in size from 5% to 20 % was observed. The shape of the 5 % (Figure 7a) and 20 % (Figure 7d) surfaces followed a similar trend in that they both demonstrated large hills with flat valleys. The largest widths identified from these two surfaces were the largest amongst the 6 μm 2D-MoS₂ surfaces (134.08 and 142.26 nm respectively) however, there was no significant difference between the values. The smallest widths were also the largest measured within the 6 μm surface category at 13.49 nm and 13.90 nm with no significant difference between them at a *p* value of 0.68.

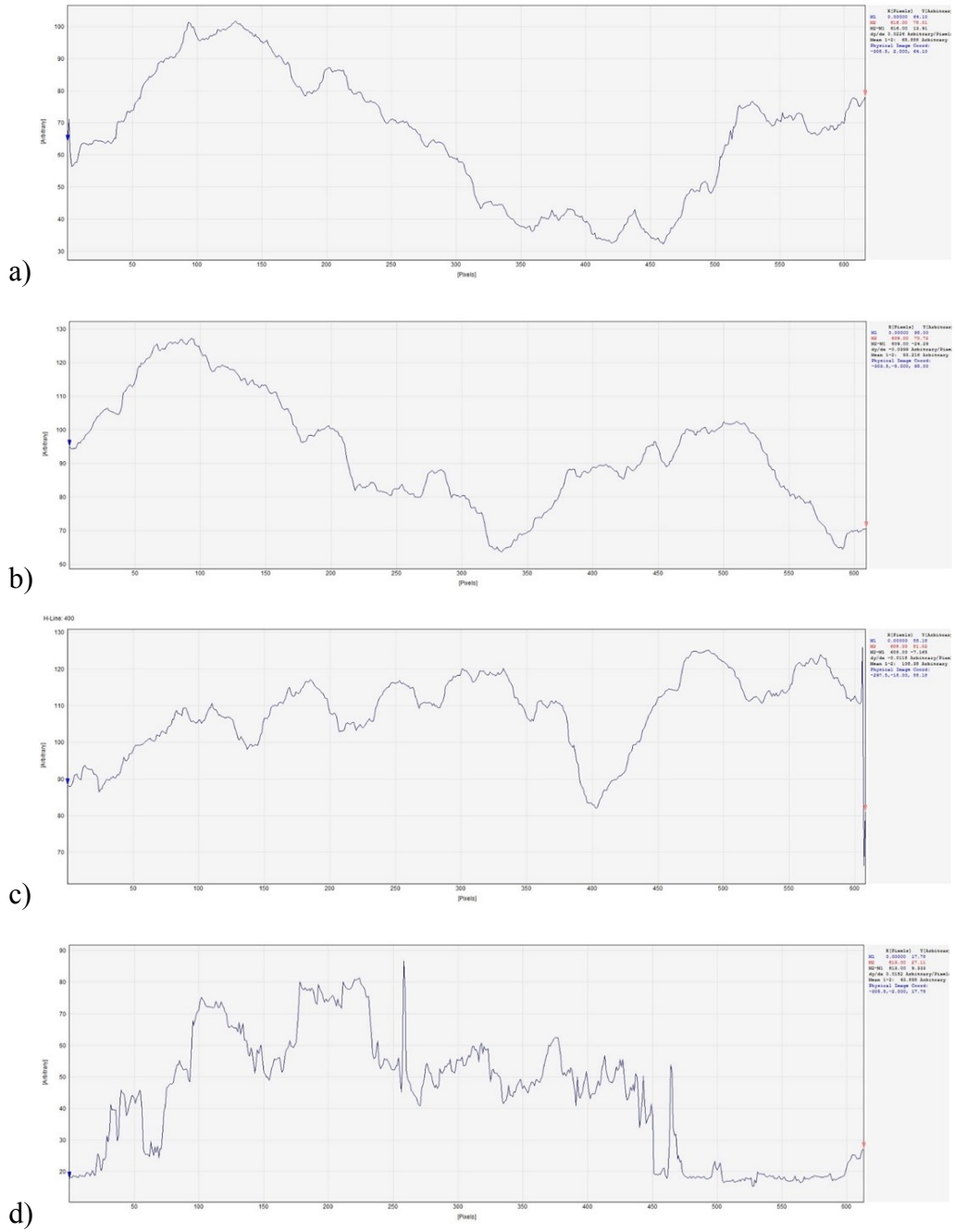


Figure 5. Line profiles taken using white light profilometry, of 90 nm 2D-MoS₂ surfaces at concentrations of a) 5 %, b) 10 %, c) 15 % and d) 20 % (n = 3).

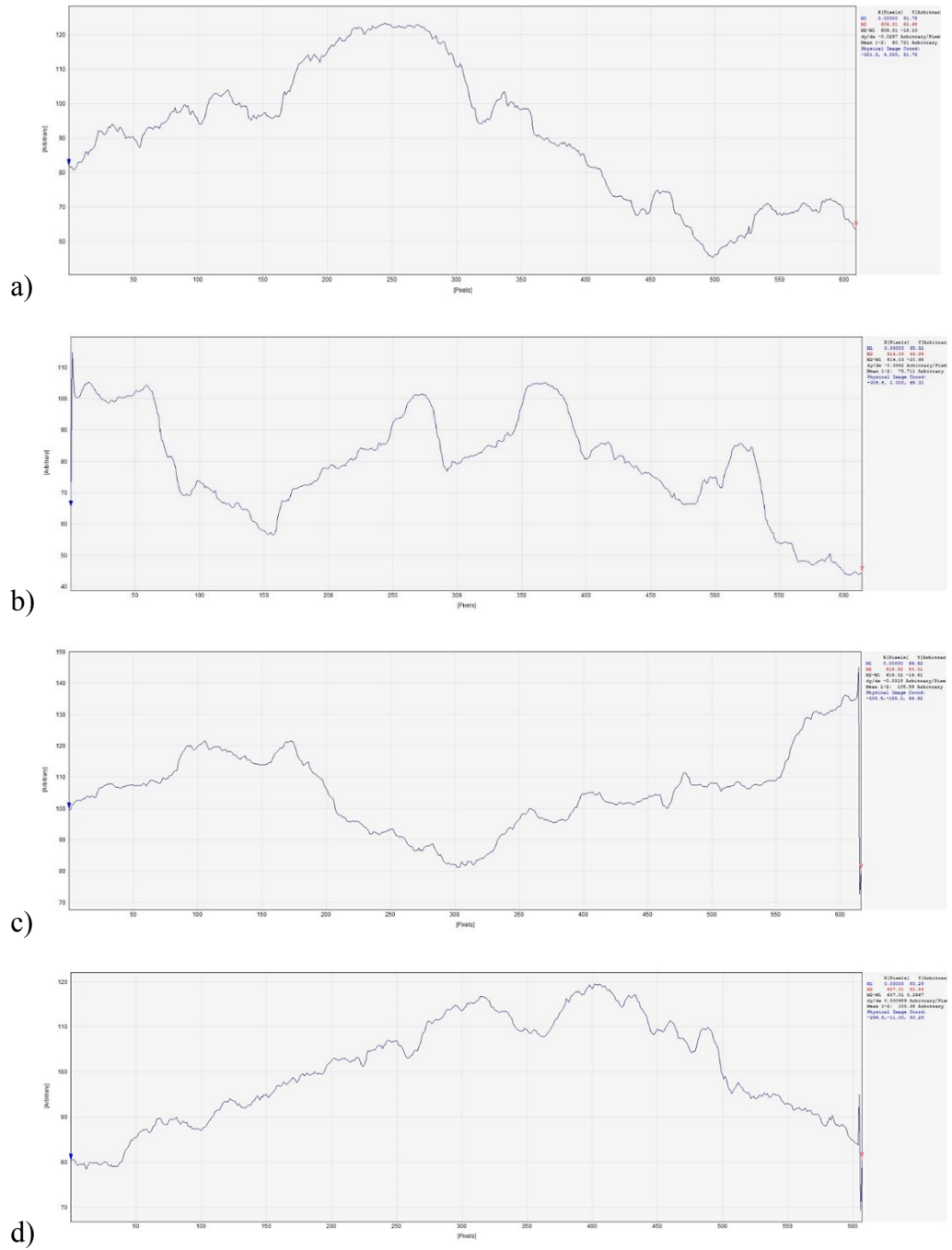


Figure 6. Line profiles taken using white light profilometry, of 2 µm 2D-MoS₂ surfaces at concentrations of a) 5 %, b) 10 %, c) 15 % and d) 20 % (n = 3).

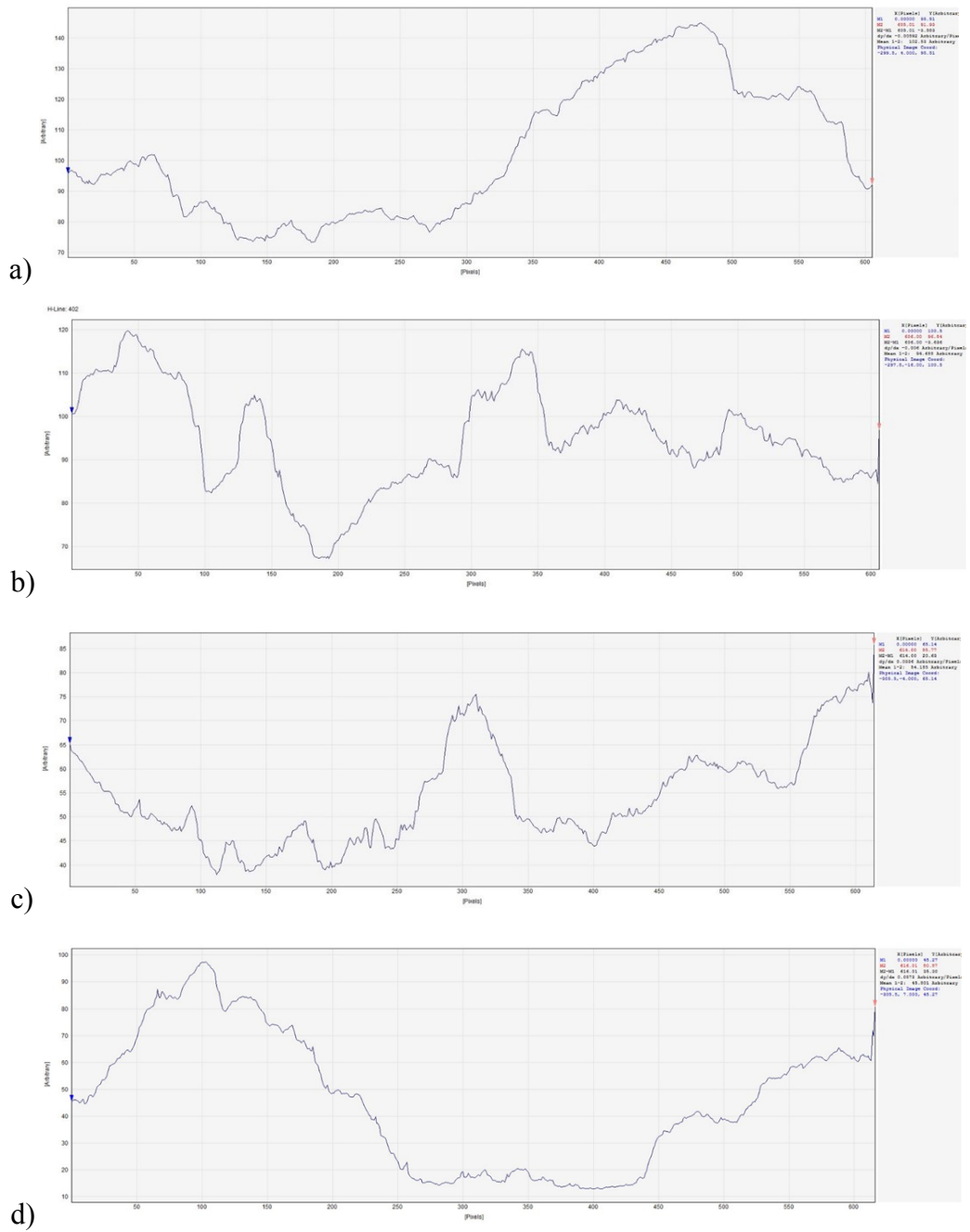


Figure 7. Line profiles taken using white light profilometry, of 6 μm 2D-MoS₂ surfaces at concentrations of a) 5 %, b) 10 %, c) 15 % and d) 20 % (n = 3).

Table 1. Average peak and valley heights across 2D-MoS₂ surfaces with increasing particle size and concentration (n = 10).

Surface Particle size and MoS₂ concentration	Largest peak/ nm	Smallest peak/ nm	Largest width/ nm	Smallest width/ nm
90 nm- 5 %	22.81	0.01	83.39	10.22
90 nm- 10 %	17.17	0.02	129.58	12.26
90 nm- 15 %	23.41	0.01	105.87	10.22
90 nm- 20 %	34.05	0.01	88.71	11.04
2 μm- 5 %	27.46	0.01	89.52	10.22
2 μm- 10 %	17.74	0.01	121.41	12.26
2 μm- 15 %	16.53	0.02	114.92	10.34
2 μm- 20 %	16.7	0.02	109.14	12.26
6 μm- 5 %	774.23	0.64	134.08	13.49
6 μm- 10 %	18.97	0.01	104.65	12.26
6 μm -15 %	1097.14	0.36	123.04	13.08
6 μm- 20 %	1133.77	0.21	142.26	13.9

3.2 Leaching of ions using inductively coupled plasma atomic emission spectroscopy

Elemental analysis using ICP-AES, of 2D-MoS₂ surfaces at particle sizes of 90 nm, 2 μm and 6 μm was carried out. Leaching of the 2D-MoS₂ surfaces was performed over 24 h, to determine the amount of molybdenum (Figure 8) or sulphur (Figure 9) that leached into the surrounding solution. An increase in MoS₂ ions as 2D-MoS₂ surface concentration increased was observed for 90 nm, 2 μm and 6 μm (0.0020 - 0.0042, 0.0016 - 0.0089 and 0.0019- 0.0039 respectively) however, no significant difference between 2D-MoS₂ particle size or molybdenum concentration per surface, and the number of molybdenum ions leached into the surrounding solution was shown. A decrease in molybdenum ion concentration was demonstrated at 90 nm 20 % 2D-MoS₂ (0.0042), however this was statistically insignificant from the other values. It should be noted that the rate of molybdenum ion leached was very low and at the limit of detection for the ICP-AES, and thus may be considered negligible. Since the key element of the 2D-MoS₂ surfaces was molybdenum, sulphur remained at a constant concentration throughout each 2D-MoS₂ particle size. The same trend was demonstrated throughout, with the exception of 2 μm at 15 % which was not significantly different from the other concentrations. 6 μm demonstrated the lowest levels of leaching through all molybdenum concentrations. Overall there was no significant difference between surface particle size and concentration against the volume of leached molybdenum or sulphur ions.

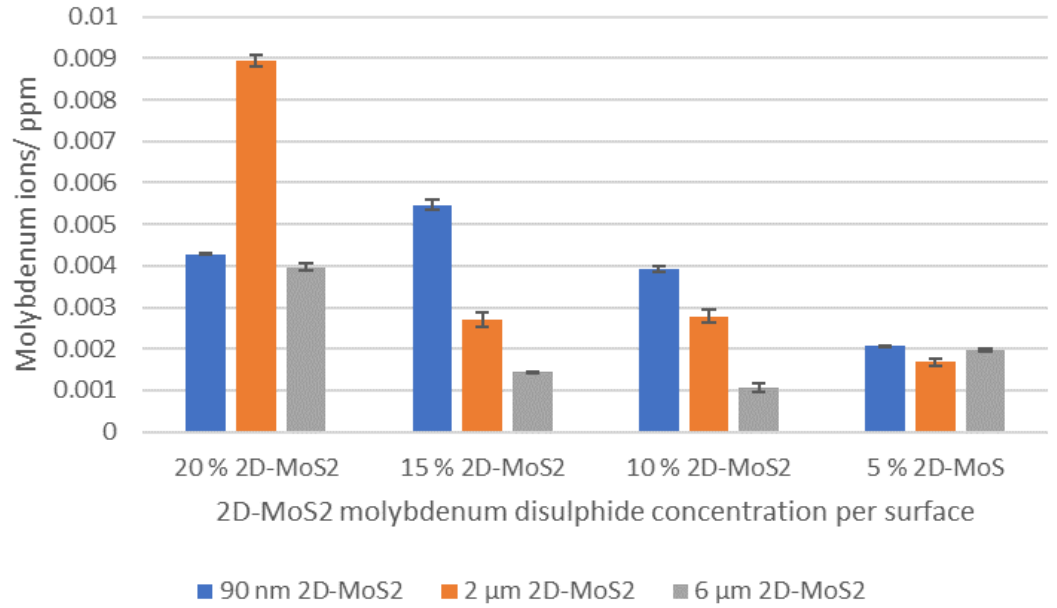


Figure 8. Mass spectrometry used for the detection of trace volumes of molybdenum from an aqueous solution of sterile distilled water and 2D-MoS₂. Note y axis scale max = 0.01ppm (n = 3)

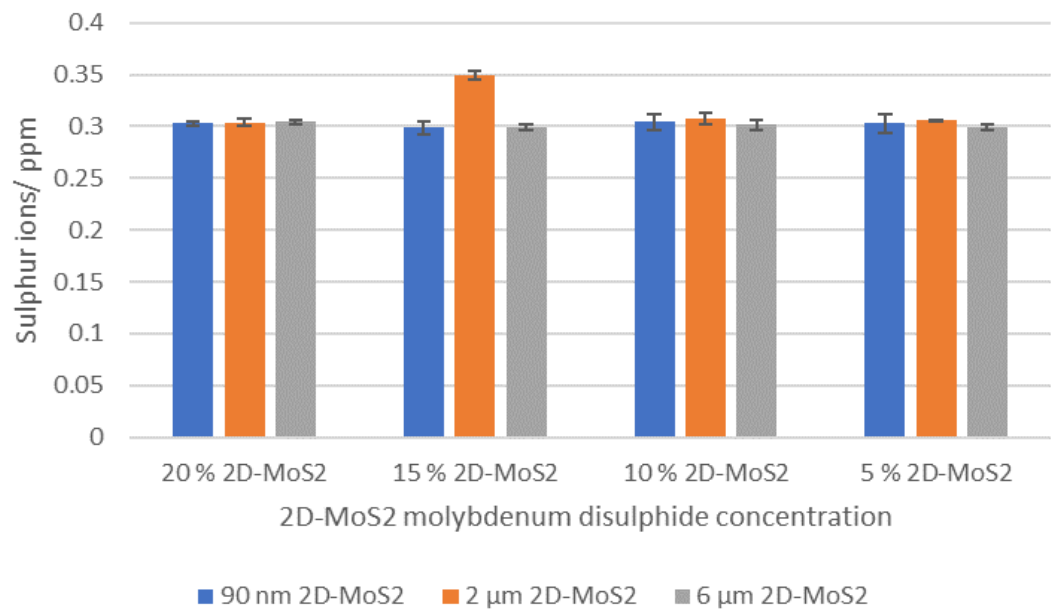


Figure 9. Average sulphur concentration measurements taken from leached MoS₂ into sterilised distilled water, detected using mass spectrometry. Note y axis scale max = 0.4ppm (n = 3)

Surface retention

3.3 Retention of *Staphylococcus aureus*

Epifluorescent microscopy was used to determine the retention of *S. aureus* on 2D-MoS₂ surfaces of particle sizes 90 nm, and 2 and 6 μm. *S. aureus* was adhered to the surfaces using retention assays. Qualitative analysis of the results demonstrated heterogeneous distribution of bacteria on the 5 % 2D-MoS₂ surface (Figure 10a), whilst the remaining 10 %, 15 % and 20 % 2D-MoS₂ surfaces from the 90 nm 2D-MoS₂ surfaces demonstrated a homogenous spread of bacteria (Figure 10b, c and d). Images of the 90 nm 2D-MoS₂ surfaces demonstrated the same trend as 2 μm 2D-MoS₂, with 5 % 2D-MoS₂ surface again (Figure. 11a) presenting a heterogeneous distribution of bacteria and the 10 %, 15 % and 20 % 2D-MoS₂ surfaces (Figure 11b, c and d) demonstrating homogenous distributions. The 6 μm 2D-MoS₂ demonstrated a heterogeneous distribution for each MoS₂ surface concentration (5 %, 10 %, 15 % and 20 %) (Figure 12 a-d).

For quantitative analysis, percentage coverage of the 2D-MoS₂ surfaces was carried out with both *S. aureus* and *P. aeruginosa*. For 90 nm 2D-MoS₂, no trend was demonstrated between the percentage of *S. aureus* coverage and the concentration of MoS₂ per surface. It was observed however, that the 90 nm 2D-MoS₂ surfaces in Figure 13, showed an opposite trend to the S_{pv} values (Figure 4b).

With the 2 μm 2D-MoS₂ particle size, a decreasing trend in the percentage coverage of bacteria occurred, as MoS₂ surface concentration increased (26.5 % - 7.72 % respectively), with the exception of 20 % 2D-MoS₂ (22.88 %). There were no trends demonstrated between these percentage coverage values and the roughness values.

S. aureus on the 6 μm 2D-MoS₂ demonstrated an increasing trend with increased surface concentration from 5 % to 15 % (7.03 % - 28.32 % respectively), with the exception of the 20 % MoS₂ surface which demonstrated a much smaller volume of coverage at 8.14 %. Like the 2 μm 2D-MoS₂ surfaces, no trends were demonstrated between percentage coverage of the surfaces and roughness values. Statistical tests demonstrated no significant difference between the 90 nm, 2 μm and 6 μm and the percentage coverage of *S. aureus* on all of the 2D-MoS₂ surfaces. Overall, an increase in particle size caused an increase in heterogeneity across the surfaces. This also

allowed the increased retention of *S. aureus* bacteria as the surfaces became more heterogeneous.

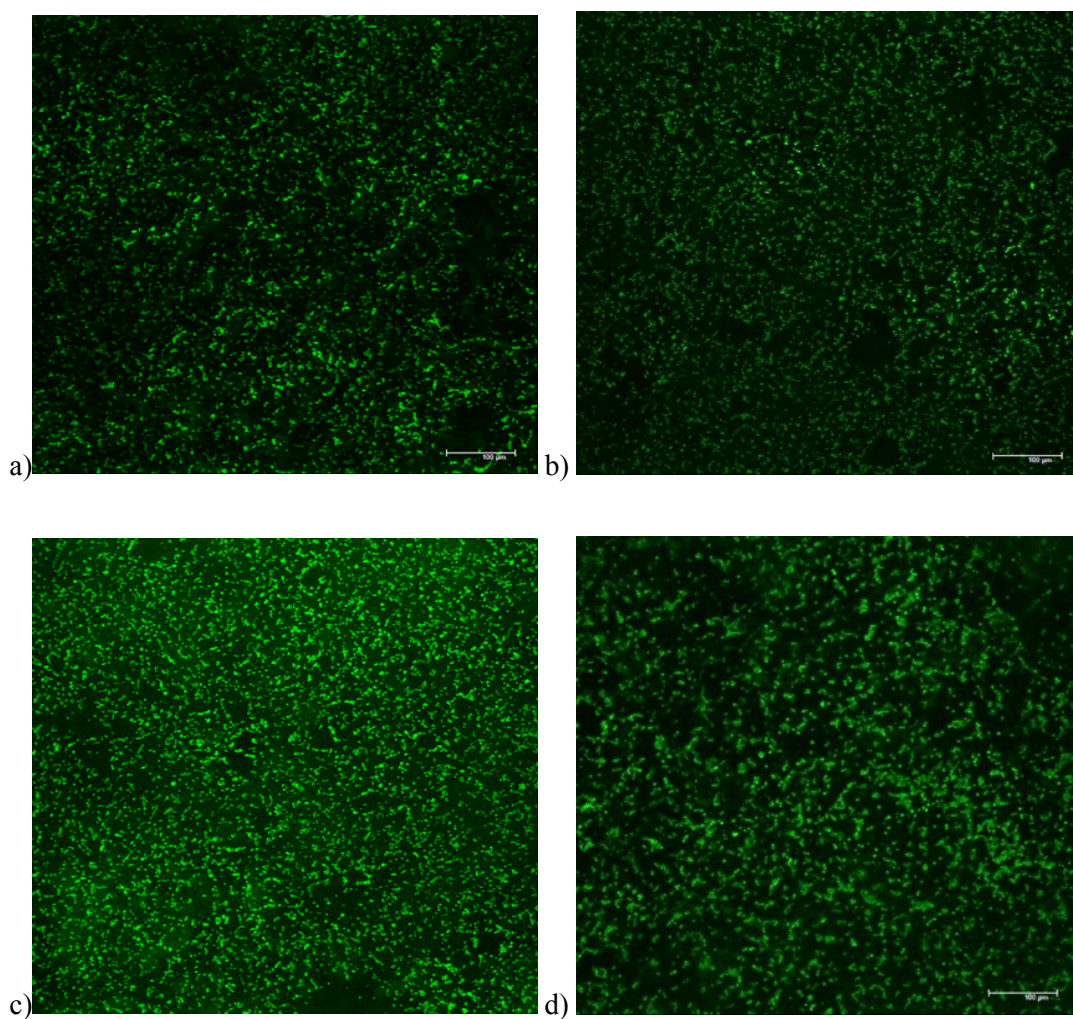


Figure 10. Epifluorescence images demonstrating the retention of *S. aureus* on 90 nm 2D-MoS₂ surfaces at concentration of a) 5 %, b) 10 %, c) 15 % and d) 20 % MoS₂ (n = 3)

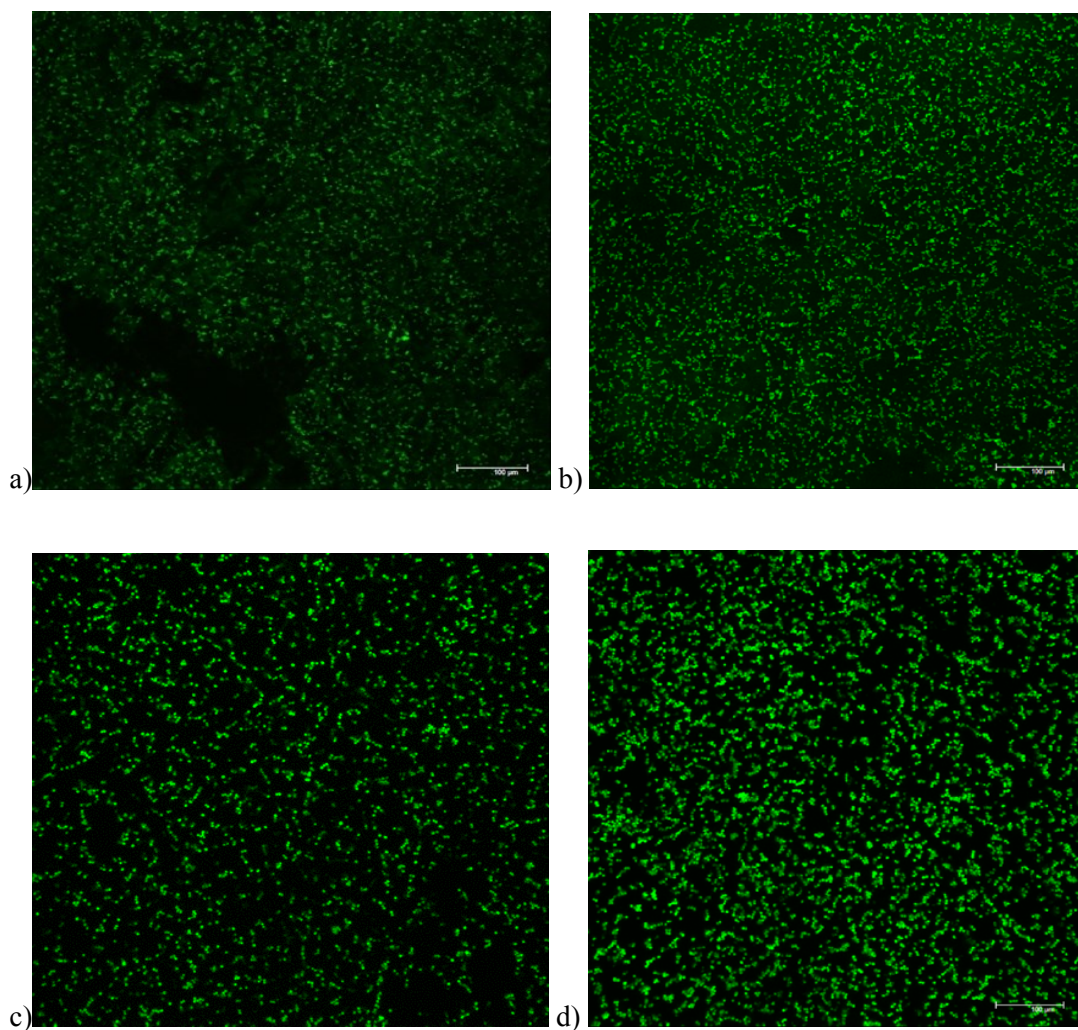


Figure 11. Epifluorescence images demonstrating the retention of *S. aureus* on 2 μm 2D-MoS₂ surfaces at concentration of a) 5 %, b) 10 %, c) 15 % and d) 20 % MoS₂ (n = 3)

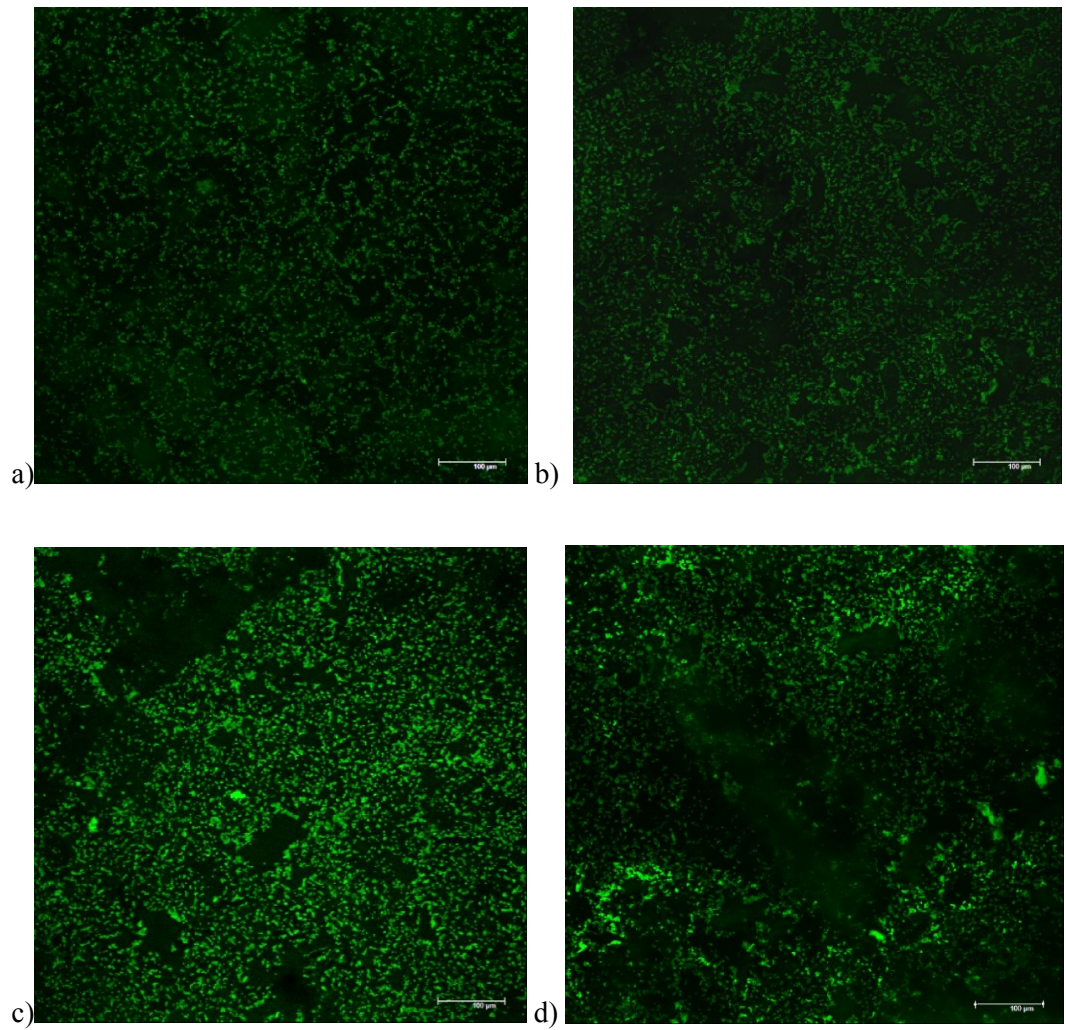


Figure 12. Epifluorescence images demonstrating the retention of *S. aureus* on 6 μm 2D-MoS₂ surfaces at concentration of a) 5 %, b) 10 %, c) 15 % and d) 20 % MoS₂ (n = 3).

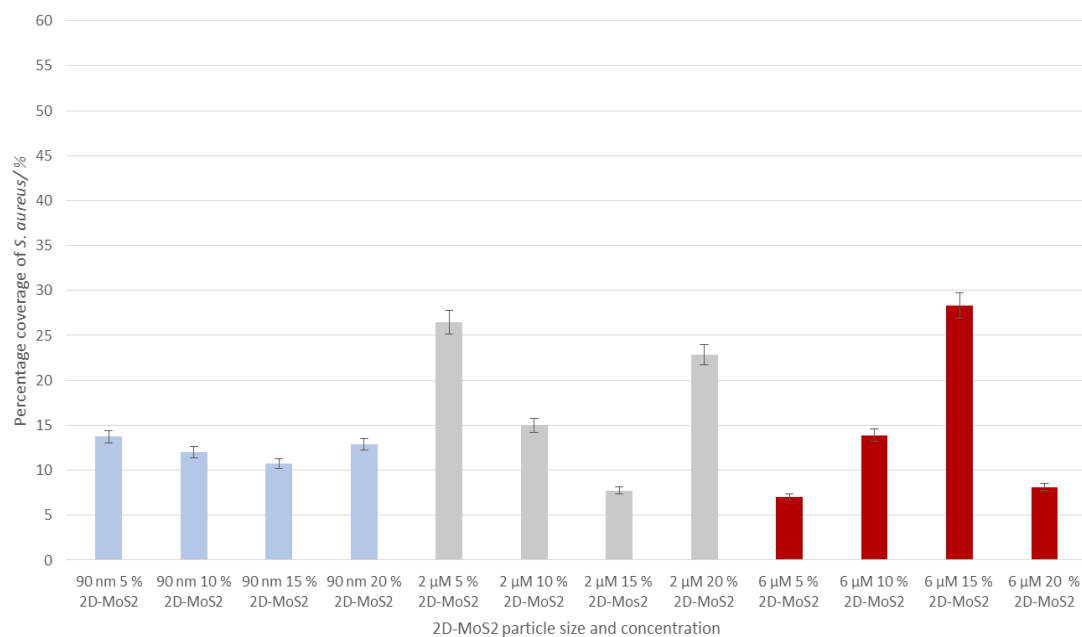


Figure 13. Percentage coverage of *S. aureus* on 90 nm, 2 μm and 6 μm 2D-MoS₂ surfaces at increasing concentrations of MoS₂ (n = 2)

3.31 Retention of *Pseudomonas aeruginosa*

P. aeruginosa was retained on 90 nm, 2 μm and 6 μm 2D-MoS₂ surfaces and analysed using epifluorescent microscopy to qualitatively identify the trends in *P. aeruginosa* distribution and quantitative analysis was used to measure the percentage coverage of *P. aeruginosa* on the surfaces. Five percent (Figure 14a) and 15 % 2D-MoS₂ (Figure 14c) at a 90 nm particle size demonstrated heterogeneous distribution of *P. aeruginosa* across the surfaces. Both 10 % (Figure 14b) and 20 % (Figure 14d) 90 nm 2D-MoS₂ showed homogenous distribution on the surfaces.

Heterogeneous distribution was demonstrated primarily by the 2 μm 2D-MoS₂ surface on the surfaces at concentrations of 5 %, 10 % and 20 % (Figure 15 a, b and d). The 15 % 2D-MoS₂ surface (Figure 15c) however, demonstrated homogenous distribution of *P. aeruginosa*.

For each surface concentration at 6 μm 2D-MoS₂ particle size, heterogeneous distribution of *P. aeruginosa* was demonstrated. This was also previously demonstrated where heterogeneous distribution of *S. aureus* was observed at all 6 μm 2D-MoS₂ surfaces concentrations (Figure 16).

The percent coverage for *P. aeruginosa* on 90 nm 2D-MoS₂ (Figure 17) demonstrated an increase in bacterial coverage of the 90 nm 2D-MoS₂ surface, as MoS₂ concentrations increased from 5 % to 15 % (34.40 % - 50.90 % respectively), with the exception of the 20 % surface which demonstrated a lower *P. aeruginosa* coverage than all previous concentrations at 26.54 %. This trend was similarly demonstrated by the S_q values for 90 nm 2D-MoS₂ when identifying surface roughness.

The 2D-MoS₂ surfaces at a particle size of 2 μm demonstrated an increasing trend of percent surface coverage as the concentrations of MoS₂ per surface increased, from 5 % to 20 % (13.04 % - 39.94 % respectively). There was however, no trend demonstrated between percentage coverage and surface roughness values (Figure 4).

Percentage coverage of *P. aeruginosa* on the 6 μm 2D-MoS₂ demonstrated a decreasing trend of bacterial coverage from 10 % to 20 % (38.59 % - 23.55 % respectively) with the exception of 5 %. No trends between percentage coverage and surface roughness were demonstrated.

Statistical tests demonstrated no significant differences between both 2 μm and 6 μm 2D₂ and bacterial coverage however, on the 90 nm 2D-MoS₂ there was demonstrated a significant difference between *S. aureus* and *P. aeruginosa* ($p = 0.002$) percentage coverage. In summary, as particle sizes of MoS₂ increased, as did the heterogeneity of the bacterial distribution on the surface.

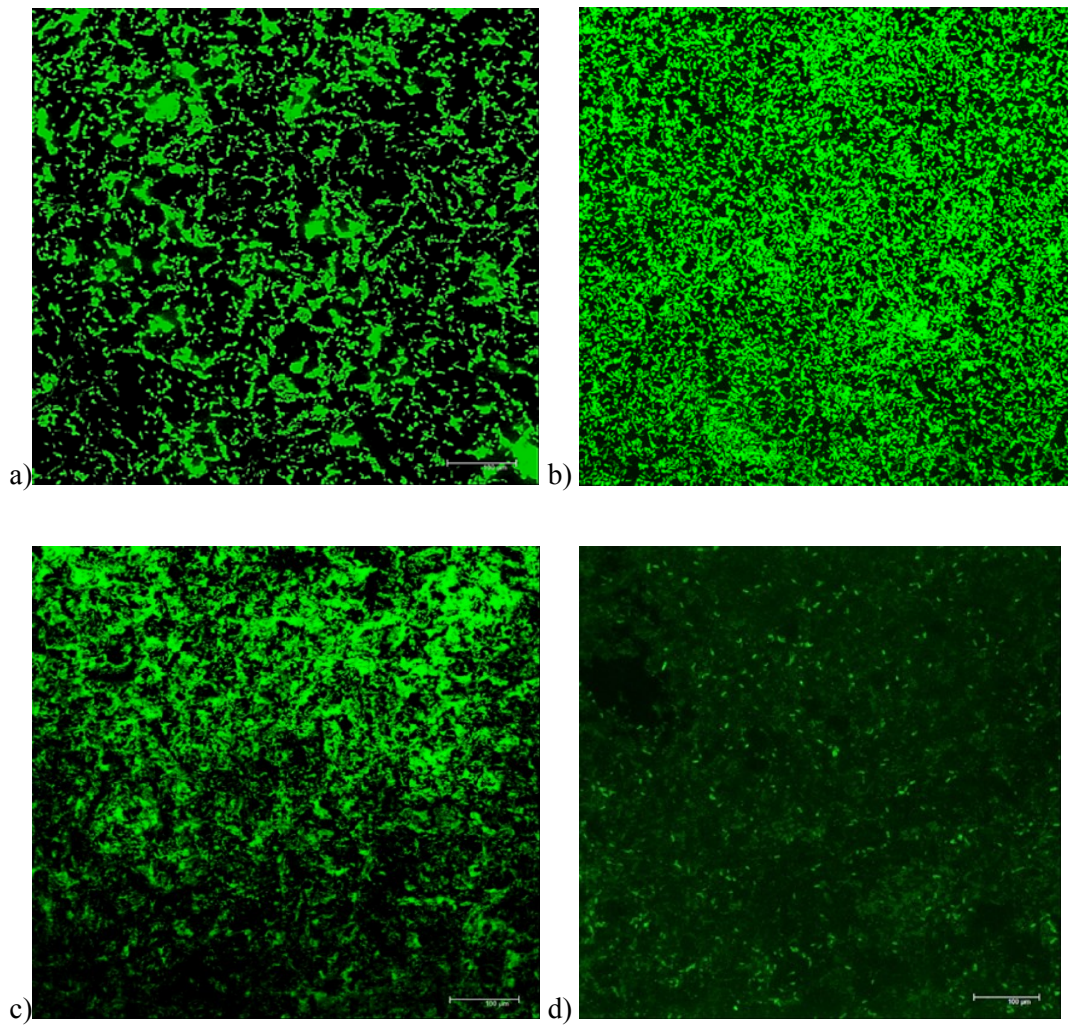


Figure 14. Epifluorescence images demonstrating the retention of *P. aeruginosa* on 90 nm 2D-MoS₂ surfaces at concentrations of a) 5 %, b) 10 %, c) 15 % and d) 20 % MoS₂ (n = 3)

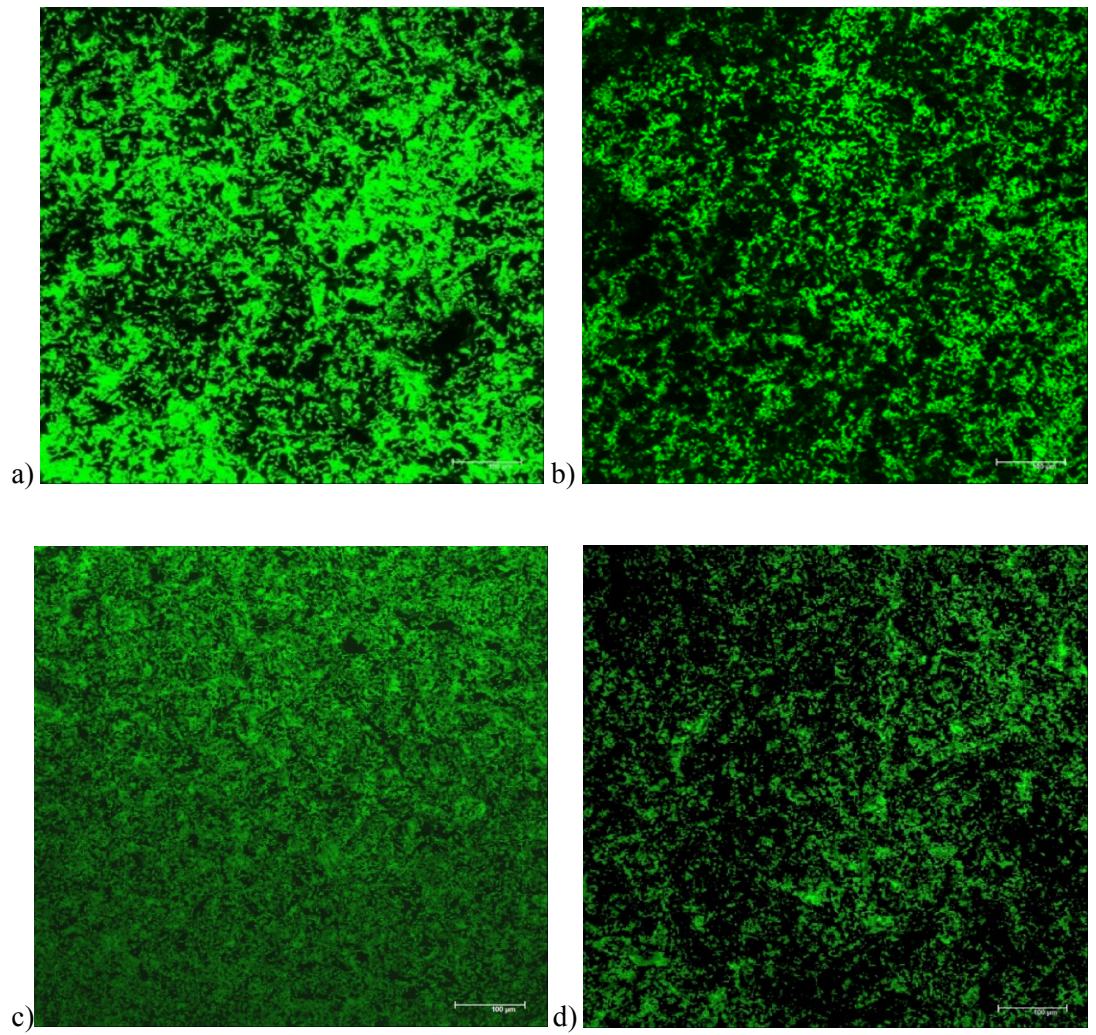


Figure 15. Epifluorescence images demonstrating the retention of *P. aeruginosa* on 2 μm 2D-MoS₂ surfaces at concentrations of a) 5 %, b) 10 %, c) 15 % and d) 20 % MoS₂ (n = 3)

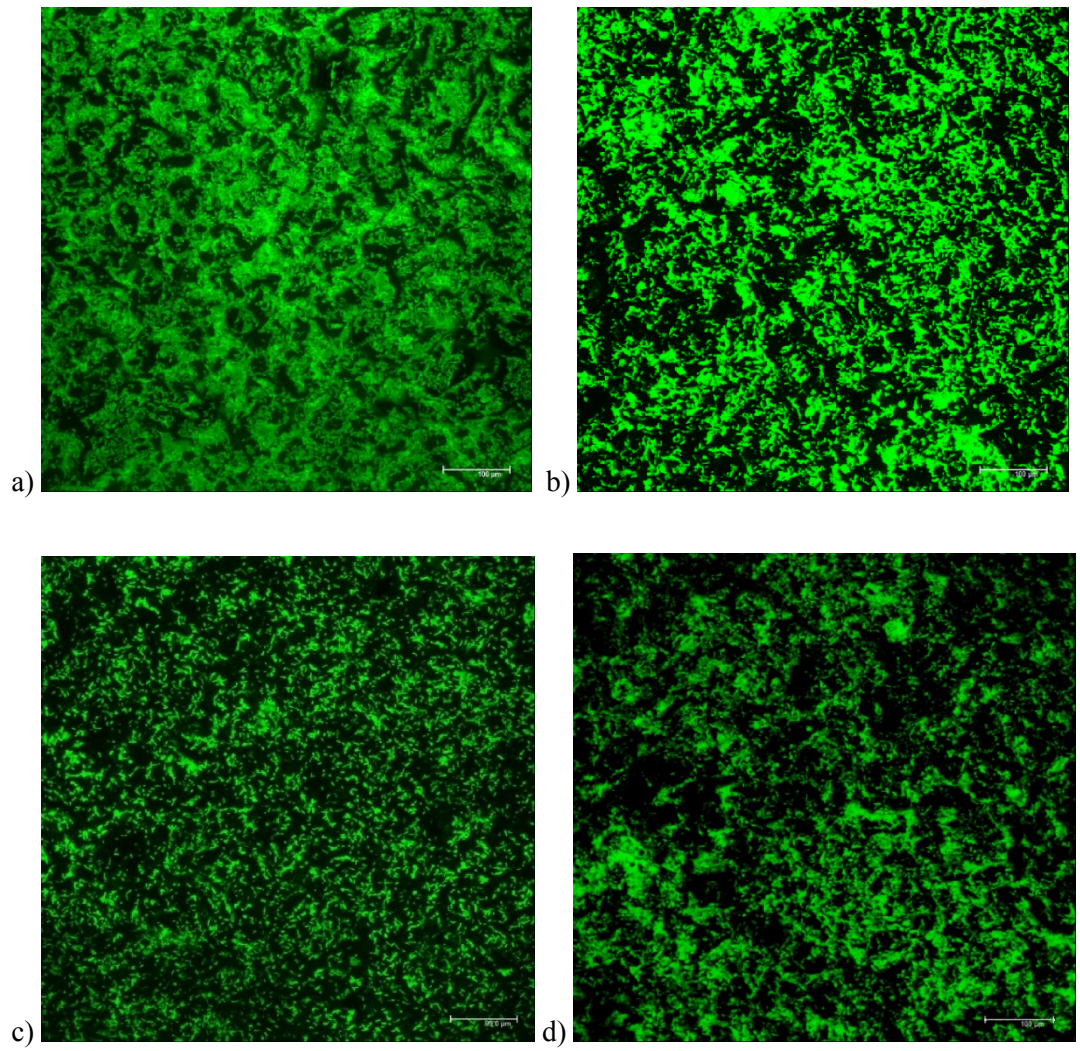


Figure 16. Epifluorescence images describing the retention of *P. aeruginosa* on 6 μm 2D-MoS₂ surfaces at concentrations of a) 5 %, b) 10 %, c) 15 % and d) 20 % MoS₂ (n = 6)

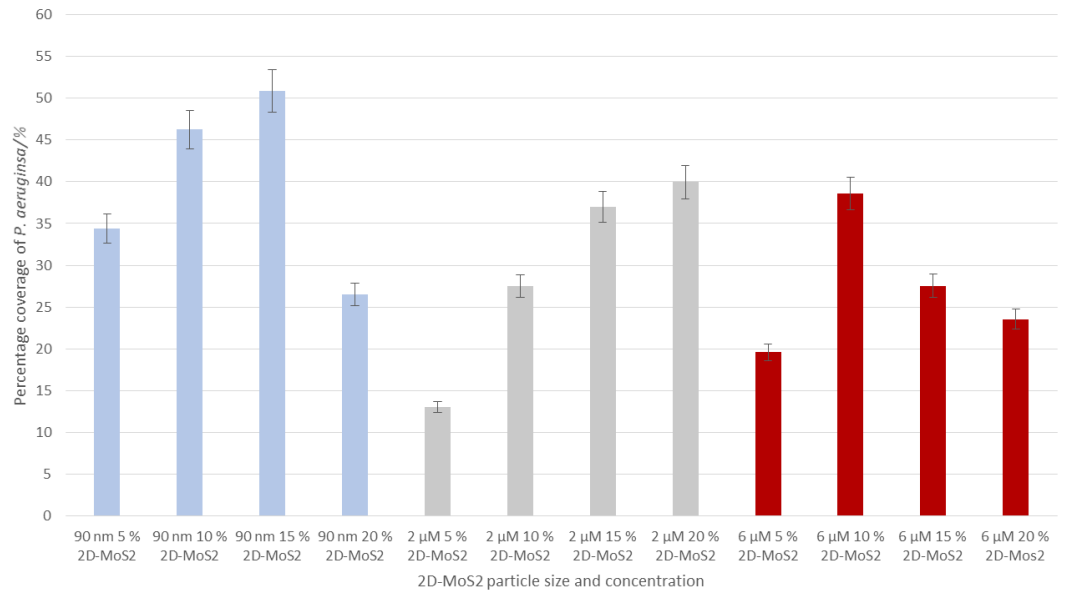


Figure 17. Percentage coverage of *P. aeruginosa* on 90 nm, 2 μm and 6 μm 2D-MoS₂ surfaces at increasing concentrations of MoS₂ (n = 2)

Antimicrobial effects of 2D-MoS₂

3.4 Zones of inhibition

Zones of inhibition were carried out to identify whether the 2D-MoS₂ surfaces would inhibit bacteria growth by metal ions leaching through the agar. The results demonstrated 0 mm zones of inhibition for both *S. aureus* and *P. aeruginosa*, for all surfaces concentrations of 5 %, 10 %, 15 % and 20 % 2D-MoS₂ surfaces. This suggested that no antimicrobial activity was demonstrated due to leaching of MoS₂ through the agar.

3.41 Crystal violet biofilm assay

Crystal violet biofilms assays were carried out identify whether 2D-MoS₂ surfaces would have an effect on bacteria within a biofilm, as oppose to their planktonic state. Assays were carried out over a 24 h period and the results showed a trend in the decrease in optical densities as concentrations of MoS₂ in the surfaces increased, for both *S. aureus* and *P. aeruginosa* (1.27 – 0.93 and 1.53 – 1.033 respectively) (Figure 19). However, statistical analysis showed no significant differences between *S. aureus* control and samples that had been treated with 2D-MoS₂. The same tests were carried out for *P. aeruginosa* and once again, no significant differences between the *P. aeruginosa* controls and MoS₂ treated samples were shown. There was also no significant differences in biofilm growth between *S. aureus* and *P. aeruginosa* at any of the surfaces concentrations tested.

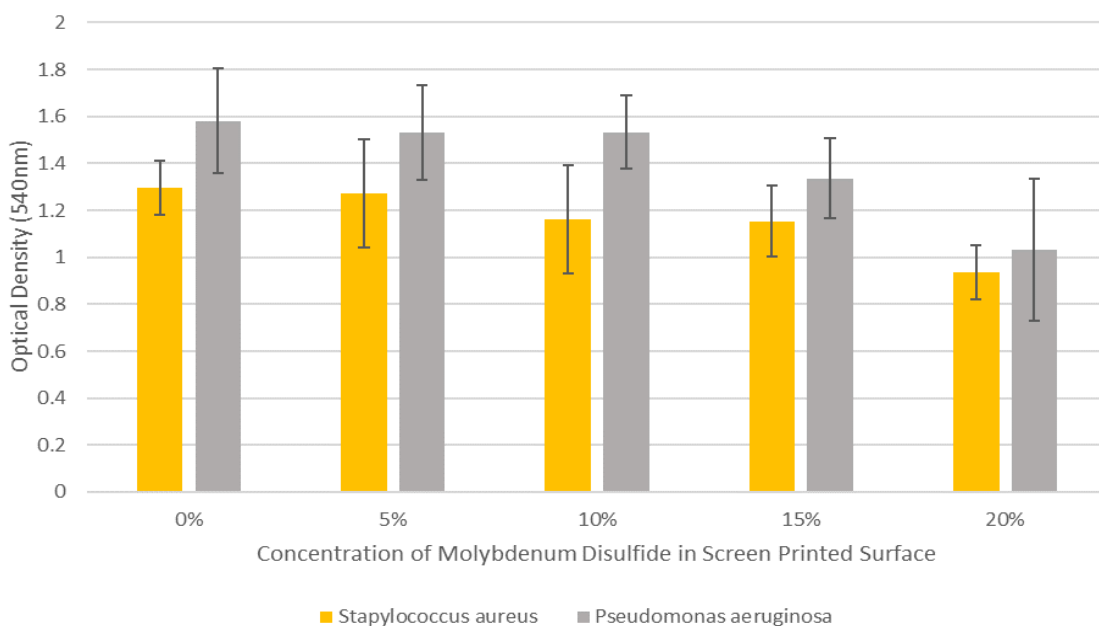


Figure 19. Average optical density reading of *S. aureus* and *P. aeruginosa* against 2D-MoS₂ at increasing concentrations of MoS₂ (5 %, 10 %, 15 % and 20 %) (n = 3)

3.42 Growth Curve of *Staphylococcus aureus*

Growth curves were carried out with *S. aureus* to identify whether 2D-MoS₂ surfaces reduced bacterial growth over a period of 24 h (Figure 20a). Control growth curves were carried out initially, to provide a baseline to which comparison of colony forming units could be made. Control growth curves for *S. aureus* demonstrated an increase in colony forming units from 2.41×10^6 at 0 h, to 3.40×10^9 at 24h. When the surfaces contained a surface particle size of 90 nm, the results showed an increase in colony forming units from 0 h to 24 h. This trend was demonstrated for all four (5 %, 10 %, 15 % and 20 %) 90 nm 2D-MoS₂ concentrations. 90 nm 2D-MoS₂ surface at 20 % MoS₂ demonstrated the smallest colony forming units increase over 24 h, demonstrating the strongest antimicrobial efficacy amongst the 90 nm particle size, due to decreased bacterial growth (2.34×10^6 - 7.58×10^8). However, statistical analysis showed no significant differences were demonstrated between the colony forming unit values of all the 90 nm 2D-MoS₂ concentrations, and the controls; with the exception of 90 nm 20 % at 4 h, where a *p* value of 0.005 was obtained. In

summary, the 90 nm 2D-MoS₂ surfaces demonstrated some antimicrobial effects towards *S. aureus*, however these results were not significant overall.

In agreement, both the 2 μm (Figure 20b) and 6 μm 2D-MoS₂ surfaces (Figure 20c), demonstrated the same trend as seen with the 90 nm particle size 2D-MoS₂ surfaces with regards to an increase in colony forming units over 24 h. Compared to the 90 nm and 6 μm surfaces, the 2 μm 2D-MoS₂ demonstrated the most reduced colony forming units at each MoS₂ concentration, equating to the most effective antimicrobial surface towards *S. aureus*. The individual MoS₂ concentrations were also not as closely distributed as the other colony forming unit curves. At 5 % 2D-MoS₂ a decrease at all time points was demonstrated (3.83×10^5 - 1.97×10^9), however, only at time points 0 h, 4 h and 6 h were significant differences from the controls observed. This was different from 10 %, 15 % and 20 %, where all three surfaces concentrations demonstrated significant differences from the controls at each time point, with the exception of hours 2 h, 3 h and 24 h. Statistical tests were carried out to identify if differences observed in the values of the lowest (5 %) and highest (20 %) concentrations were statistically significant. Significant differences were demonstrated at 0 h, 5 h, 6 h and 7 h at 2 μm 2D-MoS₂ particle size compared to the controls, demonstrating a significant antimicrobial effect from the 2 μm surface.

The results on the 6 μm 2D-MoS₂ demonstrated a reduction in colony forming units at 20 % MoS₂ (1.39×10^5 - 5.33×10^8) compared to the control for *S. aureus*. This was a much larger decrease in colony forming units than any of the lower MoS₂ concentrations (5 %, 10 % and 15 %). Overall, a greater reduction in colony forming units was demonstrated by 6 μm 2D-MoS₂, than the 90 nm surface, but was not as effective as on the 2 μm 2D-MoS₂ surface. Overall, each separate 6 μm 2D-MoS₂ surface demonstrated no significant differences between MoS₂ concentrations (5 %, 10 %, 15 % and 20 %) and the control. However, under each individual time point, 10 % 2D-MoS₂ showed significant differences from the control at 5 h and 6 h and 15 % 6 μm 2D-MoS₂ demonstrated significant differences at 0, 4 and 5 h. Unlike the previous concentrations, 6 μm 2D-MoS₂ at a 20 % MoS₂ concentration demonstrated significant differences at a greater number of time points. Hours 0, 1, 4, 5, 6 and 7 all demonstrated significant differences from the control. Overall, 6 μm 2D-MoS₂ surfaces at 20 % MoS₂ demonstrated significant antimicrobial activity towards *S.*

aureus whereas, lower concentration of MoS₂ demonstrated no significant antimicrobial affects.

Comparisons were made between the 90nm, 2 µm and 6 µm 2D-MoS₂ at each individual MoS₂ concentration (5 %, 10 %, 15 %, and 20 %), and no significant difference between the 2D-MoS₂ particle size and concentration affecting the colony forming values was observed. In summary, the 20 % MoS₂ surfaces demonstrated the greatest antimicrobial efficacy towards *S. aureus* and the 2 µm 2D-MoS₂ surfaces showed the largest decrease in *S. aureus* growth, however this difference was not significant between the 90 nm and 6 µm particle sizes.

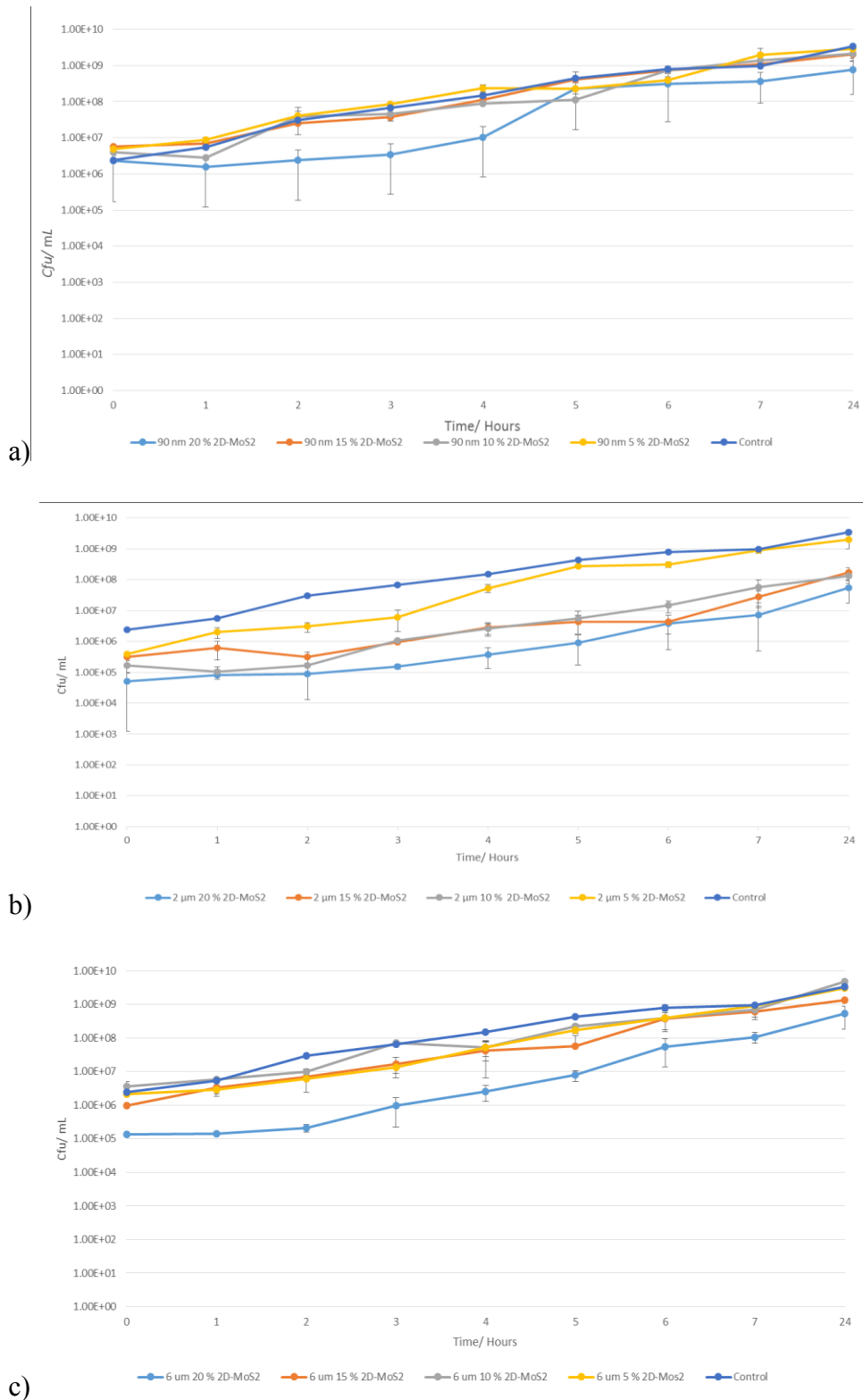


Figure 20. Average colony forming units of *S. aureus* over 24 h growth curves, tested against a) 90 nm, b) 2 μm and c) 6 μm 2D-MoS₂ particle sized surfaces, at concentrations of 5 %, 10 %, 15 % and 20 % MoS₂ (n = 2)

3.43 Growth curve of *Pseudomonas aeruginosa*

Growth curves for *P. aeruginosa* were carried out with 90 nm, 2 μm and 6 μm 2D-MoS₂ surfaces at increasing concentrations of MoS₂ (5%, 10 %, 15 % and 20 %) (Figure 21). Controls showed an increase in colony forming units from 4.95×10^6 to 8.40×10^9 (0 h – 24 h respectively). The results showed an increase in colony forming units of *P. aeruginosa* at 90 nm 2D-MoS₂ (Figure 21a). The trend was continued for all four MoS₂ concentrations however, the values were often similar to the controls at every time point. For example, at 6 h, 15 % 2D-MoS₂ colony forming units were at 1.71×10^8 , whereas the control showed a value of 2.02×10^8 , resulting in no distinct, antimicrobial MoS₂ concentration at the 90 nm particle size. There were no significant differences between colony forming units of *P. aeruginosa* at 90 nm 2D-MoS₂, at any of the four MoS₂ concentrations and the control surface. 90 nm 2D-MoS₂ demonstrated little to no antimicrobial effect towards *P. aeruginosa* for all the MoS₂ surface concentrations.

A reduction in colony forming units at all four, 2 μm 2D-MoS₂ surface concentrations was observed which suggested an increased antimicrobial activity against *P. aeruginosa* compared to 90 nm and 6 μm 2D-MoS₂ surfaces (Figure 21b). The largest decrease in colony forming units was demonstrated by 20 % MoS₂ at 1.70×10^4 - 3.67×10^8 , from hours 0 through to 24 respectively. Moreover, both 10 % and 15 % MoS₂ showed larger reductions in colony forming units than 90 nm at the same concentrations (1.85×10^5 - 1.90×10^9 and 1.46×10^5 - 1.74×10^9 respectively). While initially, demonstrating increased antimicrobial activity against *P. aeruginosa*, 5 % MoS₂ at time points of 5 h and onwards showed an increased colony forming units, thus demonstrating a lower antimicrobial efficacy. Furthermore, at 20 % 2D-MoS₂, only at 1 h, 5 h and 24 h was there a significant difference from the control shown. At 15 % 2D-MoS₂, only at hours 5 and 24, was there a significant difference shown and the remaining MoS₂ concentrations (5 % and 10 %) demonstrated no significant difference between their colony forming units and the control. Overall, 2 μm 2D-MoS₂ at 20 % MoS₂ surface demonstrated the greatest antimicrobial activity towards *P. aeruginosa* however, the antimicrobial efficacy was lower than that towards *S. aureus*.

For the 6 μm 2D-MoS₂ surface, there was no clear indication to the most effective antimicrobial surface (Figure 21c). However, a trend of increasing colony forming units as time increased was demonstrated for each 6 μm 2D-MoS₂ surface concentration of 5 %, 10 %, 15 % and 20 % (4.95×10^6 - 4.15×10^9 , 2.11×10^6 - 3.21×10^9 , 2.03×10^6 - 4.59×10^9 and 2.41×10^6 - 4.13×10^9 respectively). There were no significant differences between 5 %, 10 %, 15 % and 20 % 6 μm 2D-MoS₂ and the controls in terms of colony forming units, with the exception of hour 1 at 20 % and hour 5 at 15 % MoS₂ ($p = 0.03$ and 0.04 respectively) showing a significant difference at these time points. Significant levels between 2D-MoS₂ particle sizes at the same MoS₂ concentrations demonstrated no significant differences between the colony forming units of *P. aeruginosa* observed, and the controls. In addition, it was observed that there were no significant differences between 90 nm, 2 μm and 6 μm 2D-MoS₂ at each of their respective MoS₂ concentrations, and their effect on colony forming units between *S. aureus* and *P. aeruginosa*.

In summary, 20 % 2D-MoS₂ demonstrated the greatest antimicrobial efficacy towards both *S. aureus* and *P. aeruginosa* in all the microbiological assays used. Of these concentrations, the 2 μm surface showed the largest antimicrobial effect towards both bacteria, more significantly so towards *S. aureus* and 90 nm particle sized demonstrated the lowest antimicrobial efficacy towards *S. aureus* and *P. aeruginosa*.

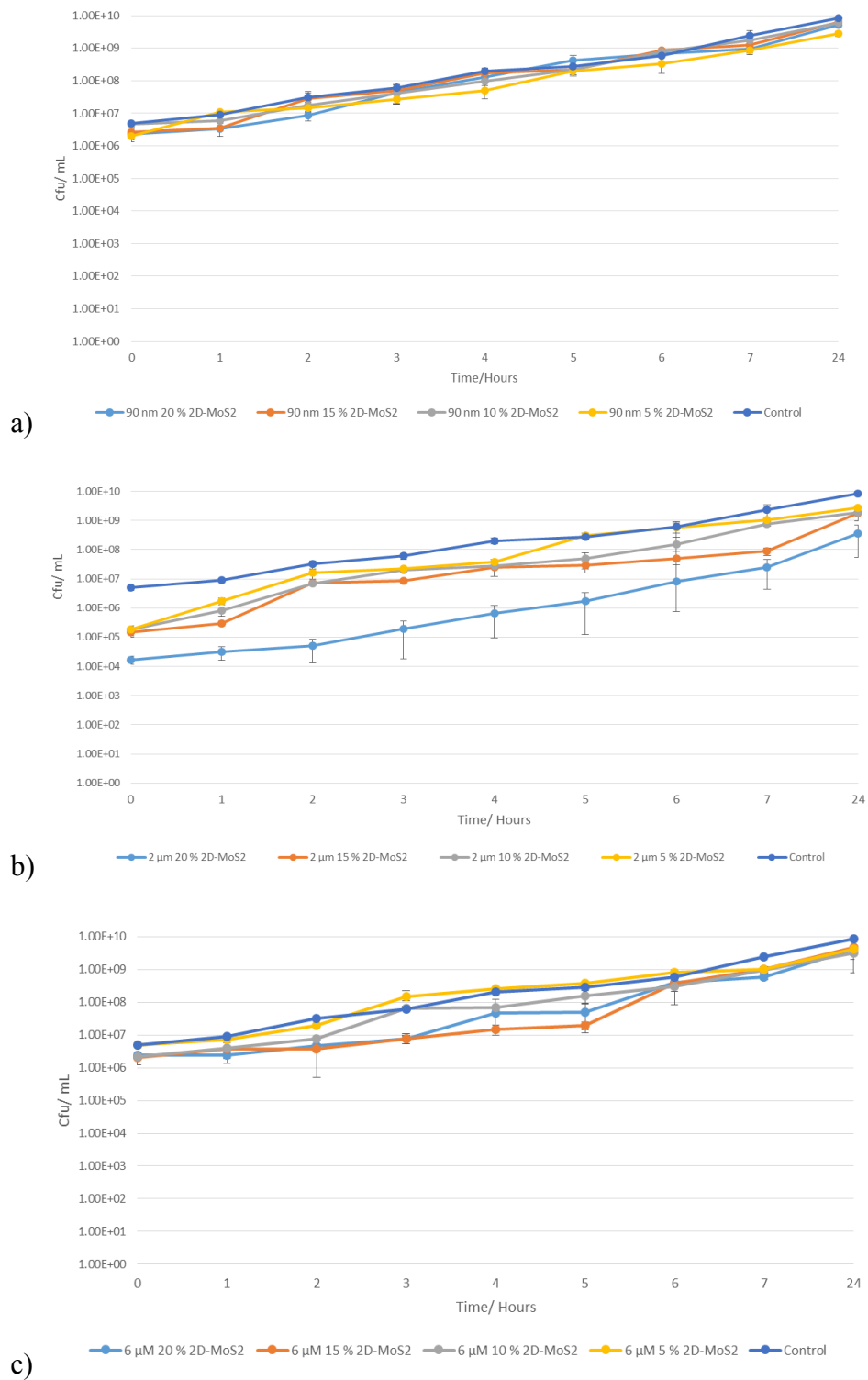


Figure 21. Average colony forming units of *P. aeruginosa* over 24 h growth curves, tested against a) 90 nm, b) 2 μm and c) 6 μm 2D-MoS₂ particle sized surfaces, at concentrations of 5 %, 10 %, 15 % and 20 % MoS₂ (n = 2)

Scanning electron microscopy of bacteria after growth curves

3.5 Staphylococcus aureus

Scanning electron microscopy was carried out on 2D-MoS₂ surfaces in order to determine morphological changes to the bacteria in the presence of 2D-MoS₂ surfaces. 2D-MoS₂ surfaces at particle sizes of 90 nm, 2 μm and 6 μm were tested and each 2D-MoS₂ particle size had four corresponding MoS₂ concentrations; 5 %, 10 %, 15, and 20 %. Initially, growth curves were carried out and at times 0 h and 24 h, 10 μL aliquot were taken from the growth curve flasks and prepared for SEM imaging. During the 0 h time-point, minimal / none 2D-MoS₂ surface contact was expected to occur. Samples were observed on silicon wafer backgrounds. The morphology of *S. aureus* remained constant throughout the growth curve. This trend was demonstrated by each 2D-MoS₂ particle size and concentration, indicating no changes in *S. aureus* cell morphology when minimal / zero 2D-MoS₂ surface contact occurred, with the exception of 15 % and 20 % at 6 μm. After 24 h of the growth curve, some *S. aureus* bacteria showed signs of damage, where some *S. aureus* bacteria showed puncture marks, and possible biofilm formation. This however, was not constant throughout the samples.

Time = 0 h

Time = 24 h

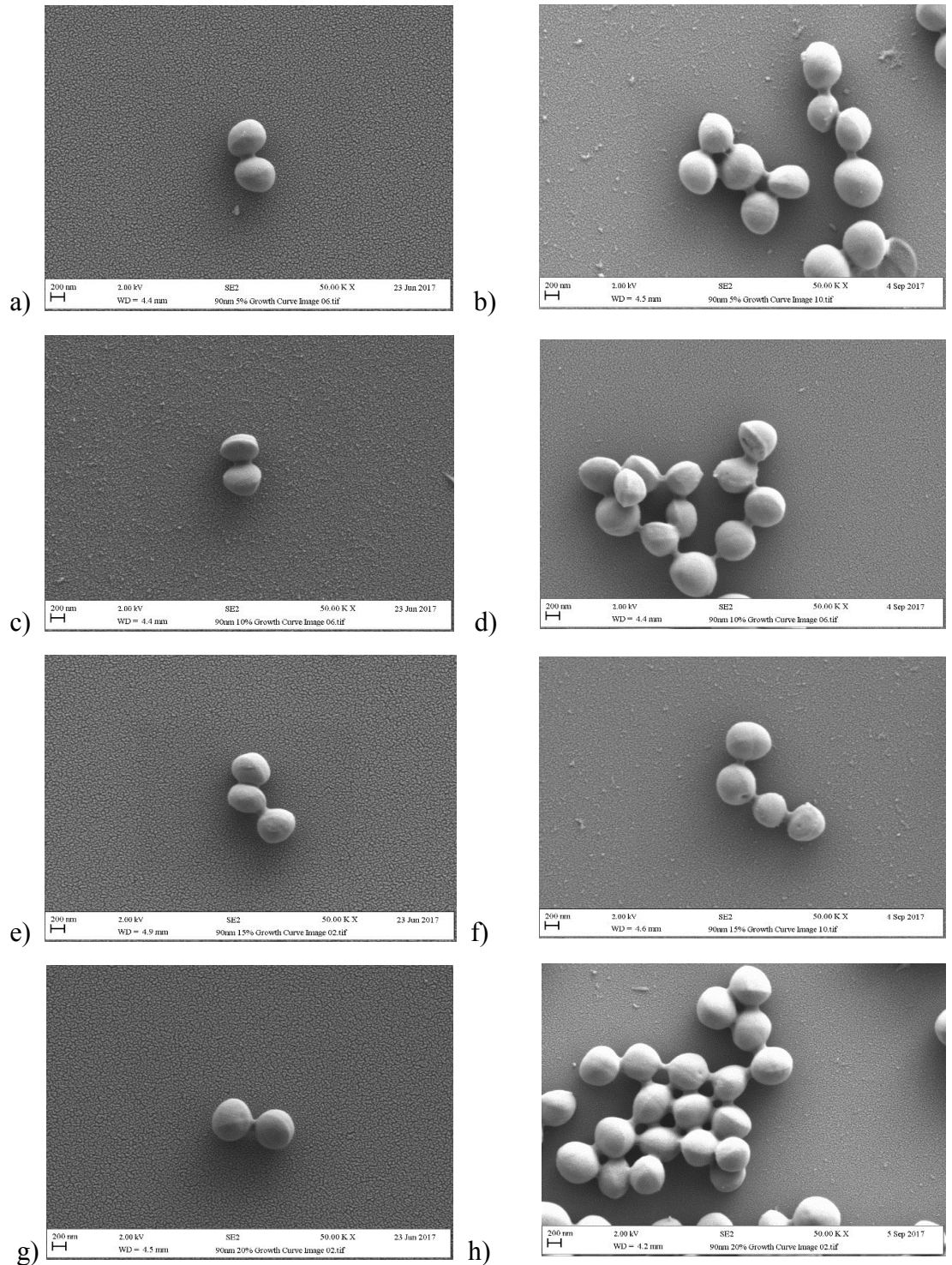
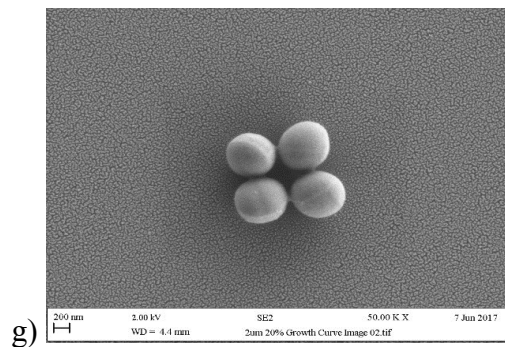
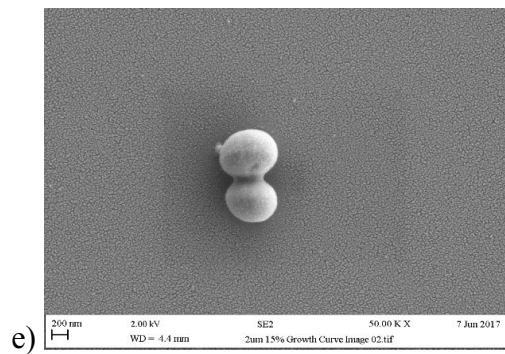
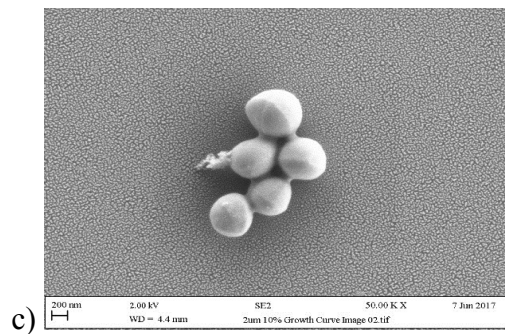
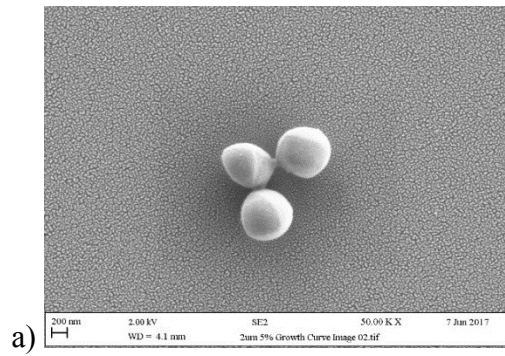


Figure 22. Scanning electron microscopy images of *S. aureus* (a, c, e and g) (0 h) alongside *S. aureus* after 2D-MoS₂ 90 nm growth curves (b, d, f and h) (24 h) at MoS₂ concentrations of a) b) 5 %, c) d) 10 %, e) f) 15 % and g) h) 20 % (n = 1)

Time = 0 h



Time = 24 h

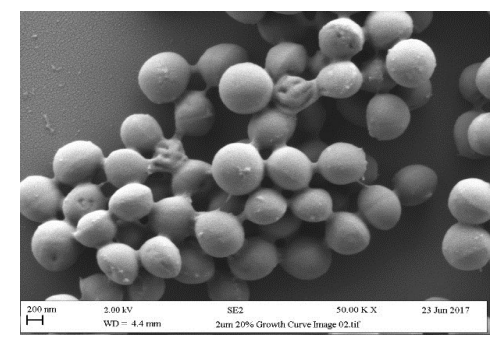
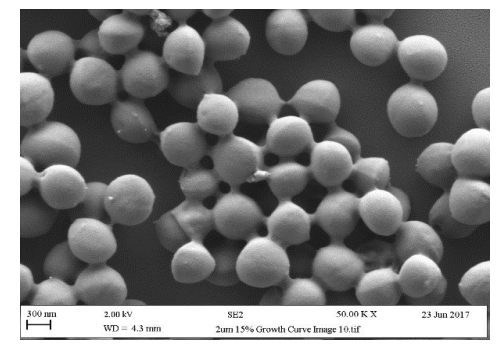
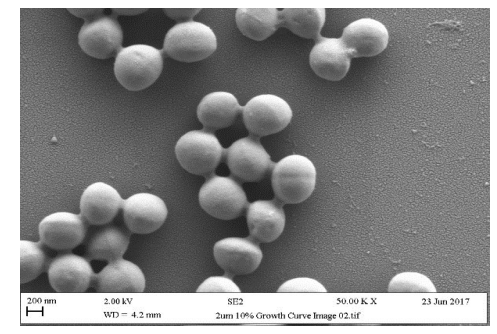
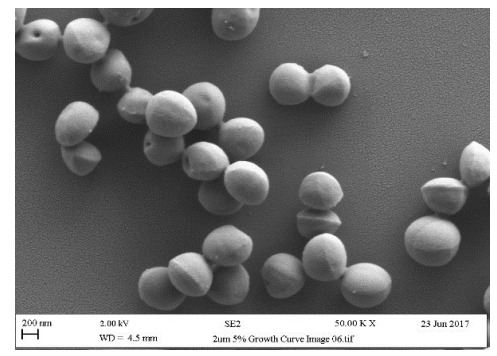
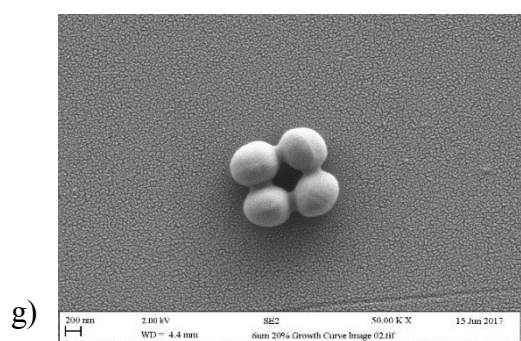
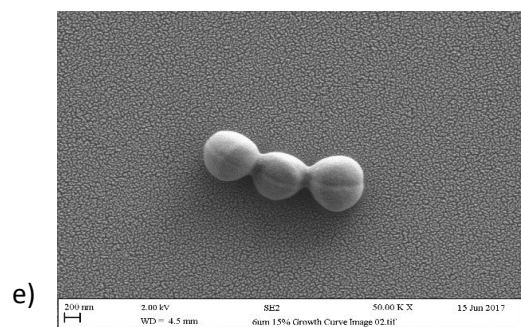
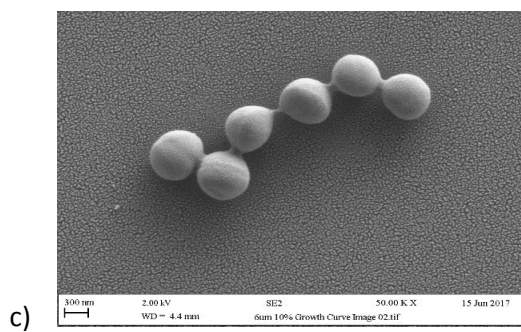
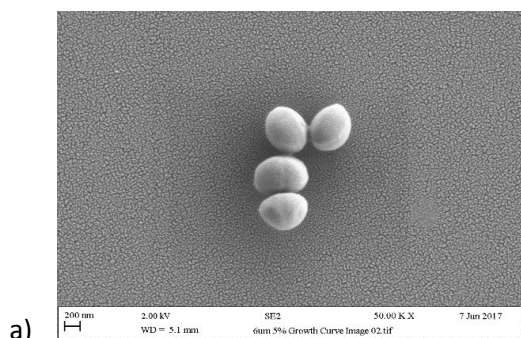


Figure 23. Scanning electron microscopy images of *S. aureus* (a, c, e and g) (0 h) alongside *S. aureus* after 2D-MoS₂ 2 μ m growth curves (b, d, f and h) (24 h) at MoS₂ concentrations of a) b) 5 %, c) d) 10 %, e) f) 15 % and g) h) 20 % (n = 1)

Time = 0 h



Time = 24 h

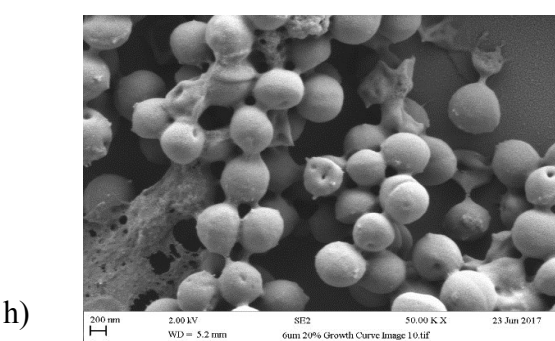
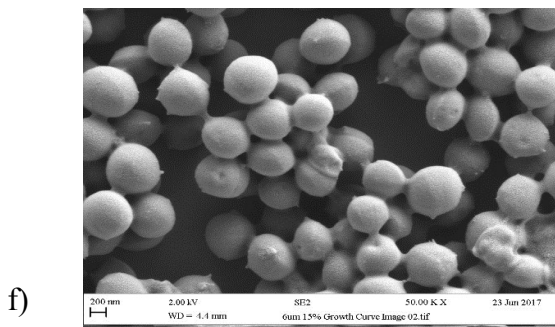
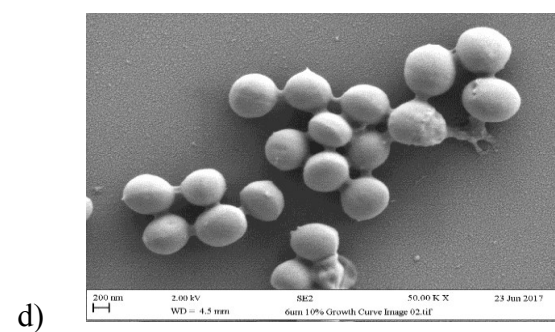
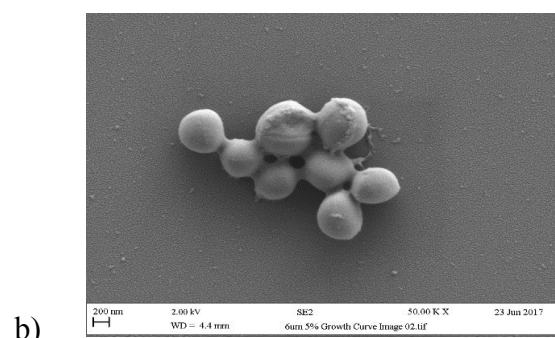


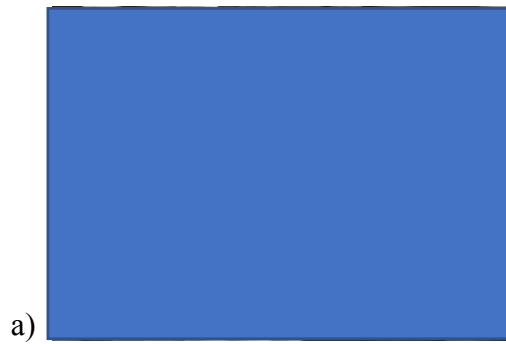
Figure 24. Scanning electron microscopy images of *S. aureus* (a, c, e and g) (0 h) alongside *S. aureus* after 2D-MoS₂ 6 μ m growth curves (b, d, f and h) (24 h) at MoS₂ concentrations of a) b) 5 %, c) d) 10 %, e) f) 15 % and g) h) 20 % (n = 1)

3.51 *Pseudomonas aeruginosa*

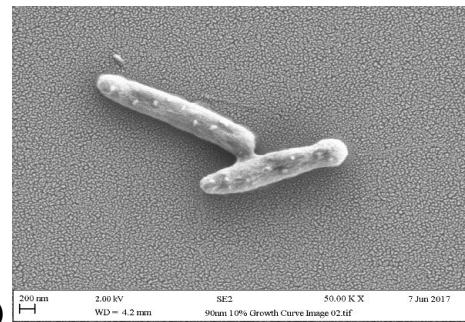
P. aeruginosa growth increased from 0 h to 24 h without inhibition from the 2D-MoS₂ surfaces at any concentration or particle sizes. However, a difference in *P. aeruginosa* morphology was demonstrated. At hour 0, *P. aeruginosa* demonstrated normal bacterial cell morphologies at all 2D-MoS₂ particle sizes and concentrations with the exception of 90 nm 20 %, 2 μm at 5 %, 10 %, 15 % and 6 μm at 10 % and 20 % MoS₂. At the aforementioned particle sizes and concentrations, *P. aeruginosa* demonstrated different morphologies. The bacteria showed a hollowed cell structure, showing an almost flattened or pressed morphology. This was demonstrated at increased magnitude after 24 h, where every *P. aeruginosa* bacterium was that shape. It was also observed that the outer membranes of these Gram negative bacteria had fused with adjacent bacteria, and demonstrated cell shrinkage at higher MoS₂ concentrations (2 μm at 15 % MoS₂).

(Please note that blank / blue spaces will be filled in after completion of missing imaging)

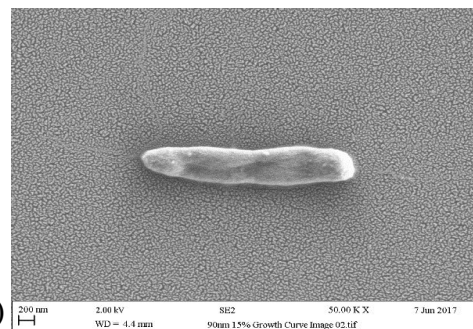
Time = 0 h



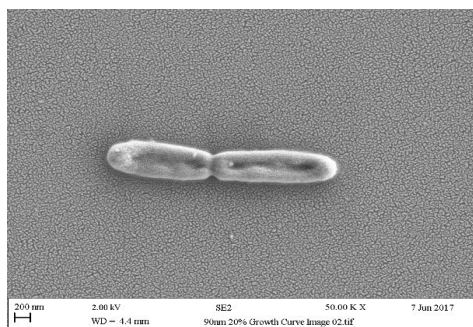
a)



c)



e)

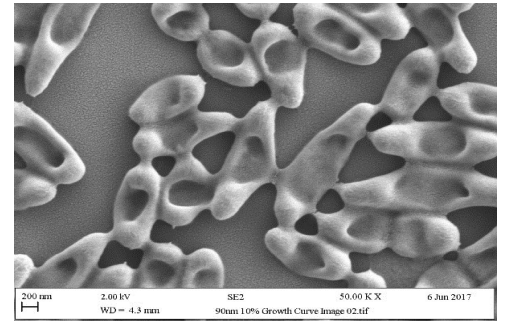


g)

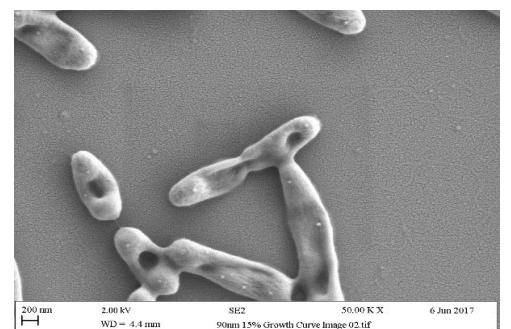
Time = 24 h



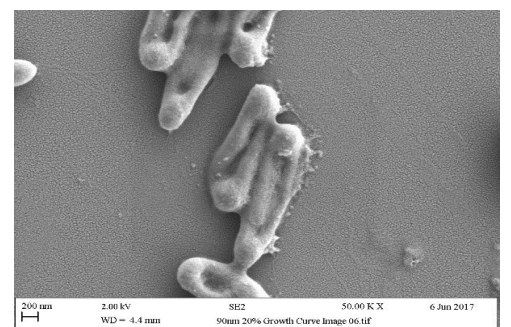
b)



d)



f)



h)

Figure 25. Scanning electron microscopy images of *P. aeruginosa* (a, c, e and g) (0 h) alongside *P. aeruginosa* after 2D-MoS₂ 90 nm growth curves (b, d, f and h) (24 h) at MoS₂ concentrations of a) b) 5 %, c) d) 10 %, e) f) 15 % and g) h) 20 % (n = 1)

Time = 0 h

Time = 24 h

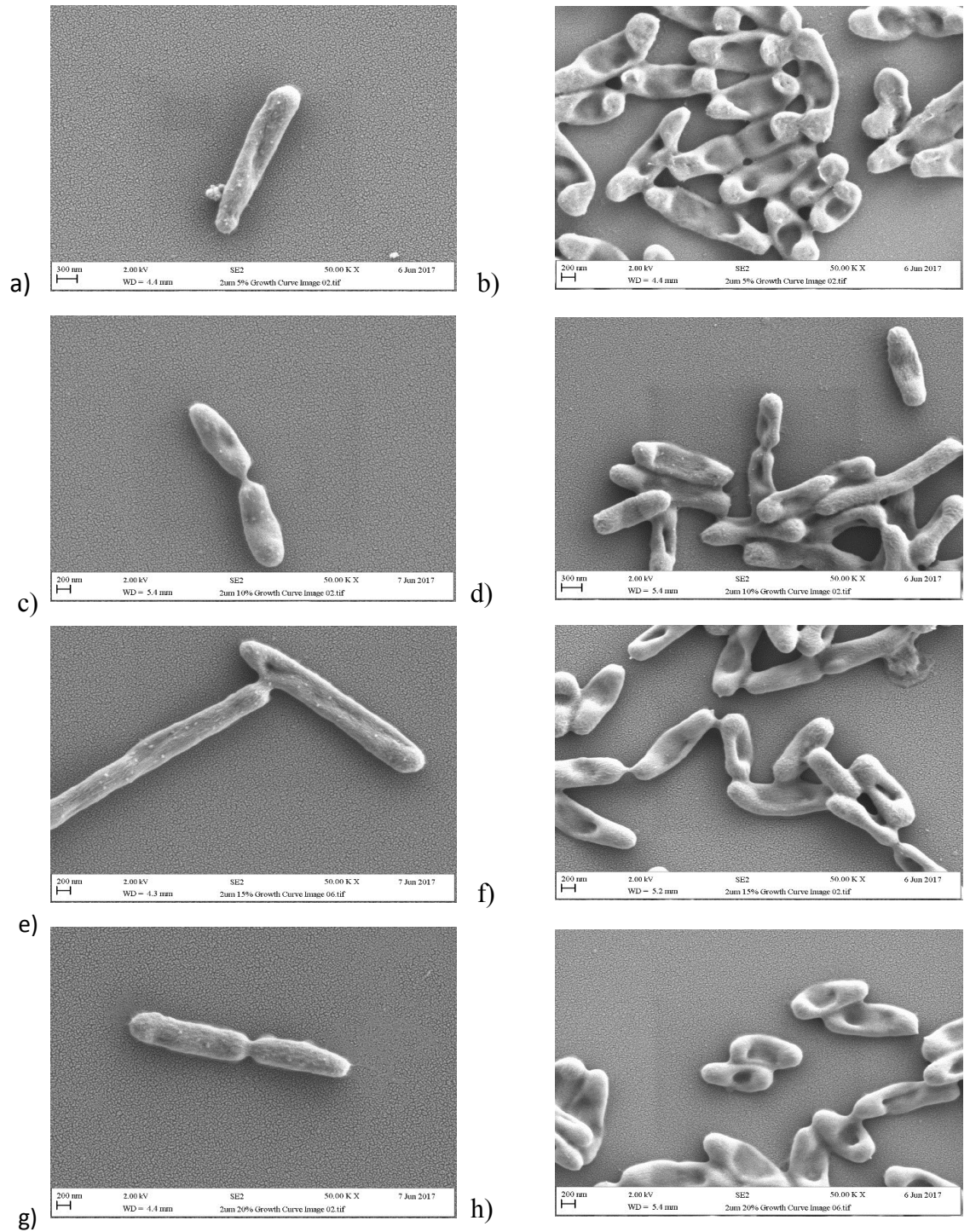


Figure 26. Scanning electron microscopy images of *P. aeruginosa* (a, c, e and g) (0 h) alongside *P. aeruginosa* after 2D-MoS₂ 2 μ m growth curves (b, d, f and h) (24 h) at MoS₂ concentrations of a) b) 5 %, c) d) 10 %, e) f) 15 % and g) h) 20 % (n = 1)

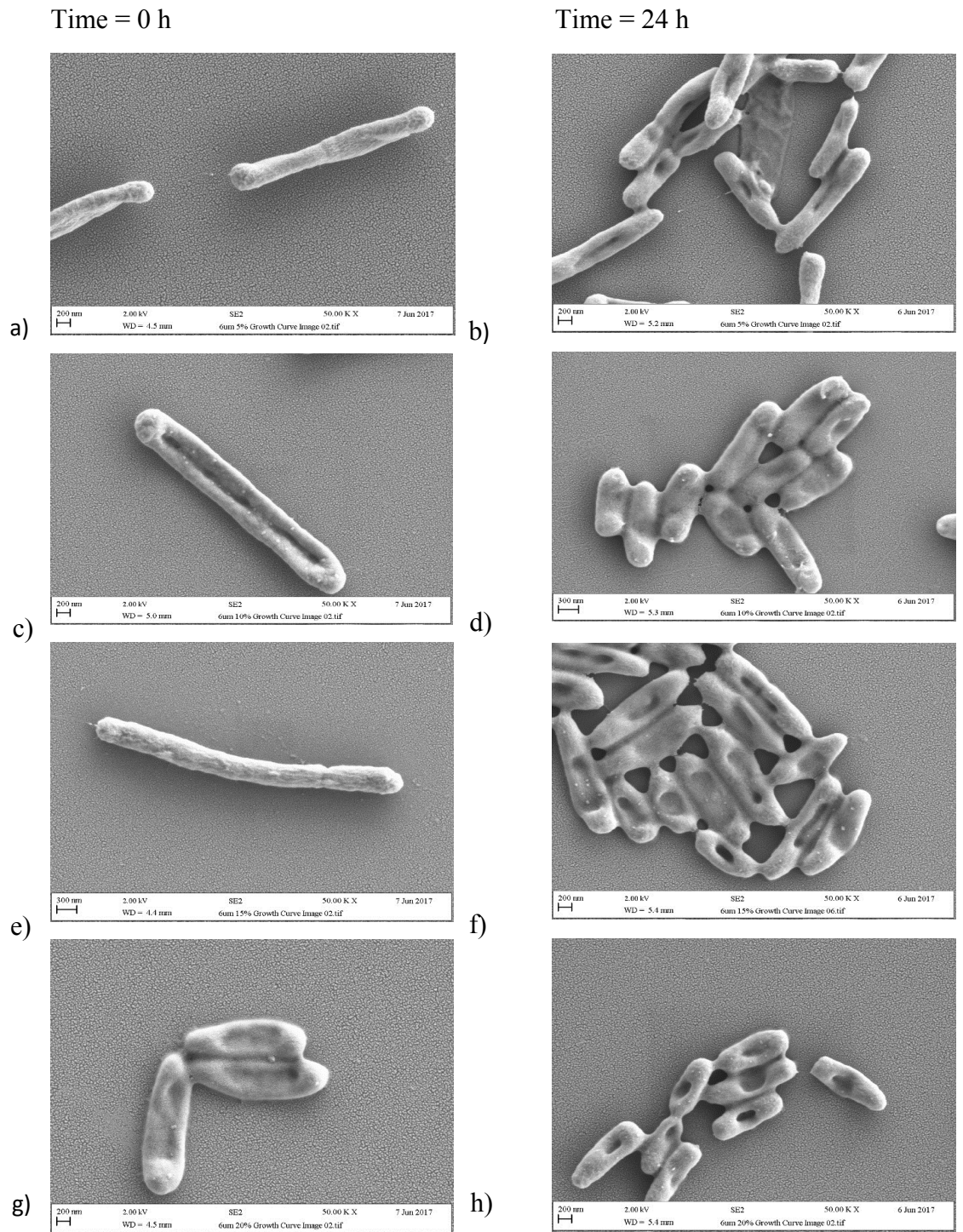


Figure 27. Scanning electron microscopy images of *P. aeruginosa* (a, c, e and g) (0 h) alongside *P. aeruginosa* after 2D-MoS₂ 6 μ m growth curves (b, d, f and h) (24 h) at MoS₂ concentrations of a) b) 5 %, c) d) 10 %, e) f) 15 % and g) h) 20 % (n = 1)

Scanning electron microscopy of retained bacteria on 2D-MoS₂ surfaces

3.6 Staphylococcus aureus

Scanning electron microscopy was carried out on the 2D-MoS₂ surfaces with attached *S. aureus* and *P. aeruginosa* at 0 h and 24 h. The 2D-MoS₂ surfaces that were tested were at particle sizes of 90 nm, 2 μm and 6 μm. These surfaces each had MoS₂ concentrations of 5 %, 10 %, 15 % and 20 %. During the growth curves, at time-point 0 h and 24 h, 2D-MoS₂ surfaces were removed from the growth curve media and prepared for SEM testing. The results showed that for *S. aureus*, there was an increase in bacterial growth from 0 h to 24 h. This was demonstrated at each 2D-MoS₂ particle size and MoS₂ concentration with the exception of 20 % 2D-MoS₂ at 90 nm particle size. *S. aureus* cells at 24 h demonstrated a different morphology when compared to 0 h. The bacteria at 24 h, showed fusion of the cell membrane to the surrounding 2D-MoS₂ surface as well as other cells. This was most prominently identified at 90 nm 10 % (24 h) and 6 μm at 20 % (24 h). In addition, when comparing the *S. aureus* that were in contact with the 2D-MoS₂ surfaces, to the bacteria on the silicon wafers, there was difference morphologies demonstrated by the bacteria. At both 0 h and 24 h on the silicon wafers, the overall *S. aureus* cell membrane showed normal morphologies. However, when in direct contact with the 2D-MoS₂ surfaces regardless of concentration or time-point, *S. aureus* demonstrated a different membrane morphology. The membrane of *S. aureus* presented as granulated (2 μm, 15 % at 0 h) and disfigured (6 μm, 20 % at 24 h); this was evident for every *S. aureus* bacteria after coming into contact with the 2D-MoS₂ surface.

Time = 0 h

Time = 24 h

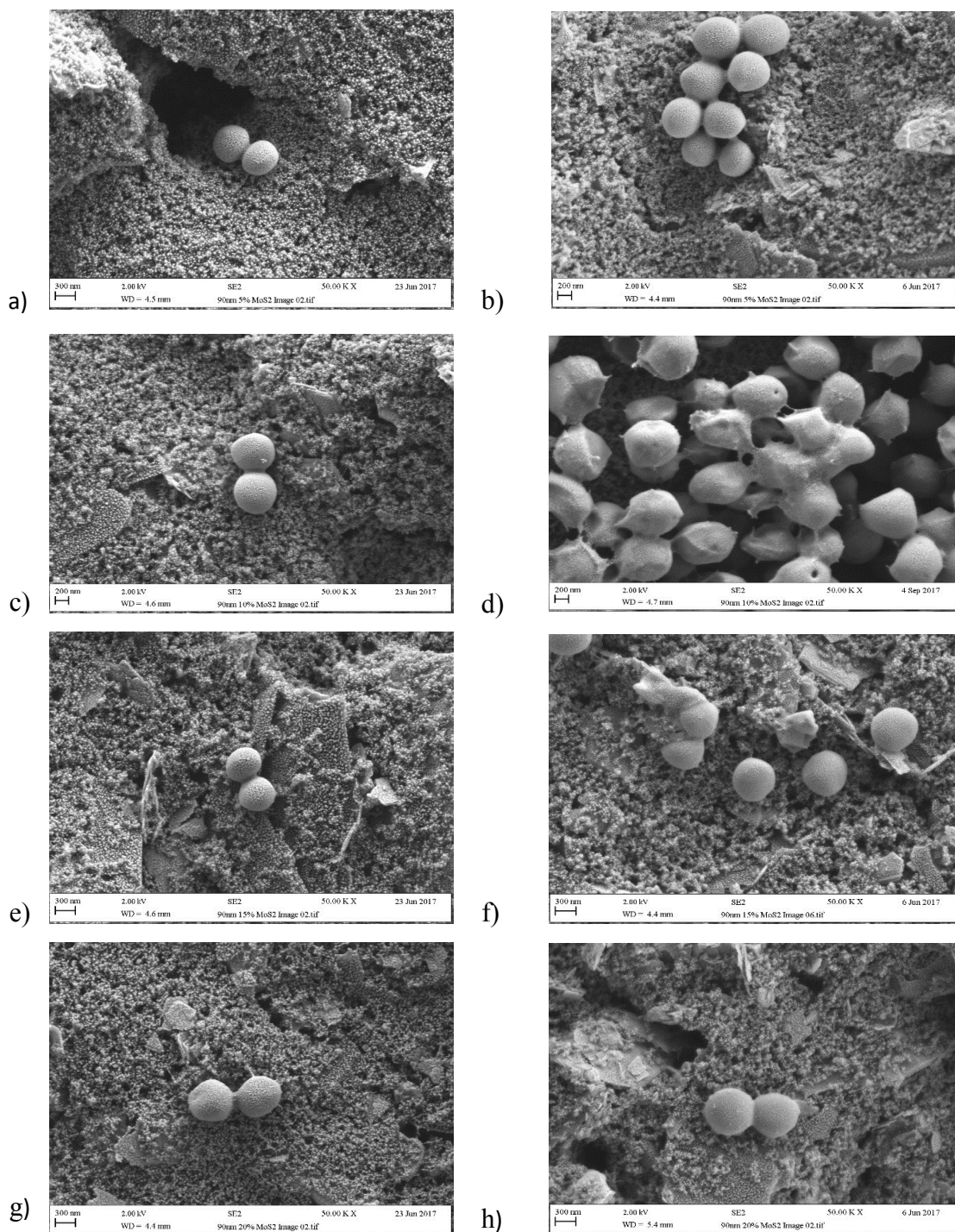
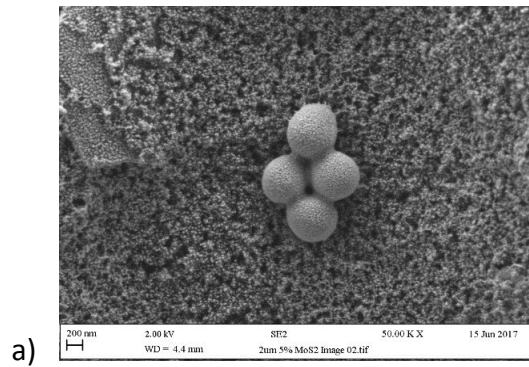
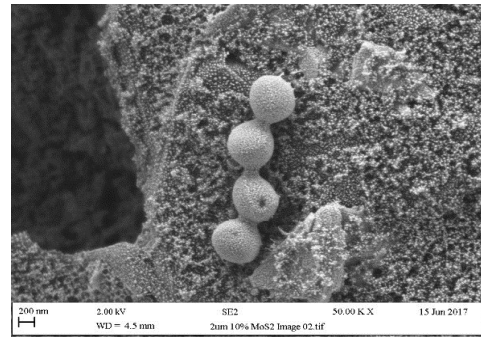


Figure 28. Scanning electron microscopy images of *S. aureus* (a, c, e, g) (0 h) on 2D-MoS₂ surfaces, alongside *S. aureus* after 24 h of 90 nm 2D-MoS₂ contact (b, d, f, h) (24 h), at MoS₂ concentrations of a) b) 5 %, c) d) 10 %, e) f) 15 % and g) h) 20 % (n = 1)

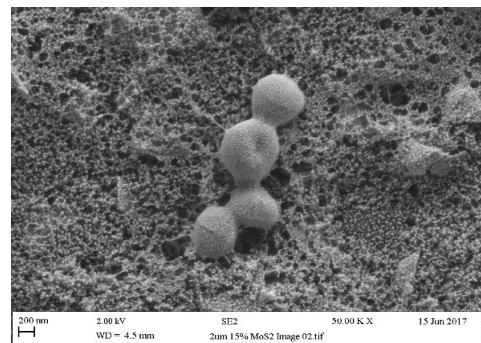
Time = 0 h



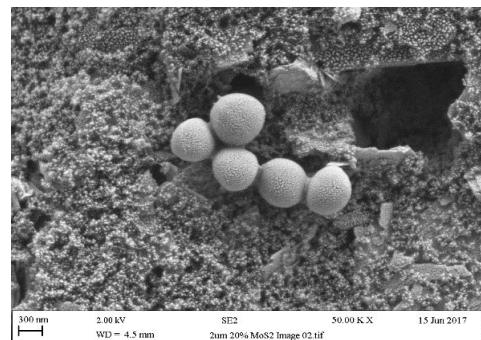
a)



c)

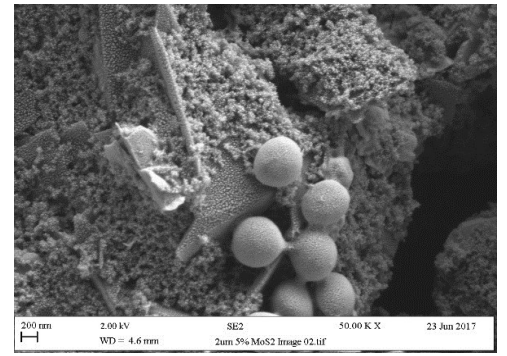


e)

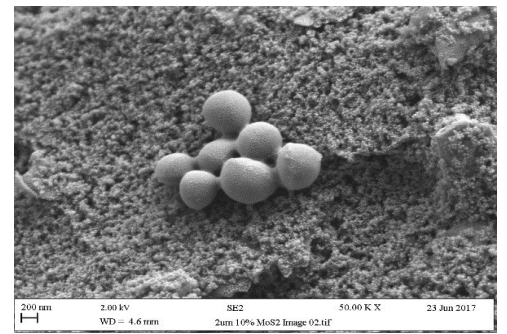


g)

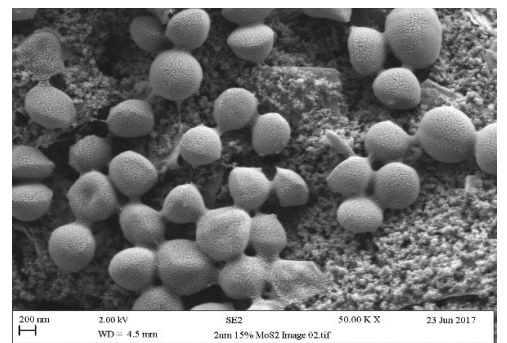
Time = 24 h



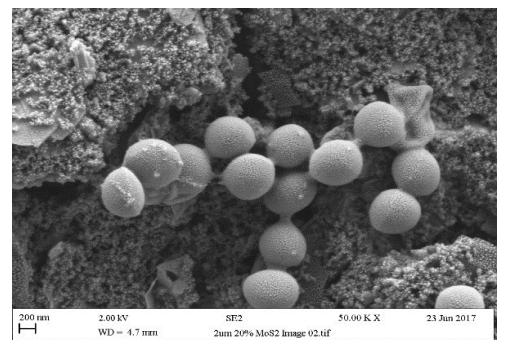
b)



d)



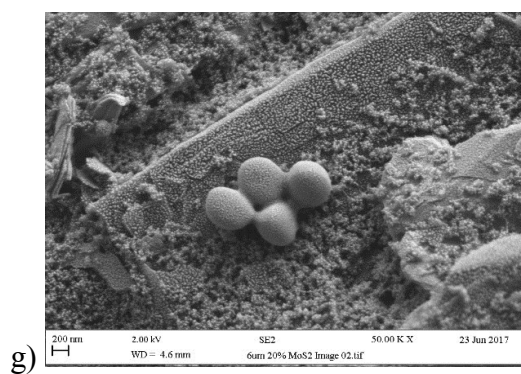
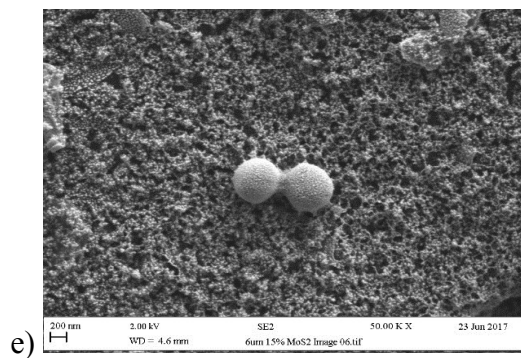
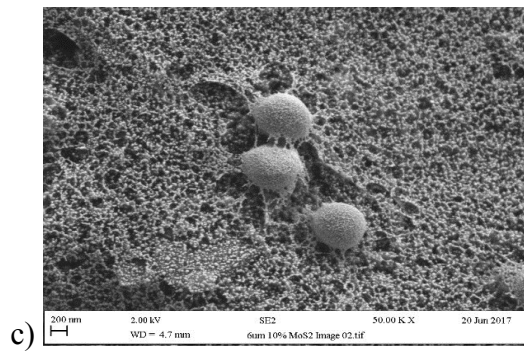
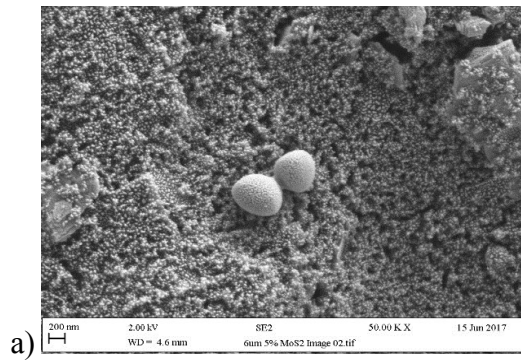
f)



h)

Figure 29. Scanning electron microscopy images of *S. aureus* (a, c, e, g) (0 h) on 2D-MoS₂ surfaces, alongside *S. aureus* after 24 h of 2 μm 2D-MoS₂ contact (b, d, f, h) (24 h), at MoS₂ concentrations of a) b) 5 %, c) d) 10 %, e) f) 15 % and g) h) 20 % (n = 1)

Time = 0 h



Time = 24 h

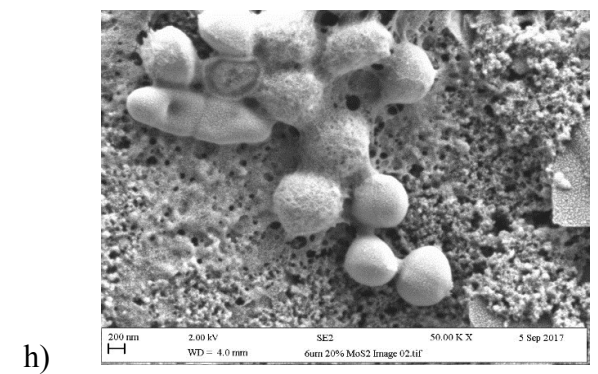
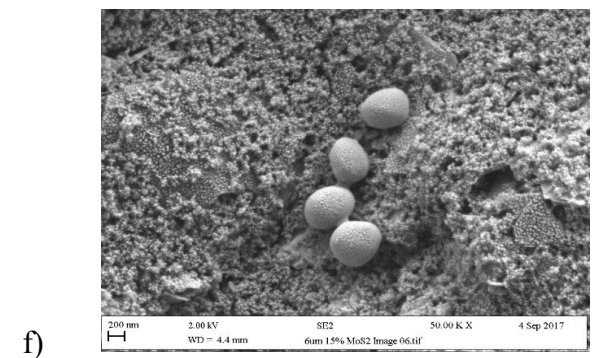
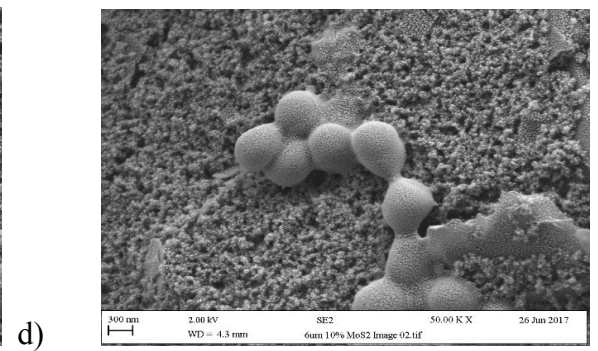
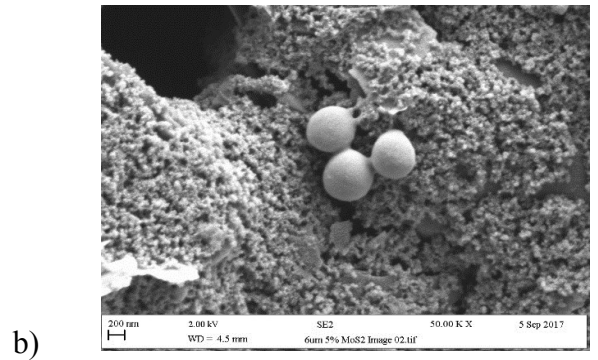


Figure 30. Scanning electron microscopy images of *S. aureus* (a, c, e, g) (0 h) on 2D-MoS₂ surfaces, alongside *S. aureus* after 24 h of 6 μm 2D-MoS₂ contact (b, d, f, h) (24 h), at MoS₂ concentrations of a) b) 5 %, c) d) 10 %, e) f) 15 % and g) h) 20 % (n = 1)

3.61 *Pseudomonas aeruginosa*

P. aeruginosa showed an increase in growth from 0 h to 24 h. This trend was demonstrated on each 2D-MoS₂ particle size and MoS₂ concentration, with the exception of 15 % 2D-MoS₂ at 90 nm particle size. *P. aeruginosa* demonstrated different morphologies at from the growth curves on the silicon wafers. The bacteria demonstrated a flattened appearance accompanied with hollowed centres. A difference between the 0 h and 24 h *P. aeruginosa* samples was also observed. At 24 h the *P. aeruginosa* bacteria were fused to the 2D-MoS₂ surfaces whereas, the 0 h bacteria were not.

Time = 0 h

Time = 24 h

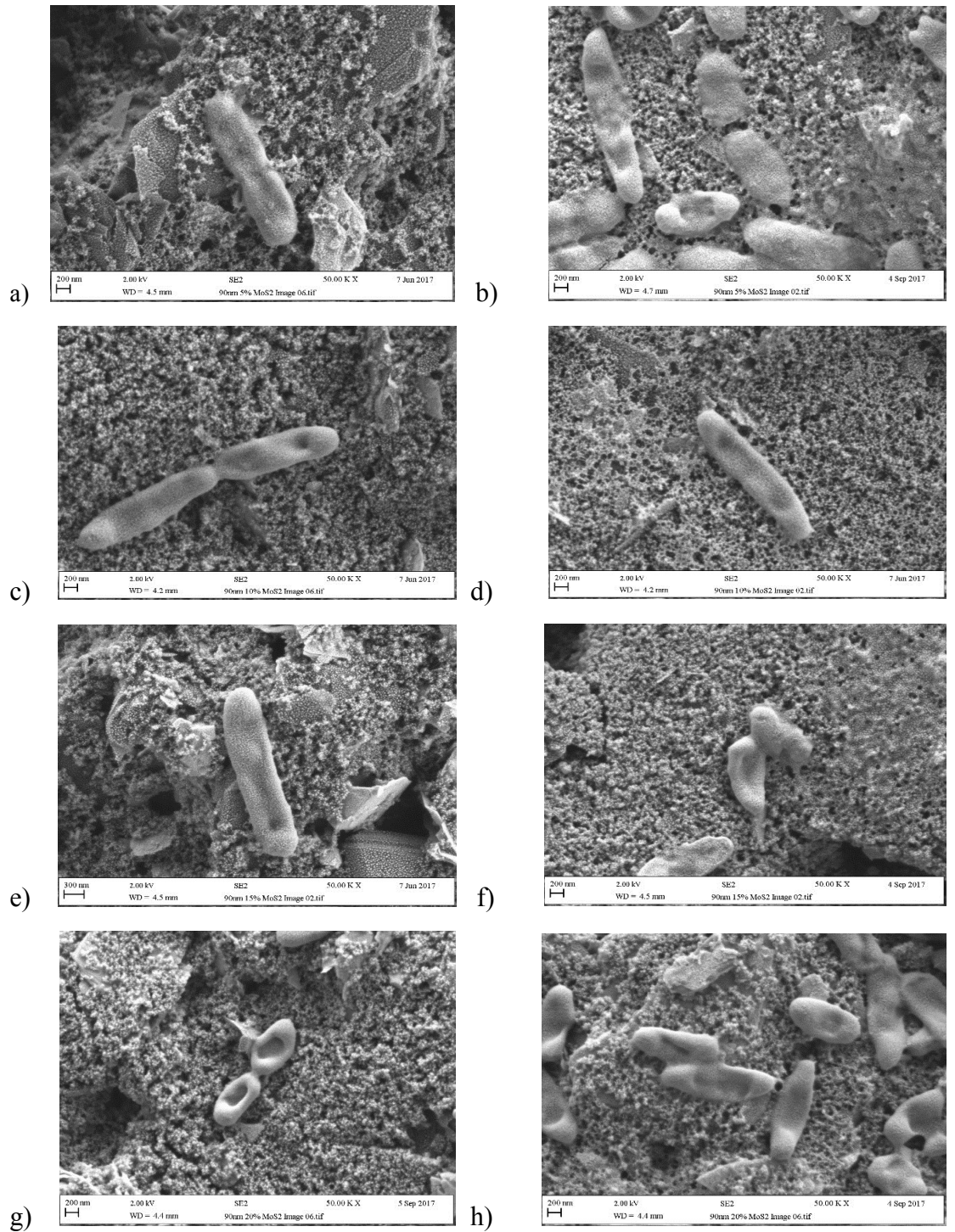


Figure 31. Scanning electron microscopy images of *P. aeruginosa* (a, c, e, g) (0 h) on 2D-MoS₂ surfaces, alongside *P. aeruginosa* after 24 h of 90 nm 2D-MoS₂ contact (b, d, f, h) (24 h), at MoS₂ concentrations of a) b) 5 %, c) d) 10 %, e) f) 15 % and g) h) 20 % (n = 1)

Time = 0 h

Time = 24 h

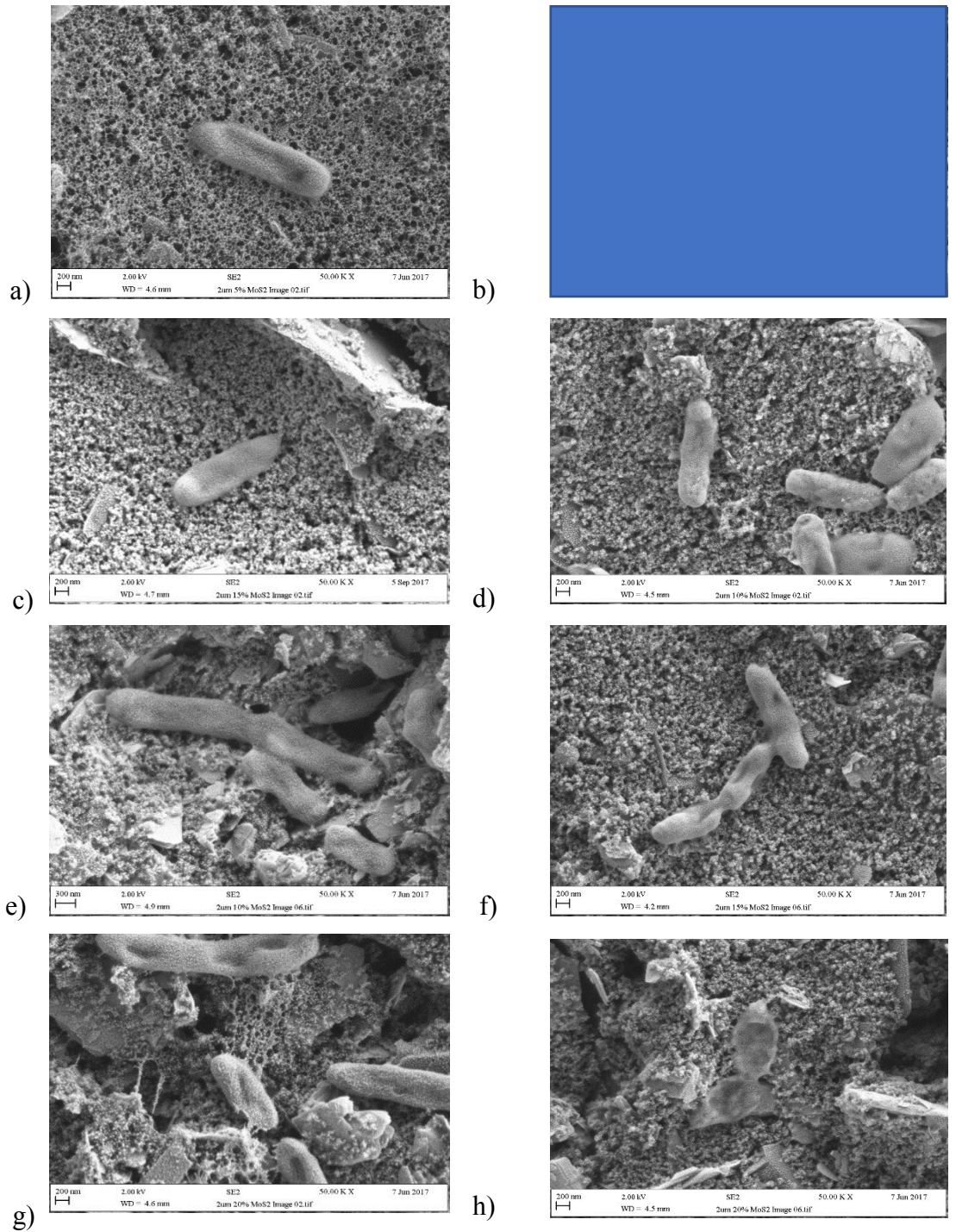


Figure 32. Scanning electron microscopy images of *P. aeruginosa* (a, c, e, g) (0 h) on 2D-MoS₂ surfaces, alongside *P. aeruginosa* after 24 h of 2 μm 2D-MoS₂ contact (b, d, f, h) (24 h), at MoS₂ concentrations of a) b) 5 %, c) d) 10 %, e) f) 15 % and g) h) 20 % (n = 1)

Time = 0 h

Time = 24 h

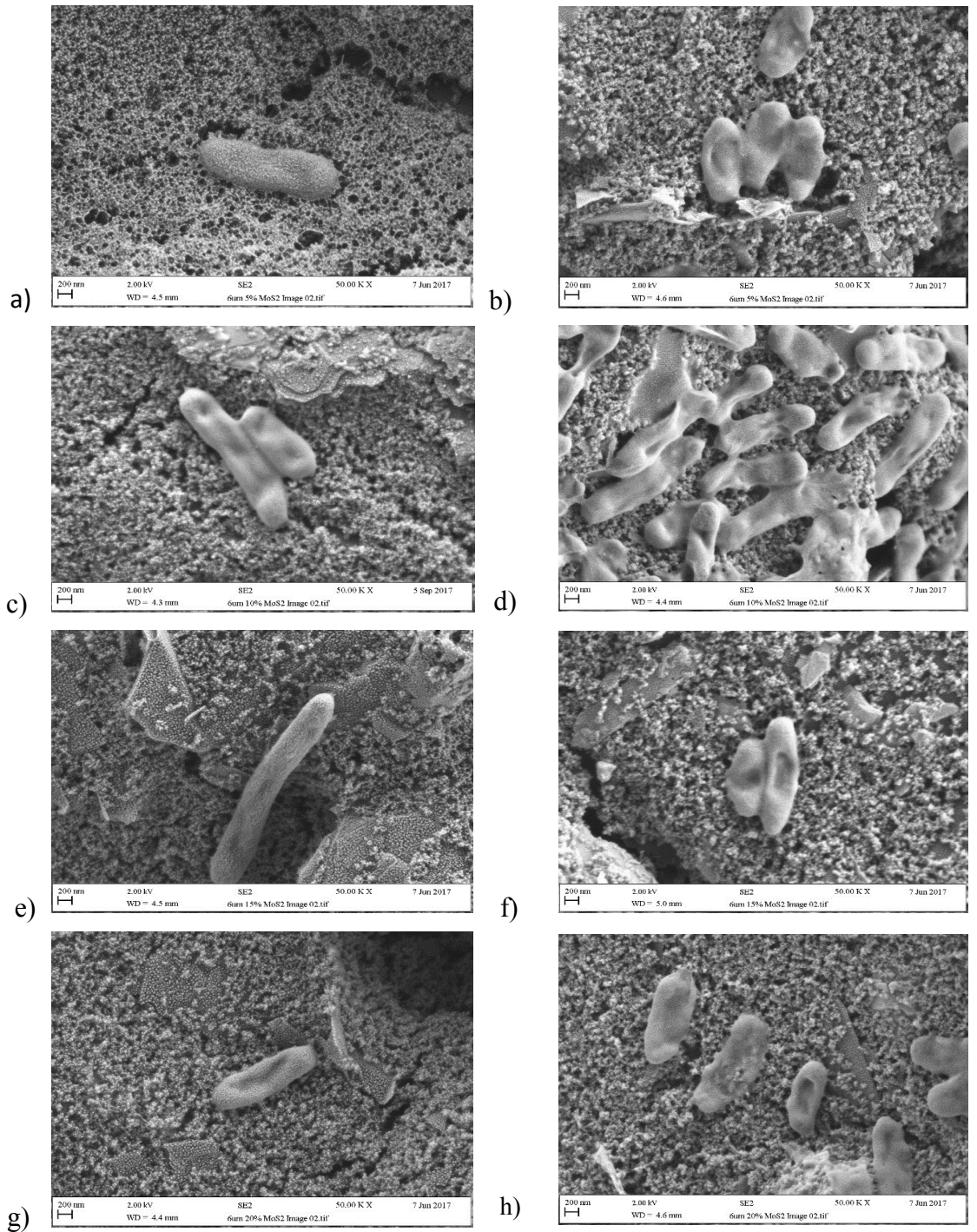


Figure 33. Scanning electron microscopy images of *P. aeruginosa* (a, c, e, g) (0 h) on 2D-MoS₂ surfaces, alongside *P. aeruginosa* after 24 h of 6 μm 2D-MoS₂ contact (b, d, f, h) (24 h), at MoS₂ concentrations of a) b) 5 %, c) d) 10 %, e) f) 15 % and g) h) 20 % (n = 1)

Renal human cell cytotoxicity

3.7 Immortalised renal human proximal tubular cell viability in response to media incubated with 2D-MoS₂ surfaces at 24, 25 and 26 hours

HK-2 cells were used in the determination of 2D-MoS₂ cell cytotoxicity due to the basic nature of the cytotoxicity tests used and the fact that the HK-2 cells were particularly effective at detecting changes at minimal substrate concentrations. Tests were carried out after 24 h of incubation with selected 2D-MoS₂ surfaces for three consecutive hours (24 h, 25 h and 26 h) and were compared to their blanks at the appropriate time-points. Absorbance readings were used to calculate the final percentage viability (Figure 34) and absorbance readings were taken at both 450 nm and 650 nm wavelengths. Blanks were carried out for each hour-point used and alongside these serum free media (SFM) controls were also analysed. Surface particle sizes of 90 nm, 2 µm and 6 µm were used for the tests at a MoS₂ concentration of 20 %, which was decided based on antimicrobial data (Figures 18 – 21). At 24 h there were no trends observed between 2D-MoS₂ particle sizes and the reduction in cell viability however, it was observed that the 2D-MoS₂ at the 90 nm particle size had the largest reduction in HK-2 cell viability (reduction of 8.1 % total cell viability) from the control. Both 2 µm and 6 µm demonstrated smaller reductions in cell viability (2.1 % and 5.6 % respectively). Serum free media control demonstrated a total of 33.1 % reduction in cell viability compared to the controls. This was statistically significant ($p = 0.001$) and was the largest overall reduction in cell viability, even more so than the HK-2 cells incubated with the 2D-MoS₂ surfaces. This trend was demonstrated throughout each hour-point from 24 h – 26 h however, SFM demonstrated smaller reductions in cell viability at 25 h and 26 h (17.8 % and 15.4 % respectively). During hours 25 and 26, trends between the 2D-MoS₂ surfaces and HK-2 cells were observed. For both hours, 90 nm 2D-MoS₂ demonstrated the lowest cell viability, at 89.8 % and 90.6 % respectively. An increase in particle size demonstrated an increase in cell viability from 2 µm (97.5 - 94.4) to 6 µm (99.8 – 97.1) at both hour points. Overall from 24 h to 26 h, the 6 µm 2D-MoS₂ particle sizes showed the smallest decrease in cell viability. There were no significant differences demonstrated by the HK-2 cell viability when incubated with the 2D-MoS₂ surfaces, compared to the blank at 24 h. This was demonstrated for all three of the time-points tested (24 h, 25 h and 26 h), where no significant differences between the surfaces and controls were

shown, with the exception of the SFM. The SFM demonstrated a significant difference with regards to reduction in cell viability at each time-point. In summary, the 6 μm 2D-MoS₂ surfaces demonstrated the smallest reduction in HK-2 cell viability over the 26 h period and would be the particle size of choice for biocompatibility.

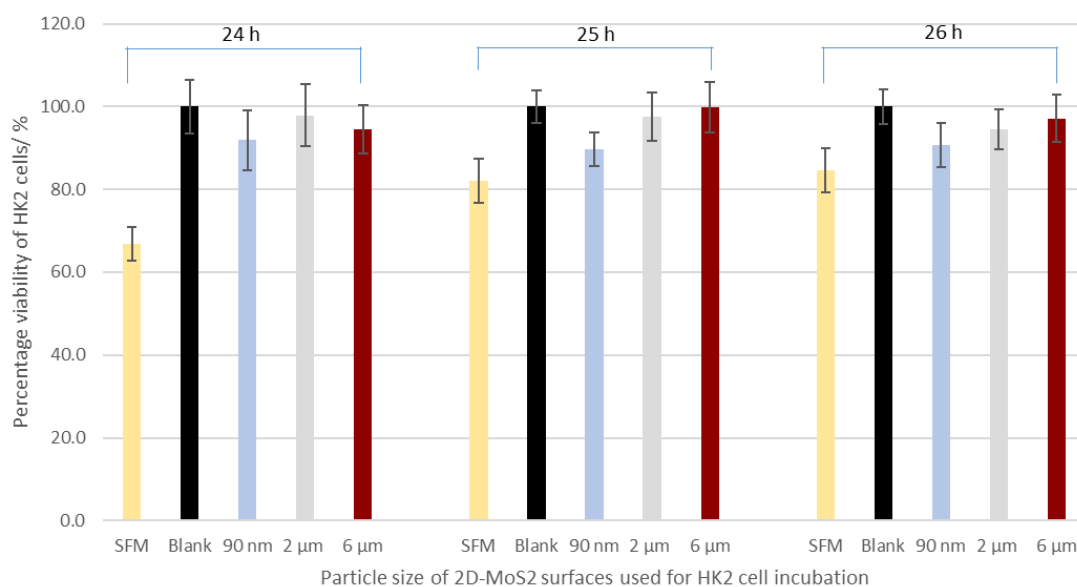


Figure 34. HK-2 cell viability when incubated with SFM and 20 % MoS₂ concentrations of 2D-MoS₂ surfaces, at particle sizes of 90 nm, 2 μm and 6 μm . Cells were tested after 24, 25 and 26 h (n = 3)

3.71 Immortalised human renal cell viability in response to media incubated with 2D-MoS₂ surface at hours 48, 49 and 50

Cell viability after 48 hours was also tested, to determine the possible effects that 2D-MoS₂ would have after prolonged contact with HK-2 cells. The absorbance readings were measured after 48 h, 49 h and 50 h. At 48 h, a decreasing trend in HK-2 cell viability was demonstrated as 2D-MoS₂ particle size of the surfaces increased from 90 nm to 2 μm , and again at 6 μm (102.4 %, 99.1 % and 83.9 % respectively). Both the 90 nm and 2 μm surfaces showed no significant differences in cell viability between themselves and the blank. The 2D-MoS₂ surface at 6 μm however, demonstrated a significant difference from the blank at a *p* value of 0.005. Similarly, to the 24, 25 and 26 h tests, the SFM samples showed a significant decrease in cell viability,

with a reduction of 19.1 % at 48 h. At hours 49 and 50, trends were demonstrated by the 2D-MoS₂ surfaces that were opposite to those showed by each 2D-MoS₂ particle size at 25 h and 26 h. A decrease in cell viability from 90 nm to 6 μm was demonstrated at both 49 h and 50 h (98.7 % - 81.3 % and 91.1 % and 89.8 % respectively). The SFM for both these two time-points, demonstrated a significant reduction ($p = 0.002$ and 0.002 respectively) in cell viability at 78.2 % for 49 h and 83.5 % at 50 h. Significance tests were carried out for both 49 and 50 h. The results demonstrated no significant differences between the 2D-MoS₂ particle sizes and the controls concerning cell viability, with the exception of 6 μm surface during 49 h. At 49 h, 6 μm showed a statistically significant reduction in cell viability ($p = 0.008$). In summary, 90 nm 2D-MoS₂ demonstrated the least bio toxicity over 50 h, which was the opposite shown after 26 h.

Comparisons between each 2D-MoS₂ surface at 24 h, 25 h and 26 h against each 2D-MoS₂ surface at 48 h, 49 h and 50, were made to identify if prolonged contact with the 2D-MoS₂ surfaces had any effect towards HK-2 cell viability. During the first hour of testing, there were no trends demonstrated, except for the SFM, which continued to show reduced cell viability compared to the 2D-MoS₂ surfaces. This was true for both 25 and 49 h however, at hours 26 and 50, an increase in viability was demonstrated by the SFM. Statistical analysis showed no significant differences between the SFM at 25 and 26 h time points against the 49 h and 50 h time-points. However, at 24 h and 48 h a significant difference was demonstrated between the HK-2 cell viabilities ($p = 0.007$). Statistical analysis was carried out between each 2D-MoS₂ particle size across each time point (24 h, 25 h and 26 h against 48 h, 49 h and 50 h respectively). This was carried out to determine whether different particle sizes of 2D-MoS₂ had differing effects after prolonged contact with the HK-2 cells. It was found that there were no significant difference between the 90 nm, 2 μm and 6 μm surfaces at 24 h against 48 h, 25 h against 49 h and 26 h against 50 h with the exception of the 6 μm particle size 2D-MoS₂ surface at hours 25 against hour 49. Here a significant difference was shown by the 6 μm surface at the two time points (25 h and 49 h) at a p value of 0.01. In summary, the 6 μm 2D-MoS₂ surfaces demonstrated the lowest HK-2 cell cytotoxicity for the first 24 h – 26 h period however, after 48 h the 90 nm 2D-MoS₂ surfaces showed the least cytotoxicity. So, if the use of the 2D-MoS₂ surface required short contact with the HK-2 cells, the 6 μm would

be the most effective. However, during periods of prolonged contact with the HK-2 cells, the 90 nm 2D-MoS₂ surface would be the ideal.

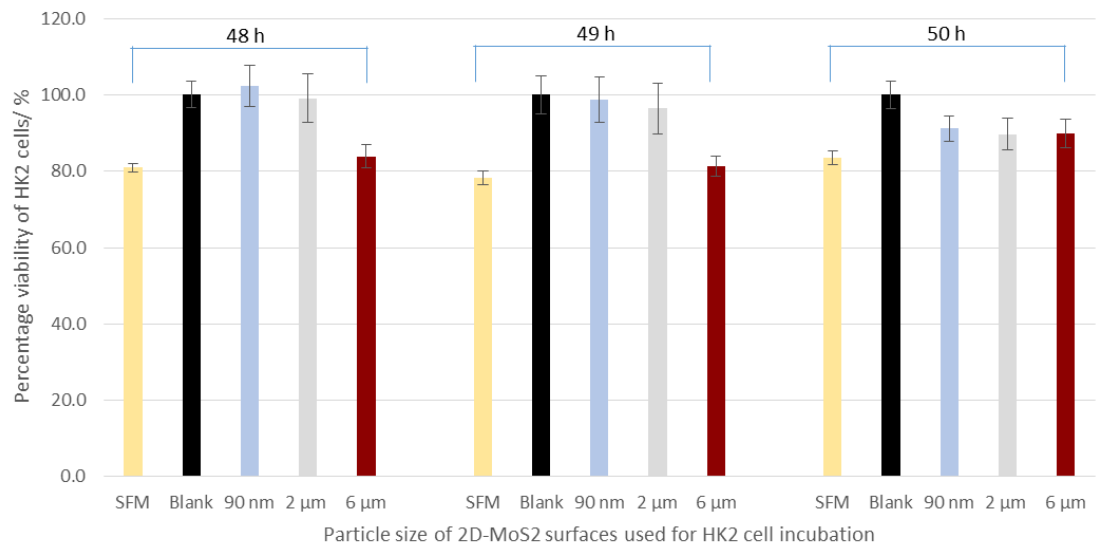


Figure 35. HK-2 cell viability when incubated with SFM and 20 % MoS₂ concentrations of 2D-MoS₂ surfaces, at particle sizes of 90 nm, 2 μm and 6 μm. Cells were tested after 48, 49 and 50 h (n = 3)

Discussion

The requirement for new antimicrobial surfaces is ever increasing. Due to the prevalent increase in antimicrobial resistant bacteria, through multiple resistance mechanisms, there is an expanding problem within the healthcare and environment sectors, due to conventional antimicrobial agents and surfaces becoming less effective. This work investigated the use of 2D-MoS₂ surfaces as a possible alternative to existing antimicrobial surfaces. Since there has been a vast amount of research in the field of metal ion toxicity towards bacterial cells, the 2D-MoS₂ surfaces containing molybdenum ions provided an opportunity to identify a novel antimicrobial surface. This suggests applications for such surfaces within the healthcare and environmental industries, such as catheter surface coatings or pin tract surfaces, where in both instances, colonisation of potential pathogenic bacteria are common.

4.0 Surface roughness

Analysis of the surfaces using optical profilometry enabled determination of the roughness values. It was shown that an increase in particle size from 90 nm to 6 µm resulted in a significant increase in all roughness values. This would have been expected since the particles for the 6 µm surfaces were significantly greater in size and demonstrated the largest roughness values. This was also shown by the average peak and valley height as the 90 nm 2D-MoS₂ particle sizes demonstrated the smallest peaks and valleys, in comparison to 6 µm that were significantly larger, demonstrated the greatest micro-topography. Thus, increasing the 2D-MoS₂ particle size, resulted in increased roughness values and the shapes of the surfaces topographies. Whitehead *et al* demonstrated that different metal coatings deposited onto surfaces presented differently shaped topographies. The shapes of the surface features affected the numbers of retained bacteria on the surfaces demonstrating that the effects of surface topographies have effects on bacterial cell retention (Whitehead *et al.*, 2015).

4.01 ICP–AES

To determine whether leached elements of the 2D-MoS₂ surfaces were molybdenum and sulphur, element analysis was carried out using ICP–AES. The results determined that the molybdenum concentrations in the diluent increased as the surface concentrations of 2D-MoS₂ increased however the levels were very low and on the limit of the ICP-AES detection threshold. These results however, were not significantly different. In addition, sulphur concentrations were tested to ensure that molybdenum was the only increasing element in terms of concentration. It was demonstrated that sulphur concentrations between each 2D-MoS₂ surface concentration remained the same, identifying that molybdenum was the element released in greater concentrations from the surfaces. This meant that any changes observed when increasing 2D-MoS₂ concentrations, was due to the molybdenum ions and not the sulphur. A study in 2017 used ICP–AES to measure the molybdenum and sulphur based species in 2D-MoS₂ powders and found that soluble concentration of molybdenum were very low and reached the very limit of ICP–AES detection (Wang *et al.*, 2016). This was similarly found during the ICP–AES analysis of this study where the concentration of MoS₂ detected was pushing the lower limits of ICP–AES detection. It was reported in a study in 2014 that between 5 – 80 µg/ mL was sufficient enough to initiate an antimicrobial effect towards *Escherichia coli*, causing a total loss in viability of over 90 %. It was also stated that at 1 µg/ mL, there was no sufficient evidence to show that any antimicrobial effect had occurred (Yang *et al.*, 2014). This would mean that it required between 5 – 80 ppm to kill 90 % of *E. coli* within a sample and 1 ppm produced no antimicrobial effect. This was much greater than the 0.009 ppm identified in the leaching of the 20 % 2D-MoS₂ surfaces.

4.02 2D-MoS₂ retention of bacteria

The 90 nm 2D-MoS₂ surfaces demonstrated the most homogenous distribution of both *S. aureus* and *P. aeruginosa* across all concentrations. 2D-MoS₂ surfaces at a particle size of 2 µm showed similar homogeneity to the 90 nm surfaces with regards to both *S. aureus*, but showed primarily heterogeneous distribution for *P. aeruginosa*. Heterogeneous distribution was demonstrated by 6 µm sized 2D-MoS₂ surfaces for both *S. aureus* and *P. aeruginosa*. It was observed that an increase in 2D-MoS₂ particle size meant an increase in heterogeneity amongst bacterial distribution. It was also shown that *P. aeruginosa* after carrying out

retention assays, had a greater affinity towards binding to the 2D-MoS₂ surface, resulting in increased *P. aeruginosa* retention. A study conducted in 2015 demonstrated that bacterial retention was influenced greatly through surface roughness and whether the surface is hydrophilic or hydrophobic. Although hydrophobicity assays were not carried out in this study due to time constraints, it may have been an influencing factor (Whitehead *et al.*, 2015).

4.03 Zones of inhibition

Although minimal leaching was demonstrated using ICP-AES, there was no leaching of the 2D-MoS₂ surfaces through agar when conducting the ZoI tests. The SEM images of the bacterial damage when in contact with the 2D-MoS₂ surfaces along with recent studies suggesting that 2D-MoS₂ required contact with the bacteria to produce a kill. In comparative work, TiN/Ag coatings were used as antimicrobial surfaces, and it was described that the silver particles were only tens of nm in diameter (similar to the 90 nm 2D-MoS₂ surfaces) and was concluded that the leaching rate of the silver particles was too low in an aqueous environment (Kelly *et al.*, 2009). Furthermore, it was demonstrated during ZoI testing that no leaching of the 2D-MoS₂ surfaces occurred which may have been due to a handful of factors such as, the agars used might interfere with the MoS₂ particles, preventing their dispersion. Moreover, the ZoI method involves the leaching of an object into the agar matrix, this however, becomes difficult if the antimicrobial is attached or part of the surface, as the 2D-MoS₂ are. A study published in 2016 demonstrated the effects of molybdenum (Mo) nanoparticles and their effectiveness during ZoI testing. Using a well diffusion method, Mo nanoparticles demonstrated strong antimicrobial activity against *E. coli* since it was not bound to a surface and was instead in solution (Fakhri and Nejad, 2016).

4.04 Growth Curve

It was shown throughout the growth curves that 2 µm was the most effective particle size of 2D-MoS₂ at inhibiting both *S. aureus* and *P. aeruginosa* growth, demonstrating significant reductions in bacterial colony forming units across all time-points. The higher the concentration of MoS₂, the greater the reduction in bacterial colony forming units for both Gram positive and Gram negative bacteria. A study in 2011 displayed the bacteriostatic effects of Zinc nanoparticles on the

growth of Gram negative bacteria over a 14-hour growth curve. The bacteria were under agitation during incubation, similarly to the 2D-MoS₂ surfaces. The results showed the gradual shortening of the log phase of bacterial growth, which was theorised to be indicating a bacteriostatic effect (Chatterjee, *et al.*, 2011).

4.05 Bacterial biofilms

Bacteria within a biofilm are much more difficult to kill since they are protected by a polymeric matrix as well as other dead bacterial aggregates, effective inhibition of bacteria is often difficult (Jhajharia *et al.*, 2015). It was observed that an increased concentration of MoS₂ lead to a decrease in biofilm formation. The mechanism of producing ROS to disrupt bacterial cell membranes is a potential mechanism of action for the 2D-MoS₂ surfaces. A study in 2014 found that using surfaces coated with metal oxide particles, that could release ROS through a biofilm of *P. aeruginosa*, had significantly inhibited the bacteria growth, as well as further biofilm formation through bactericidal effects (Dwivedi *et al.*, 2014). This was detected using absorbance measurements via crystal violet staining, which was the same method used during this study. The decrease in absorbance reading was proportionate to the decrease in biofilm biomass.

4.06 2D-MoS₂ effects on bacteria

Both Gram positive and Gram negative bacteria were tested and demonstrated different susceptibilities towards the 2D-MoS₂ surfaces. On average, a greater reduction of colony forming units was demonstrated by *S. aureus*, the Gram positive bacteria. In a study conducted in 2016, MoS₂ was tested as an antimicrobial against *S. aureus*. During the study, it was displayed that the MoS₂ would bind to the bacteria through van der Waals forces. After aggregation, the microbial cells would enter a state of arrest, thus forming MoS₂ - *S. aureus* conjugates, inhibiting cellular function and replication (Zhang *et al.*, 2016). An initial possibility for the differences between Gram positive and negative bacteria may have been due to the obvious differences in membrane morphology. Gram negative bacteria such as *P. aeruginosa* are innately more resistant towards antimicrobial agents due to their outer membrane structure and morphology (Sousa and Pereira, 2014). This outer membrane is absent in Gram positive bacteria, reducing its protection from the environment by preventing cytoplasm access to toxic molecules, such as heavy metals and providing a stabilizing

layer around the cell (Silhavy *et al.*, 2010). A study from 2017 described the resistance of *P. aeruginosa* to other transition metals in the environment. *P. aeruginosa* was demonstrated the ability to remove up to 90 % of the metal ions (Giovanella *et al.*, 2017). *P. aeruginosa*'s outer membrane however, was still was not enough to prevent bacterial damage as Kim *et al* described the effects of MoS₂ against the Gram negative bacteria. The work evaluated the destruction of outer cell membranes using SEM at a magnification of 10,000 x. The morphologies of the bacteria were described as severely damaged with holes in the cellular membrane after 3 h of incubation with the MoS₂ surfaces. Moreover, the study concluded that direct contact with the surfaces was required for cellular damage to occur (Kim *et al*, 2017).

Previous studies have proposed several antimicrobial mechanisms of 2D materials, which include the physical interaction between bacterial cells or chemical oxidation of intracellular components. The 2D compound graphene oxide (GO), shares properties similar to that of 2D-MoS₂, with its proposed mechanism of action being through direct contact with bacteria. Graphene oxide may act as a sharp blade causing physical stress to bacterial cells by piercing or penetrating the bacterial membranes (Yadav *et al.*, 2017). It is theorised that 2D-MoS₂ does not share this antimicrobial property, but instead, through its increased oxidation capacity, is able to induce ROS release towards bacteria (Kim *et al.*, 2017). Reduction of molecular oxygen (O₂) by high energy exposure or electron transfer leads to the production of highly reactive ROS (Sharma *et al*, 2012).

It was demonstrated that the ZoI did not produce any zones of inhibition, due to the fact that the 2D-MoS₂ surfaces required direct contact with the bacteria to result in a kill. In agreement with this, it was described in current literature in 2014, that the antibacterial pathway for MoS₂ needed contact with the bacteria to induce membrane stress. Evidence for this was provided via SEM analysis, where the *S. aureus* bacteria observed had not been sliced or broken, instead having morphological changes to their membranes, preventing cell function (Yang *et al.*, 2014). The morphology of the *S. aureus* was similarly observed in a study in 2016, where the shape of the *Staphylococcal* species had been imaged using SEM. The bacteria demonstrated membrane morphologies that been stretched, possibly due to the binding and fusing of the bacteria to the 2D-MoS₂

rough surface. The bacteria in contact with the 2D-MoS₂ showed cell granulation and deformed membranes, some of which had fused together due to membrane depolarisation (Pandit *et al.*, 2016). The membrane disfiguration of bacterial cells was repeatedly demonstrated during SEM analysis in this study, showing strong evidence for the proposed mechanism as the control image showed spherical smooth *S. aureus* cells whose morphology remains distinct of *S. aureus*. This exact mechanism was demonstrated by 2D-MoS₂ at particle sizes of 90 nm, 2 µm and 6 µm when describing the SEM images. Furthermore, when the *S. aureus* bacteria that was not in direct contact with the 2D-MoS₂ surface demonstrated that the bacterial membrane morphology remained whole and unaltered, suggesting that direct contact with the 2D-MoS₂ surface was a factor in damaging the bacteria.

Following contact with the 2D-MoS₂ surfaces, the cell membrane of *P. aeruginosa*, seemed to have entirely collapsed after 24 h. This was demonstrated on the surfaces of all particle sizes and concentrations, meaning that the chemistry of the MoS₂ itself, and not the different particle sizes, was the primary factor in the bacterial cell disruption. Although it was clear that the cells had collapsed, there was not scope in this project to determine if *P. aeruginosa* death had occurred. The hollowed morphology of the *P. aeruginosa* cells could have been due to ROS release however, there may have been another mechanism of action causing this such as interactions with the sharp edges of the 2D-MoS₂ surface. It was identified that the 2D-MoS₂ contained sharp edges on its metal particles, meaning that slicing of the bacterial cell membranes could be a possibility (Kim *et al.*, 2017). This was also demonstrated in a study conducted in 2013, although 2D-MoS₂ was not the 2D material used, graphene was believed to share similar properties to 2D-MoS₂. The study showed that under SEM, the jagged or sharp edges of the graphene sheets could easily pierce cell membranes, leading to a disruption in cell function (Li *et al.*, 2013). This coupled with the fact that when incubating the bacteria for 24 h during the growth curves, bacterial cells were under continuous agitation allowing the interaction of bacteria with the sharp 2D-MoS₂ particles.

4.07 Cytotoxicity of MoS₂

Two dimensional materials can be damaging to mammalian cells, mainly due to cell membrane damage via oxidative stress. The excessive accumulation of ROS

can damage the cell membrane and reduce its stability. The results showed that 6 μm surfaces resulted in the smallest reduction in HK-2 cell viability, which was concurrent with the leaching results from the ICP-AES, as 6 μm particle sizes leached the least at all concentrations. From the bio toxicity analysis, it was observed that minor increments of HK-2 cell viability were reduced, more so at increased particle sizes of 2D-MoS₂ after increased exposure. This was demonstrated by a paper published in 2016, which evaluated the cytotoxic and genotoxic effects of 2D-MoS₂ sheets what had been produced through chemical vapour deposition (CVD). The effect of MoS₂ was tested on human epithelial keratinocyte (HEK293f) cells, and used SEM to detect changes in their cell morphologies, of which there were none. This indicated no impact on cell morphology, thus HEK cell viability was tested. Using both Live dead fluorescence for detection of acute tissue toxicity and ROS monitoring to identify apoptosis, it was evaluated that MoS₂ had no significant effect on cellular viability of the HEK cells (Appel *et al.*, 2016).

It was found that 2D-MoS₂ was highly detrimental to specific proteins and was observed that the helical structures of proteins such as HP35 had been severely destroyed by the MoS₂ surface (Gu *et al.*, 2016). Using this information, it was hypothesised that the reduction in cell viability from the 24 h reading would occur due to it having some negative effects towards organic components. As surface particle size increased, there was a reduction in cell viability. This was concurrent with results from this study, where an increase in MoS₂ particle size, demonstrated a significant reduction in cell viability. The objective of this study was to identify the antimicrobial effects 2D-MoS₂ surfaces while also identifying their cytotoxicity towards human cells. Using the 2 μM sized surface as the most effective antimicrobial surface, the cytotoxicity was lower than that of 6 μM 2D-MoS₂ after 48 h. This meant that it would kill the greatest number of bacteria whilst maintaining reduced human cell death / damage. This was different from 90 nm 2D-MoS₂, where the cytotoxicity of the 90 nm surface was closer to that of the controls at 48, 49 and 50 h, resulting in minimal cytotoxicity towards HK-2 cells. However, 90 nm was determined to have the weakest antimicrobial efficacy throughout the study, providing the lowest values in terms of bacterial cell death, regardless of Gram positive or Gram negative being a factor, often having little to no antimicrobial effect.

Prolonged exposure to the 2D-MoS₂ surfaces at increased particle sizes resulted in decreased HK-2 cell viability. Given the increased exposure time increasing the likelihood of a greater number of cells coming into contact with the surfaces, would result in increased release of ROS. These ROS are produced typically when in contact with the surface, therefore requiring a longer timeframe to accumulate which would eventually lead to them becoming unstable (Fan *et al.*, 2015). This would lead to an overall decrease in cellular function and damage, presenting with a decreased cell viability. Another possible reason for decreased HK-2 cell viability may have been due to slicing of cells by MoS₂ particles. Due to the sizes of mammalian cells being much larger than bacteria (10 x), they would be less effected by surface area of the 2D-MoS₂ inserts. The, 6 μm 2D-MoS₂ contained larger MoS₂ particles than the other surface sizes. This may have been a factor due to HK-2 cells coming into contact with the peaks of the sharp edges, since the HK-2 cells were too large to reside in the recesses of the 2D-MoS₂ surfaces, and being sliced open, resulting in a potential lower viable HK-2 cell yield. It was shown that the SFM during testing demonstrated lower than expected HK-2 cell viabilities. When conducting the toxicity tests, under a microscope, it was identified that the HK-2 cells in the wells containing the SFM had areas on the plate that had no cells present. This may have been a reason for the significantly reduced cell viability of the SFM wells. It was a possibility that the HK-2 cells did not favour the location or environment of the SFM wells, since growth did originally occur before treatment of SFM, the SFM itself was not the growth inhibiting factor.

5.0 Future work

The work in this study described the surface topography of 2D-MoS₂, its antimicrobial properties and the effects of 2D-MoS₂ against HK-2 cells however, there are still topics on which further research would be beneficial.

Firstly, multifractal analysis would be used to quantitatively analyse the density, cell dispersion and clustering of retained bacteria on the 2D-MoS₂ surfaces (Wickens *et al.*, 2014). This is an approach to obtain numerical data on the effects that surface topography will have on the microbial cells retention. With regards to adhesion of bacteria to a surface, microbial adhesion to hydrocarbon assay (MATH) would be an additional step to take in order to further this research. Determining the physiochemistry's of the 2D-MoS₂ surface would be a beneficial method to this study. Identifying changes in hydrophobicity of a surface are important factors since it may affect the preferential binding to the 2D-MoS₂ surfaces by different bacterial species. In addition, the assessment of the electron donating or accepting potential, along with the hydrophobicity of the bacteria would be an ideal assessment for the hygienic qualities of the surfaces (Tetlow *et al.*, 2017).

It was suggested that the mechanism of action for the 2D-MoS₂ surfaces was through either ROS release or slicing of cell membranes using the sharp edges of the 2D-MoS₂ particles. To further this project, molecular analysis of these mechanisms must be done, in order to find the actual mechanism in which 2D-MoS₂ affects bacterial cells. Uy *et al* in 2011 described a method using an Acridan lumigen PS-3 assay for the detections of ROS in culture medium.

Molecular analysis of bacterial would be an important step in identifying the potential of 2D-MoS₂ as an antimicrobial surface. When certain species of bacteria are exposed to a hostile environment, they can enter a state of low metabolic activity known as viable but not culturable (VBNC) (Li *et al.*, 2014). Analysis would be carried out with the DNase I protection assay as described by Pawlowski *et al*, 2011,

who successfully identified the viability of a Gram negative pathogen at otherwise undetectable levels.

6.0 Conclusion

The results demonstrated that an increase in MoS₂ particle size increased and influenced the surface topographies. Significant differences were shown by the 2D-MoS₂ surfaces at increasing particle sizes and concentrations. ICP-AES revealed that only the 20 %, 2 µm 2D-MoS₂ surface increased in Mo, while maintaining the same levels of sulphur in the surfaces however, the rate of leaching was very small and at the limit of detection. This in part may explain why no leaching through the agar occurred in the zone of inhibition assays. The pattern of retention of the bacteria changed from homogenous at lower 2D-MoS₂ particle sizes, to more heterogeneous at particle sizes of 6 µm. *P. aeruginosa* bacteria were also shown to have a greater affinity to binding to the 2D-MoS₂ surface.

The 2D-MoS₂ surface at each concentration demonstrated some level of antimicrobial activity. The results of the study concluded that the 2 µm surface showed the greatest antimicrobial efficacy, whereas the 90 nm surface demonstrated the weakest antimicrobial activity against both *S. aureus* and *P. aeruginosa*. When encased in a 24 h biofilm, both *S. aureus* and *P. aeruginosa* showed significantly reduced growth at 20 % concentrations of MoS₂. Furthermore, after analysing the bacterial damage via SEM, it was clear that the morphologies of the bacteria had been injured. Using current literature, it was suggested that ROS was a possible mechanism of action and had been damaging bacterial cell membranes through ROS release.

Toxicity towards human cells was tested in order to identify a potential application for the 2D-MoS₂ surfaces *in vivo*. The results showed that after a short incubation time that 6 µm 2D-MoS₂ surfaces demonstrated the lowest cytotoxicity. This was directly comparable to the ICP-AES results that showed 6 µm surfaces leached the least. Moreover, after prolonged exposure to the surfaces, 6 µm demonstrated increased HK-2 cell toxicity and 90 nm 2D-MoS₂ showed the lowest cytotoxicity.

This work suggests that the 2D-MoS₂ surfaces were antimicrobial towards both Gram positive and Gram negative bacteria. The antimicrobial efficacies of these surfaces were most effective at 2 μm particles sizes. However, the 2D-MoS₂ 90 surfaces at 48 h were the least cytotoxic. This means that for 2D-MoS₂ surfaces to achieve the most effective antimicrobial and demonstrate the lowest cytotoxicity, compromises must be made. With a possible solution to this being, a 2D-MoS₂ particle surface produced combining different particle sizes. A compromise between antimicrobial activity and cytotoxicity depending on the application or intended use for the 2D-MoS₂ surface would be the most effective use.

Bibliography

Alam, F. and Balani, K. (2017). Adhesion force of *Staphylococcus aureus* on various biomaterial surfaces. *Journal of the Mechanical Behavior of Biomedical Materials*, 65, pp.872-880.

Ansari, S., Prasad, H., Gautam, R., Rayamajhi, N., Shrestha, S., Upadhyay, G. Chapagain, M. (2014). Threat of drug resistant *Staphylococcus aureus* to health in Nepal. *Bio Med Central*. 14(157), 1-2.

Appel, J., Li, D., Podlevsky, J., Debnath, A., Green, A., Wang, Q. and Chae, J. (2016). Low Cytotoxicity and Genotoxicity of Two-Dimensional MoS₂ and WS₂. *ACS Biomaterials Science & Engineering*, 2(3), pp.361-367.

Bos, R., van der Mei, H. and Busscher, H. (1999). Physico-chemistry of initial microbial adhesive interactions – its mechanisms and methods for study. *FEMS Microbiology Reviews*, 23(2), pp.179-230.

Bruins M, S. Kapil, F.W. Oehme Microbial resistance to metals in the environment *Ecotox. Environ. Safe.*, 45 (2000), pp. 198-207

Cabot, G, Laura, Z, Moya, B, Juan, C, Navas, A, Blazquez, J, Antonio, O. (2016). Evolution of *Pseudomonas aeruginosa* Antimicrobial Resistance and Fitness under Low and High Mutation Rates. *Antimicrobial Agents and Chemotherapy*. 60 (3), p1767-1778.

Cao, F., Ju, E., Zhang, Y., Wang, Z., Liu, C., Li, W., Huang, Y., Dong, K., Ren, J. and Qu, X. (2017) 'An Efficient and Benign Antimicrobial Depot Based on Silver-Infused MoS₂'. *ACS Nano*, 11(5) pp.4651-4659.

Chudobova, D., Dostalova, S., Ruttkay-Nedecky, B., Guran, R., Rodrigo, M., Tmejova, K., Krizkova, S., Zitka, O., Adam, V. and Kizek, R. (2015). The effect of metal ions on *Staphylococcus aureus* revealed by biochemical and mass spectrometric analyses. *Microbiological Research*, 170, pp.147-156.

Costa, F., Carvalho, I., Montelaro, R., Gomes, P. and Martins, M. (2011). Covalent immobilization of antimicrobial peptides (AMPs) onto biomaterial surfaces. *Acta Biomaterialia*, 7(4), pp.1431-1440.

Crawford, R. (2008). *Staleya guttiformis* attachment on poly (tert-butylmethacrylate) polymeric surfaces. *Micron*, 39(8), pp.1197-1204.

- Davies, J. and Davies, D. (2010). Origins and Evolution of Antibiotic Resistance. *Microbiology and Molecular Biology Reviews*, 74(3), pp.417-433.
- Driscoll, J. A., Brody, S. L. & Kollef, M. H.(2007). *The epidemiology, pathogenesis and treatment of Pseudomonas aeruginosa infections*. *Drugs* 67, pp.351–368.
- Donlan, R M. (2002). Biofilms: Microbial Life on Surfaces. *Emerging Infectious Diseases*. 8 (9), 881-882.
- Donlan, R. and Costerton, J. (2002). Biofilms: Survival Mechanisms of Clinically Relevant Microorganisms. *Clinical Microbiology Reviews*, 15(2), pp.167-193.
- Dwivedi, S., Wahab, R., Khan, F., Mishra, Y., Musarrat, J. and Al-Khedhairi, A. (2014). Reactive Oxygen Species Mediated Bacterial Biofilm Inhibition via Zinc Oxide Nanoparticles and Their Statistical Determination. *PLoS ONE*, 9(11), pp. 111289.
- Fakhri, A. and Nejad, P. (2016). Antimicrobial, antioxidant and cytotoxic effect of Molybdenum trioxide nanoparticles and application of this for degradation of ketamine under different light illumination. *Journal of Photochemistry and Photobiology B: Biology*, 159, pp.211-217.
- Fan, J., Li, Y., Nguyen, H., Yao, Y. and Rodrigues, D. (2015). Toxicity of exfoliated-MoS₂ and annealed exfoliated-MoS₂ towards planktonic cells, biofilms, and mammalian cells in the presence of electron donor. *Environ. Sci.: Nano*, 2(4), pp.370-379.
- Foster, T., Geoghegan, J., Ganesh, V. and Höök, M. (2013). Adhesion, invasion and evasion: the many functions of the surface proteins of *Staphylococcus aureus*. *Nature Reviews Microbiology*, 12(1), pp.49-62.
- Gaze, W. Krone, S. Larsson, J. Li, X.-Z. Robinson, J. Simonet, P. Zhu, Y.-G. (2013). Influence of Humans on Evolution and Mobilization of Environmental Antibiotic Resistome. *Emerging Infectious Diseases*, 19(7), 1.pp. 1
- Giovanella, P., Cabral, L., Costa, A., de Oliveira Camargo, F., Gianello, C. and Bento, F. (2017). Metal resistance mechanisms in Gram-negative bacteria and their potential to remove Hg in the presence of other metals. *Ecotoxicology and Environmental Safety*, 140, pp.162-169.
- González-Bello, C. (2017). Antibiotic adjuvants – A strategy to unlock bacterial resistance to antibiotics. *Bioorganic & Medicinal Chemistry Letters*.

- Gu, Z Yang, Z Kang, S Yang, J.R Luo, J Zhou, R. (2016). Robust Denaturation of Villin Headpiece by MoS₂ Nanosheet: Potential Molecular Origin of the Nanotoxicity. *Scientific Reports*. 6 (1), pp .10
- Hall-Stoodley, L., Costerton, J. and Stoodley, P. (2004). Bacterial biofilms: from the Natural environment to infectious diseases. *Nature Reviews Microbiology*, 2(2), pp.95-108.
- Hobman, J Crossman, LC. (2015). Bacterial antimicrobial metal ion resistance. *Journal of Medical Microbiology*. 64 (5), 471-497.
- Heesemann, J. (1993). [Mechanisms of resistance to beta-lactam antibiotics]. *Infection*. 21 Suppl 1. S4-9.
- Heilmann, C. (2011). Adhesion Mechanisms of Staphylococci. *Advances in Experimental Medicine and Biology*, pp.105-123.
- Hirsch, E. and Tam, V. (2010). Impact of multidrug-resistant *Pseudomonas aeruginosa* infection on patient outcomes. *Expert Review of Pharmacoeconomics & Outcomes Research*, 10(4), pp.441-451.
- Ivanova, E., Mitik-Dineva, N., Wang, J., Pham, D., Wright, J., Nicolau, D., Mocanasi, R. and Santajit, S. and Indrawattana, N. (2016). Mechanisms of Antimicrobial Resistance in ESKAPE Pathogens. *BioMed Research International*, 2016, pp.1-8.
- Jhajharia, K., Mehta, L., Parolia, A. and Shetty, K. (2015). Biofilm in endodontics: A review. *Journal of International Society of Preventive and Community Dentistry*, 5(1), p.1.
- Kelly, P., Li, H., Whitehead, K., Verran, J., Arnell, R. and Iordanova, I. (2009). A study of the antimicrobial and tribological properties of TiN/Ag nanocomposite coatings. *Surface and Coatings Technology*, 204(6-7), pp.1137-1140.
- Kim, T Kwon, B Yoon, J Park, I Bang, G Park, Y Seo, Y Choi, S . (2017). Antibacterial Activities of Graphene Oxide–Molybdenum Disulfide Nanocomposite Films. *ACS Appl. Mater. Interfaces*. 9 (9), pp 7908–7917.
- Whitehead, K.A. Verran, J. (2009). The effect of substratum properties on the survival of attached microorganisms on inert surfaces. *Marine and Industrial Biofouling*. 4 (1), p13–33.
- Laverty, G Gorman, S Gilmore, B. (2014). Biomolecular Mechanisms of *Pseudomonas aeruginosa* and *Escherichia coli* Biofilm Formation. *Pathogens*. 3 (3), p597-598.
- Lemire, J Harrison, J Turner, R. (2013). Antimicrobial activity of metals: mechanisms, molecular targets and applications. *NATURE REVIEWS MICROBIOLOGY*. 11 (1), 371–384.

- Li, C., Xu, Y., Jiang, W., Dong, X., Wang, D. and Liu, B. (2013). Effect of NaCl on the heavy metal tolerance and bioaccumulation of *Zygosaccharomyces rouxii* and *Saccharomyces cerevisiae*. *Bioresource Technology*, 143, pp.46-52.
- Li, Y., Yuan, H., von dem Bussche, A., Creighton, M., Hurt, R., Kane, A. and Gao, H. (2013). Graphene microsheets enter cells through spontaneous membrane penetration at edge asperities and corner sites. *Proceedings of the National Academy of Sciences*, 110(30), pp.12295-12300.
- liopoulos, G, Blazquez, J. (2003). Hypermutation as a Factor Contributing to the Acquisition of Antimicrobial Resistance. *Clinical infectious Diseases*. 37 (9), 1201-1209.
- Lister, P, Wolter, D, Hanson, N. (2009). Antibacterial-Resistant *Pseudomonas aeruginosa*: Clinical Impact and Complex Regulation of Chromosomally Encoded Resistance Mechanisms. *Clinical Microbiology Reviews*. 22 (4), p582–610.
- Liu, G. (2009). Molecular Pathogenesis of *Staphylococcus aureus* Infection. *Pediatric Research*, 65(5 Part 2), pp.71R-77R.
- Livermore, D. (2002). Multiple Mechanisms of Antimicrobial Resistance in *Pseudomonas aeruginosa*: Our Worst Nightmare?. *Clinical Infectious Diseases*, 34(5), pp.634-640.
- Lowy, F. (2003). Antimicrobial resistance: the example of *Staphylococcus aureus*. *Journal of Clinical Investigation*. 9 (1), 1265–1273
- Novick, R. (2003). Autoinduction and signal transduction in the regulation of Staphylococcal virulence. *Molecular Microbiology*, 48(6), pp.1429-1449.
- Ohlsen K, T. Ternes, G. Werner, U. Wallner, D. Löffler, W. Ziebuhr. (2003). Impact of antibiotics on conjugational resistance gene transfer in *Staphylococcus aureus* in sewage Environ .*Microbiol .* , 5 pp. 711-716
- Pandit, S, Karunakaran, S, Boda, S K, Basu, B. (2016). High Antibacterial Activity of Functionalized Chemically Exfoliated. *ACS Appl. Mater. Interfaces*. 8 (46), pp 31567–31573.
- Paraje, M. G. "Antimicrobial resistance in biofilms." *Science against microbial pathogens: communicating current research and technological advances*(2011): 736-744.
- Pawlowski, D., Metzger, D., Raslawsky, A., Howlett, A., Siebert, G., Karalus, R., Garrett, S. and Whitehouse, C. (2011). Entry of *Yersinia pestis* into the Viable but Nonculturable State in a Low-Temperature Tap Water Microcosm. *PLoS ONE*, 6(3), p.e17585.

- Rağbetli, C., Parlak, M., Bayram, Y., Guducuoglu, H. and Ceylan, N. (2017). *Evaluation of Antimicrobial Resistance in Staphylococcus aureus Isolates by Years*.
- Renner, L and Weibel, D. (2011). Physicochemical regulation of biofilm formation. *MRS Bulletin*. 36 (5), p347–355.
- Sefton, A. (2002) 'Mechanisms of Antimicrobial Resistance'. *Drugs*, 62(4) pp.557-566.
- Seniya C, S.K. Verma, S.S. Trivedia, R.Verma, H.S. Vijayarti, S. VyasMetal Stress and Antibiotic Susceptibility Profile of Some Bacterial and Fungal Strains *J. Pure Appl. Microbiol.*, 6 (2012), pp. 1727-1734
- Sharma P, Jha AB, Dubey RS, Pessarakli M. (2012). Reactive Oxygen Species, Oxidative Damage, and Antioxidative Defense Mechanism in Plants under Stressful Conditions. *Journal of Botany*. 250 (2), pp 585-600.
- Silhavy, T., Kahne, D. and Walker, S. (2010). The Bacterial Cell Envelope. *Cold Spring Harbor Perspectives in Biology*, 2(5), pp.a000414-a000414.
- Somorjai, G. and Li, Y. (2010). Impact of surface chemistry. *Proceedings of the National Academy of Sciences*, 108(3), pp.917-924.
- Stewart, P. and William Costerton, J. (2001). Antibiotic resistance of bacteria in biofilms. *The Lancet*, 358(9276), pp.135-138.
- Tenover, F. (2006). Mechanisms of antimicrobial resistance in bacteria. *American Journal of Infection Control*, 34(5), pp.3-10.
- Ternes, T. and Joss, A. (2010). *Human pharmaceuticals, hormones and fragrances*. London: IWA Publishing, pp.212.
- Tuson, H and Weibel, D. (2013). Bacteria-surface interactions. *Soft Matter*. 9 (18), p4368–4380
- Tetlow, L., Lynch, S. and Whitehead, K. (2017). The effect of surface properties on bacterial retention: A study utilising stainless steel and TiN/25.65at.%Ag substrata. *Food and Bioproducts Processing*, 102, pp.332-339.
- Tsukatani, T., Suenaga, H., Shiga, M., Noguchi, K., Ishiyama, M., Ezoe, T. and Matsumoto, K. (2012). Comparison of the WST-8 colorimetric method and the CLSI broth microdilution method for susceptibility testing against drug-resistant bacteria. *Journal of Microbiological Methods*, 90(3), pp.160-166.

Uy B, McGlashan S, Shaikh S. (2011). Measurement of Reactive Oxygen Species in the Culture Media Using Acridan Lumigen PS-3 Assay. *Journal of Biomolecular Techniques*. 22 (3), 95–107.

Ventola, C L. (2015). The Antibiotic Resistance Crisis. *Pharmacy and Therapeutics*. 40 (4), 277–283

Yadav, N., Dubey, A., Shukla, S., Saini, C., Gupta, G., Priyadarshini, R. and Lochab, B. (2017). Graphene Oxide-Coated Surface: Inhibition of Bacterial Biofilm Formation due to Specific Surface–Interface Interactions. *ACS Omega*, 2(7), pp.3070-3082.

Yang, X., Li, J., Liang, T., Ma, C., Zhang, Y., Chen, H., Hanagata, N., Su, H. and Xu, M. (2014). Antibacterial activity of two-dimensional MoS₂ sheets. *Nanoscale*, 6(17), pp.10126-10133.

Yayan, J., Ghebremedhin, B. and Rasche, K. (2015). Antibiotic Resistance of *Pseudomonas aeruginosa* in Pneumonia at a Single University Hospital Center in Germany over a 10-Year Period. *PLOS ONE*, 10(10), pp.10

Yilmaz, M., Elaldi, N., Balkan, İ., Arslan, F., Batirel, A., Bakıcı, M., Gozel, M., Alkan, S., Çelik, A., Yetkin, M., Bodur, H., Sınırtaş, M., Akalın, H., Altay, F., Şencan, İ., Azak, E., Gündeş, S., Ceylan, B., Öztürk, R., Leblebicioglu, H., Vahaboglu, H. and Mert, A (2016). Mortality predictors of *Staphylococcus aureus* bacteraemia: a prospective multicenter study. *Annals of Clinical Microbiology and Antimicrobials*. 15 (7)

Wang, Z., von dem Bussche, A., Qiu, Y., Valentin, T., Gion, K., Kane, A. and Hurt, R. (2016). Chemical Dissolution Pathways of MoS₂ Nanosheets in Biological and Environmental Media. *Environmental Science & Technology*, 50(13), pp.7208-7217.

Zhang, W., Shi, S., Wang, Y., Yu, S., Zhu, W., Zhang, X., Zhang, D., Yang, B., Wang, X. and Wang, J. (2016). Versatile molybdenum disulfide based antibacterial composites for in vitro enhanced sterilization and in vivo focal infection therapy. *Nanoscale*, 8(22), pp.11642-11648.

